Evaluated Nuclear Data for Nuclides within the Thorium–Uranium Fuel Cycle

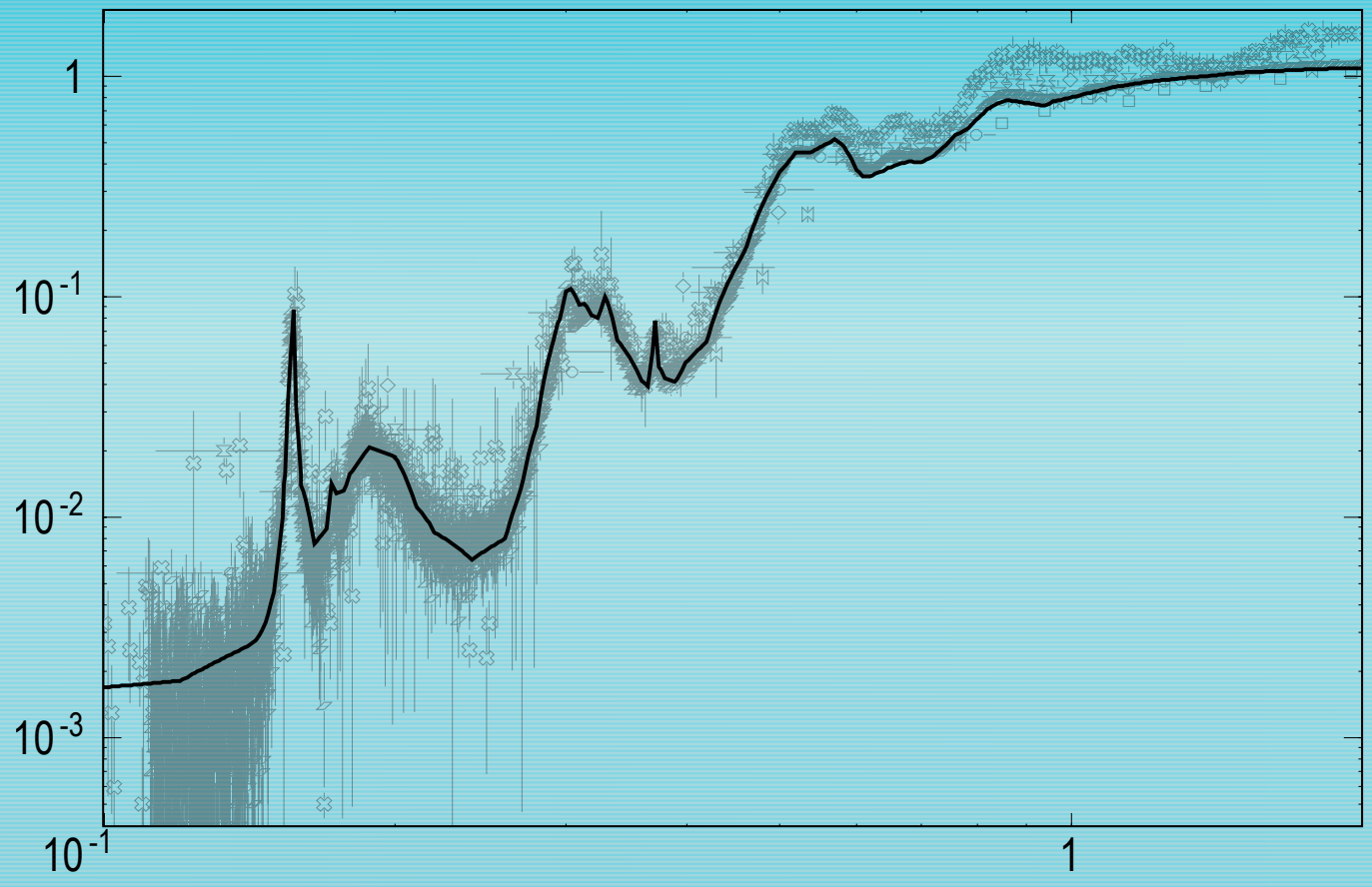

IAEA
International Atomic Energy Agency

EVALUATED NUCLEAR DATA FOR NUCLIDES WITHIN THE THORIUM–URANIUM FUEL CYCLE

The following States are Members of the International Atomic Energy Agency:

AFGHANISTAN
ALBANIA
ALGERIA
ANGOLA
ARGENTINA
ARMENIA
AUSTRALIA
AUSTRIA
AZERBAIJAN
BAHRAIN
BANGLADESH
BELARUS
BELGIUM
BELIZE
BENIN
BOLIVIA
BOSNIA AND HERZEGOVINA
BOTSWANA
BRAZIL
BULGARIA
BURKINA FASO
BURUNDI
CAMBODIA
CAMEROON
CANADA
CENTRAL AFRICAN REPUBLIC
CHAD
CHILE
CHINA
COLOMBIA
CONGO
COSTA RICA
CÔTE D'IVOIRE
CROATIA
CUBA
CYPRUS
CZECH REPUBLIC
DEMOCRATIC REPUBLIC OF THE CONGO
DENMARK
DOMINICAN REPUBLIC
ECUADOR
EGYPT
EL SALVADOR
ERITREA
ESTONIA
ETHIOPIA
FINLAND
FRANCE
GABON
GEORGIA
GERMANY
GHANA
GREECE
GUATEMALA
HAITI
HOLY SEE
HONDURAS
HUNGARY
ICELAND
INDIA
INDONESIA
IRAN, ISLAMIC REPUBLIC OF
IRAQ
IRELAND
ISRAEL
ITALY
JAMAICA
JAPAN
JORDAN
KAZAKHSTAN
KENYA
KOREA, REPUBLIC OF
KUWAIT
KYRGYZSTAN
LATVIA
LEBANON
LESOTHO
LIBERIA
LIBYAN ARAB JAMAHIRIYA
LIECHTENSTEIN
LITHUANIA
LUXEMBOURG
MADAGASCAR
MALAWI
MALAYSIA
MALI
MALTA
MARSHALL ISLANDS
MAURITANIA
MAURITIUS
MEXICO
MONACO
MONGOLIA
MONTENEGRO
MOROCCO
MOZAMBIQUE
MYANMAR
NAMIBIA
NEPAL
NETHERLANDS
NEW ZEALAND
NICARAGUA
NIGER
NIGERIA
NORWAY
OMAN
PAKISTAN
PALAU
PANAMA
PARAGUAY
PERU
PHILIPPINES
POLAND
PORTUGAL
QATAR
REPUBLIC OF MOLDOVA
ROMANIA
RUSSIAN FEDERATION
SAUDI ARABIA
SENEGAL
SERBIA
SEYCHELLES
SIERRA LEONE
SINGAPORE
SLOVAKIA
SLOVENIA
SOUTH AFRICA
SPAIN
SRI LANKA
SUDAN
SWEDEN
SWITZERLAND
SYRIAN ARAB REPUBLIC
TAJIKISTAN
THAILAND
THE FORMER YUGOSLAV REPUBLIC OF MACEDONIA
TUNISIA
TURKEY
UGANDA
UKRAINE
UNITED ARAB EMIRATES
UNITED KINGDOM OF GREAT BRITAIN AND NORTHERN IRELAND
UNITED REPUBLIC OF TANZANIA
UNITED STATES OF AMERICA
URUGUAY
UZBEKISTAN
VENEZUELA
VIETNAM
YEMEN
ZAMBIA
ZIMBABWE

The Agency's Statute was approved on 23 October 1956 by the Conference on the Statute of the IAEA held at United Nations Headquarters, New York; it entered into force on 29 July 1957. The Headquarters of the Agency are situated in Vienna. Its principal objective is "to accelerate and enlarge the contribution of atomic energy to peace, health and prosperity throughout the world''.

EVALUATED NUCLEAR DATA FOR NUCLIDES WITHIN THE THORIUM–URANIUM FUEL CYCLE

INTERNATIONAL ATOMIC ENERGY AGENCY
VIENNA, 2010

COPYRIGHT NOTICE

Marketing and Sales Unit, Publishing Section
International Atomic Energy Agency
Vienna International Centre
PO Box 100
1400 Vienna, Austria
fax: +43 1 2600 29302
tel.: +43 1 2600 22417
email: sales.publications@iaea.org
http://www.iaea.org/books

Printed by the IAEA in Austria
May 2010
STI/PUB/1435

IAEA Library Cataloguing in Publication Data

Evaluated nuclear data for nuclides within the thorium–uranium fuel cycle. —
Vienna : International Atomic Energy Agency, 2010.
p. ; 29 cm.
STI/PUB/1435
ISBN 978–92–0–101010–0
Includes bibliographical references.

1. Nuclear fuels. 2. Thorium. 3. Uranium. 4. Nuclides. I. International Atomic Energy Agency.

IAEAL 10–00627

FOREWORD

With the increasing awareness of global changes to the environment, nuclear power is slowly regaining a position of acceptance as an appropriate option for energy supply with negligible emission of greenhouse gases. This acceptability is subject to the following conditions: increased inherent safety, reduction of the risk of proliferation of fissile material and a viable solution to the problems of long term radioactive waste disposal. New concepts in nuclear technology for power production are being investigated to satisfy these requirements. The thorium based nuclear fuel cycle offers many advantages, including a much smaller buildup of long lived higher actinides, which are the main source of long term residual radioactivity arising from nuclear waste, and the fact that the world reserves of thorium are much larger than those of uranium. Additionally, it is well established that thorium fuel is more proliferation resistant. These advantages have resulted in a growing interest in innovative fuel cycle concepts based on thorium. Unfortunately, due to the previous lack of interest in the thorium fuel cycle, the quality of nuclear data for the relevant materials is lower than that for comparable materials in the uranium or mixed oxide (plutonium) fuel cycles. Uncertainties in the nuclear data are in some cases a factor of three larger than the target accuracies set by the designers of nuclear plants.

Numerous activities are in progress in many countries that anticipate the use of thorium based fuel for accelerator driven systems applicable to power production and radioactive waste transmutation. Active design efforts in India are focused on an advanced heavy water reactor concept that uses thorium fuel. There is a need for improved evaluated nuclear data, and at a review meeting in May 1999 the International Nuclear Data Committee (INDC) endorsed a project entitled "Nuclear Data for the Th–U Fuel Cycle" with a high priority. This project was initiated as a coordinated research project (CRP) in the IAEA programme and budget plan for 2002.

The nuclides of primary interest for evaluation relevant to the thorium–uranium (Th–U) fuel cycle are ^{232}Th, ^{231,233}Pa and ^{232,233,234,236}U. Historically, production of complete evaluated data files for important nuclides was primarily the domain of laboratories with long traditions in nuclear data evaluation. The evaluation efforts were usually part of national projects in countries with strong nuclear power programmes; the user was subsequently charged with the task of deciding which competing evaluation to trust, modify and adopt. This CRP, dedicated to the neutron cross-sections of nuclides of the Th–U fuel cycle, has been organized to produce more than just assessments of existing evaluations with minor improvements. Data validation was integrated into the evaluation process, which ensured prompt feedback on potential weaknesses to the evaluators, and thus improved the quality and final performance of the evaluations.

The main goal of this CRP was an improvement of evaluated nuclear data files that will allow more accurate design calculations of innovative fuel cycle concepts involving the Th–U fuel cycle. The research activities resulted in new evaluated nuclear data files for ^{232}Th and ^{231,233}Pa, and improvements to existing evaluations for ^{232,233,234,236}U. Basic evaluated nuclear data files, as well as the processed libraries in ACE format for the MCNP family of Monte Carlo codes and in MATXS format for deterministic codes, are available from the IAEA at http://www-nds.iaea.org/Th-U/.

The IAEA wishes to thank all participants who contributed to the CRP and to this publication. Thanks are also due to the US Cross Section Evaluation Working Group (CSEWG) for providing evaluated data files from the ENDF/B-VII.0 library and to V.M. Maslov for making available his extensive sets of actinide evaluated data. The technical officers responsible for this publication were A. Trkov, R. Capote and A.L. Nichols of the Division of Physical and Chemical Sciences.

CONTRIBUTING AUTHORS

Capote, R.	International Atomic Energy Agency
Leal, L.	Oak Ridge National Laboratory, United States of America
Liu, Ping	China Institute of Atomic Energy, China
Liu, Tingjin	China Institute of Atomic Energy, China
Schillebeeckx, P.	Institute for Reference Materials and Measurements, Belgium
Sin, M.	University of Bucharest, Romania
Sirakov, I.	Bulgarian Academy of Sciences, Bulgaria
Trkov, A.	International Atomic Energy Agency

TECHNICAL ASSISTANCE

Nichols, A.L.	International Atomic Energy Agency

EDITORIAL NOTE

CONTENTS

1. INTRODUCTION

Past developments in nuclear technology have been streamlined towards the adoption of uranium in thermal and fast reactors in order to improve the utilization of natural uranium resources. After the accidents at Three Mile Island and Chernobyl, opposition to nuclear technology rose significantly: restructuring of industry to reduce energy consumption was progressively implemented, and new reserves of natural gas and oil were discovered. Thus, the continued development of nuclear technology almost stopped, apart from safety related issues. The lack of an increase in demand for nuclear fuel removed the urgency to develop fast breeder reactors. Furthermore, when considering economic and safety aspects, this type of reactor had no advantages compared with conventional thermal reactors. Therefore, development of this technology was terminated in a significant number of countries, including France, which was the most advanced in this field and had a full scale fast breeder reactor in operation for some time.

With increasing awareness of global changes to the environment, nuclear power is slowly regaining a position of acceptance as an appropriate option for energy supply with negligible emission of greenhouse gases. This acceptability is subject to the condition of increased inherent safety, reduction of the risk of fissile material proliferation and a viable solution to the problems of long term radioactive waste disposal. New concepts of nuclear technology for power production are being investigated to satisfy these needs, and the thorium based nuclear fuel cycle offers many advantages:

(a) Neutron capture by ^{232}Th yields ^{233}U, which is a highly efficient nuclear fuel — the thermal breeder (or near-breeder) reactor concept based on thorium fuel is feasible.
(b) The buildup of long lived higher actinides, which are the main source of long term residual radioactivity in nuclear waste, is much smaller in thorium fuel — this behaviour can be used to advantage in the design of critical, as well as subcritical, accelerator driven systems (ADSs).
(c) Thorium fuel is more proliferation resistant due to highly radioactive constituents that cannot be separated out by chemical means — handling of such material in improvised clandestine laboratories is practically impossible.
(d) The world reserves of thorium are much larger than the reserves of uranium.

The above advantages have resulted in an increasing interest in innovative fuel cycle concepts based on thorium. Unfortunately, due to the previous lack of interest in the thorium fuel cycle, the quality of nuclear data for the relevant materials is lower than that for comparable materials in the uranium or mixed oxide (plutonium) fuel cycle. Uncertainties in the nuclear data are in some cases a factor of three larger than the target accuracies set by the designers of nuclear plants [1.1].

Numerous activities are in progress in many countries that anticipate the use of thorium based fuel for ADSs applicable to power production and radioactive waste transmutation [1.2]. Active design efforts are focused on an advanced heavy reactor concept in India that uses thorium fuel [1.3]. Important new experimental measurements of the cross-sections of materials relevant to the Th–U fuel cycle have been reported, or are in progress [1.4]. These data have to be evaluated, verified and validated on integral benchmarks to ensure valid design calculations. There is a definite need for improved evaluated nuclear data, and the International Nuclear Data Committee (INDC) endorsed a project entitled “Nuclear Data for Th–U Fuel Cycle” with high priority at a review meeting in May 1999. This project was initiated within the IAEA programme and budget plan for 2002.

The overall objectives of the IAEA coordinated research project (CRP) on evaluated nuclear data for the Th–U fuel cycle were as follows:

(a) Incorporate newly available experimental information into evaluated nuclear data files, which can be processed and used by designers of nuclear plants;
(b) Activate available human resources and facilitate the interaction and sharing of work to complete the task as defined above in a timely and professional manner;

(c) Produce improved evaluated nuclear data files that will allow more accurate design calculations of innovative fuel cycle concepts involving the Th–U fuel cycle — the nuclides of primary interest for evaluation are ^{232}Th, ^{231}Pa, ^{233}Pa and ^{232,233,234,236}U.

The first Research Coordination Meeting (RCM) was held in Vienna, Austria, from 25 to 29 August 2003, the second RCM from 6 to 9 December 2004, and the third and last RCM from 29 January to 2 February 2006 [1.5–1.7]. Evaluated nuclear data files were produced for the nuclides listed above. Some data were adopted from existing data files, and others are completely new evaluations.

Activities within the CRP that are included within this report are identified with the following:

(a) Critical assessments of the available experimental information with an emphasis on new data, and renormalization to modern cross-section standards (if necessary);
(b) Derivation (or adjustment) of resonance parameters for the resolved resonance range (RRR) and the unresolved resonance range (URR), including resonance covariance data;
(c) Derivation of nuclear model input parameters consistent with state of the art theoretical models, and reproduction of the experimentally measured cross-sections as much as possible;
(d) Construction of the cross-section covariance matrix prior by means of Monte Carlo calculations through random variation of nuclear model input parameters;
(e) Adjustment of the covariance matrix by the introduction of experimentally measured cross-sections;
(f) Assembly of the evaluated data in ENDF-6 format;
(g) Verification of the formatted data to ensure that they are formally correct, internally consistent, and do represent the experimental data from which they were derived;
(h) Processing of the data into application libraries for validation purposes;
(i) Preliminary validation of processed data against existing externally provided benchmark tests.

The aforementioned activities resulted in new evaluated nuclear data files for ^{232}Th, ^{231}Pa and ^{233}Pa, and improvements to existing evaluations for ^{232,233,234,236}U. The evaluations of neutron cross-sections are described separately for individual nuclides or groups of nuclides; evaluation procedures in the resonance range and in the fast energy range are given in the various subsections. Recommendations on the selection of fission product yields and decay data are also given, followed by the results of data validation by means of benchmark studies.

REFERENCES TO SECTION 1

[1.1] PRONYAEV, V.G., in Summary Report of the Consultants' Meeting on Assessment of Nuclear Data Needs for Thorium and Other Advanced Cycles, Rep. INDC(NDS)-408, IAEA, Vienna (1999).
[1.2] INTERNATIONAL ATOMIC ENERGY AGENCY, Feasibility and Motivation for Hybrid Concepts for Nuclear Energy Generation and Transmutation (Proc. Mtg Madrid, 1997), Rep. IAEA-TC-903.3, IAEA, Vienna (1998).
[1.3] HERMAN, M., Long Term Needs for Nuclear Data Development (Proc. Mtg Vienna, 2000), Rep. INDC(NDS)-428, IAEA, Vienna (2001).
[1.4] SHIBATA, K. (Ed.), Nuclear Data for Science and Technology (Proc. Int. Conf. Tsukuba, 2001), J. Nucl. Sci. Technol. **39** Suppl. 2 (2002).
[1.5] TRKOV, A. (Ed.), Evaluated Nuclear Data for Th–U Fuel Cycle, Summary Report of the 1st Research Coordination Mtg, Rep. INDC(NDS)-447, IAEA, Vienna (2003).
[1.6] SCHILLEBEECKX, P., TRKOV, A. (Eds), Evaluated Nuclear Data for Th–U Fuel Cycle, Summary Report of the 2nd Research Coordination Mtg, Rep. INDC(NDS)-468, IAEA, Vienna (2004).
[1.7] SCHILLEBEECKX, P., TRKOV, A. (Eds), Evaluated Nuclear Data for Th–U Fuel Cycle, Summary Report of the 3rd Research Coordination Mtg, Rep. INDC(NDS)-494, IAEA, Vienna (2006).

2. GENERAL EVALUATION METHODOLOGY

At the start of the project, the Japanese JENDL-3.3 [2.1] and the Russian BROND-2.2 [2.2] libraries were available. A number of new evaluations for the relevant nuclides were submitted to the IAEA from the Joint Institute for Power and Nuclear Research at Minsk [2.3]. Studies were also in progress at the Los Alamos National Laboratory (LANL) in the United States of America (USA), to review and improve the evaluated nuclear data for the uranium isotopes for the ENDF/B-VII.0 library [2.4]. During project implementation, the European JEFF-3.1 library was released [2.5]. These evaluations were the key references against which any improved evaluations were to be compared.

The following work was agreed on the basis of detailed reviews of the available evaluated data files for the relevant nuclides presented at the first RCM and consideration of the activities in progress at the participating laboratories at the time:

(a) Perform a detailed evaluation for ^{232}Th, including nuclear model calculations and a new resonance analysis based on new measurements at the Institute for Reference Materials and Measurements (IRMM) laboratory at Geel in Belgium and n_TOF experiments at CERN;
(b) Apply the same procedure in order to evaluate the cross-sections for ^{231}Pa and ^{233}Pa above the resonance range, while adopting the resonance data from available evaluations after careful review;
(c) Adopt evaluations for the uranium radionuclides from newly revised files from LANL, with modifications where necessary;
(d) Adopt fission product yield data from the JEFF-3.1 library after review;
(e) Adopt decay data from the JEFF-3.1 library after review.

The ENDF/B-VII library was released in December 2006 after the project terminated [2.4]. Evaluations resulting from the IAEA project for ^{232}Th and ^{231,233}Pa have been included in the final version of the ENDF/B-VII.0 library.

REFERENCES TO SECTION 2

[2.1] SHIBATA, K., et al., Japanese Evaluated Nuclear Data Library Version 3 Revision-3: JENDL-3.3, J. Nucl. Sci. Technol. **39** (2002) 1125–1136.
[2.2] MANOKHIN, V.N., et al., BROND-2.2: Russian Evaluated Neutron Reaction Data Library, Rep. IAEA-NDS-90, Rev. 8, IAEA, Vienna (1994).
[2.3] MASLOV, V.M., et al., Evaluated Neutron Nuclear Data for Pu, Am and Cm Isotopes, Rep. INDC(BLR)-2-11, IAEA, Vienna (1995–1998); http://www-nds.iaea.org/minskact/
[2.4] CHADWICK, M.B., et al., ENDF/B-VII.0: Next Generation Evaluated Nuclear Data Library for Nuclear Science and Technology, Nucl. Data Sheets **107** (2006) 2931–3060.
[2.5] KONING, A., et al. (Eds), The JEFF-3.1 Nuclear Data Library, JEFF Rep. 21, NEA No. 6190, Organisation for Economic Co-operation and Development, Paris (2006).

3. NEUTRON CROSS-SECTIONS OF THORIUM-232

3.1. EVALUATION IN THE RESOLVED RESONANCE RANGE

The resonance parameters of ^{232}Th were obtained from a sequential Bayes analysis by means of the SAMMY code. The analysed experimental database included neutron transmission data from the ORELA facility by Olsen and Ingle [3.1], capture data from the GELINA facility by Schillebeeckx [3.2], and capture data from the n_TOF facility at CERN in the energy range from 1 eV to 4 keV provided by Gunsing [3.3]. Capture data of Chrien et al. [3.4] and Lundgren [3.5] in the thermal energy range were normalized to a value of 7.35 b as recommended by Trkov [3.6], and fitted by SAMMY along with the total cross-section of Olsen [3.7] up to an energy of 1 eV.

The contribution of the external resonances (negative energy resonances and resonances at energies larger than 4 keV) was obtained from two fictitious resonances, one at –2000 eV and the other at 6000 eV. Parameters defining these resonances allow the representation of the Olsen transmission data for thick samples with an average accuracy of 1%. A constant value of the scattering radius of $R' = 9.686$ fm was found to be adequate for the entire energy range analysed, in agreement with the evaluated value of Olsen [3.7]. A ladder of seven s wave negative energy resonances from –3 to –110 eV was used to aid in fitting the thermal energy range. The resonances at –3.52 eV were used to adjust the cross-sections at 0.0253 eV.

The resonance set contains 244 s wave and 669 p wave resonances. Large s wave resonances were identified from their shape; some other resonances were assigned as s wave because they led to reduced neutron widths that were too large when assigned p wave. A large number of resonances assigned p wave are not seen in the experimental data; they were used to obtain agreement with the Wigner distribution of the spacing and the Porter–Thomas distribution of the reduced neutron width. A set of resonances that does not contain p wave resonances of reduced neutron width smaller than 1.6 meV results in a calculated average capture cross-section that is too small by 0.5% at energies below 1 keV, and too small by about 3% in the energy range 3–4 keV.

The prior values of the resonance parameters in the SAMMY fit were those from the Olsen evaluation [3.7], with a constant value of 24.4 meV for the capture width of all the resonances. A value of 24.4 meV was maintained for the p wave resonances. The capture width in the SAMMY fit was allowed to vary for the large s wave resonances, because for most of these resonances the capture area is sensitive to the capture width. However, the average of the capture width agrees within 4% with a value of 24.4 meV.

The cross-sections calculated at 0.0253 eV with the resonance parameters are 20.40 and 7.34 b for the total and capture cross-sections, respectively, compared with 20.38 and 7.40 b, respectively, calculated from the ENDF/B-VI database. The capture resonance integral in the energy range 0.5–4000 eV is 81.74 b from the present evaluation and 83.62 b from ENDF/B-VI, i.e. the present value is 2.3% lower than that from ENDF/B-VI. The total cross-section calculated with the resonance parameters is not consistent with the experimental data of Olsen in the energy range near 0.0253 eV, due to the Bragg scattering effect in the measured total cross-section.

Average capture cross-sections calculated in several energy ranges are compared with the ENDF/B-VI values in Table 3.1 (using a calculation with the SAMMY code). The covariance matrix of the resolved resonance parameters is a by-product of the fitting procedure with the SAMMY code.

3.2. EVALUATION IN THE UNRESOLVED RESONANCE RANGE

The neutron induced total and capture cross-sections of ^{232}Th in the URR have a strong impact on the performance and safety assessment of fast reactor systems based on the Th–U fuel cycle [3.8]. A sensitivity study of a fusion–fission hybrid system by Cheng and Mathews [3.9] demonstrated that the production rate of ^{233}U can be predicted within 1%, provided that the ^{232}Th(n, γ) cross-section between 3 and 3000 keV is known to within 2%. Bartine confirmed for fast breeder reactors that the most important region for capture in ^{232}Th lies between 10 and 100 keV [3.10]. The importance of the ^{232}Th(n, γ) cross-section was also noted by Salvatores [3.11], who stated that a 10% uncertainty in the data can produce a 30% uncertainty in the proton current requirement to operate an ADS at the subcritical level of $k_{\text{eff}} \approx -0.97$.

TABLE 3.1. AVERAGE CAPTURE CROSS-SECTIONS CALCULATED IN SEVERAL ENERGY RANGES COMPARED WITH VALUES FROM THE ENDF/B-VI DATABASE

Energy range (eV)	Present results (b)	ENDF/B-VI results (b)	Difference	
			(b)	(%)
0.1–1.0	1.475	1.63	0.155	10.5
1.0–20	0.212	0.335	0.123	58
20–100	25.92	26	0.08	0.3
100–500	9.049	9.356	0.307	3.4
500–1000	3.115	3.284	0.169	5.4
1000–1000	2.063	2.177	0.114	5.5
2000–3000	1.584	1.65	0.066	4.2
3000–4000	1.141	1.267	0.126	11

3.2.1. Review of experimental data and evaluated data files prior to the CRP

The most recent and complete survey of experimental data in the URR was reported by Maslov et al. in 2003 [3.12]. Other reviews of total and capture cross-section data in the URR can be found in the studies by de Saussure and Macklin [3.13], Meadows et al. [3.14], Ohsawa and Ohta [3.15], and Ohsawa and Inoue [3.16]. These reviews indicated that large discrepancies exist between the experimental data that were available before the IAEA initiated the CRP. Therefore, the nuclear data relevant to the thorium fuel cycle did not have the same level of accuracy as those of the U–Pu fuel cycle.

Several total cross-section measurements have been performed for ^{232}Th in the MeV region. However, documented experimental data for neutron energies below 100 keV are rather scarce and large discrepancies exist for energies below 40 keV. The experimental data of Uttley et al. [3.17], Kobayashi et al. [3.18], Iwasaki et al. [3.19], Poenitz and Smith [3.20], Vertebnyj et al. [3.21] and Grigor'ev et al. [3.22] are compared in Fig. 3.1 with the cross-section recommended by Soukhovitskii et al. and based on the dispersive coupled channel optical model (DCCOM) [3.23]. The cross-sections calculated by Capote [3.24] are compared in Fig. 3.2 with the evaluations performed by Maslov et al. [3.12] (adopted for JEFF-3.1), and with the ENDF/B-VI.8 and the JENDL 3.3 libraries, respectively. Wisshak et al. [3.25] have reported the results of capture cross-section measurements that were performed at the 3.75 MV van de Graaff accelerator by means of a 4π BaF_2 total absorption detector. While a comparison of the results of these measurements with the data obtained by Macklin and Winters [3.26] and Kobayashi et al. [3.27] shows reasonable agreement at neutron energies above 15 keV (Fig. 3.3), discrepancies of up to 40% are observed at lower neutron energies. The data of Macklin and Winters and Kobayashi et al. represent measurements at a time-of-flight facility based on determining the total energy by means of C_6D_6 and C_6F_6 detectors, respectively.

The data of Kobayashi et al. [3.27] have been adopted in the JENDL 3.3 and the CENDL evaluations [3.28]. The ENDF/B-VI evaluation in the URR is based on a combination of parameters resulting from measurements in the RRR and the capture data of Macklin and Halperin in the URR [3.29]. This evaluation does not include the 1.113 correction factor to the capture data mentioned by Macklin and Winters [3.26]. Thus, the significant discrepancies in experimental data result in similar differences between the capture cross-sections in the evaluated data files, as illustrated in Fig. 3.4, in which the capture cross-sections of the JENDL 3.3, BROND 3 and ENDF/B-VI libraries, and the evaluation of Maslov et al. [3.12], are compared. The data in Figs 3.3 and 3.4 illustrate the status of the ^{232}Th(n, γ) excitation function, which was far from the requested 2% uncertainty before the start of the CRP.

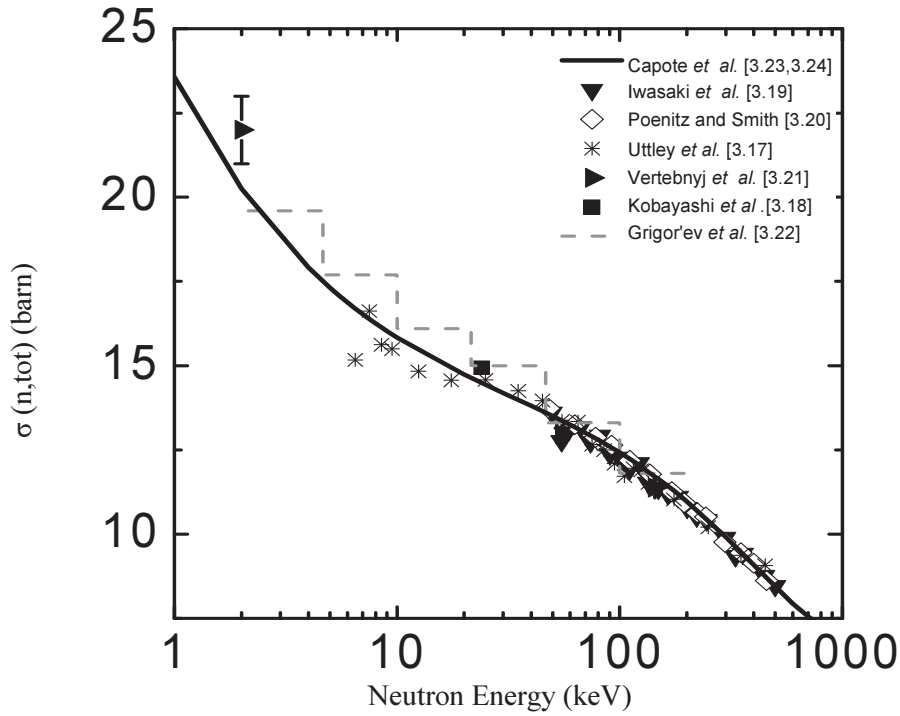

FIG. 3.1. Comparison of the total cross-section data obtained by Iwasaki et al. [3.19], Poenitz and Smith [3.20], Uttley et al. [3.17], Kobayashi et al. [3.18], Vertebnyj et al. [3.21] and Grigor'ev et al. [3.22] with the evaluation of Soukhovitskii et al. [3.23] and Capote [3.24].

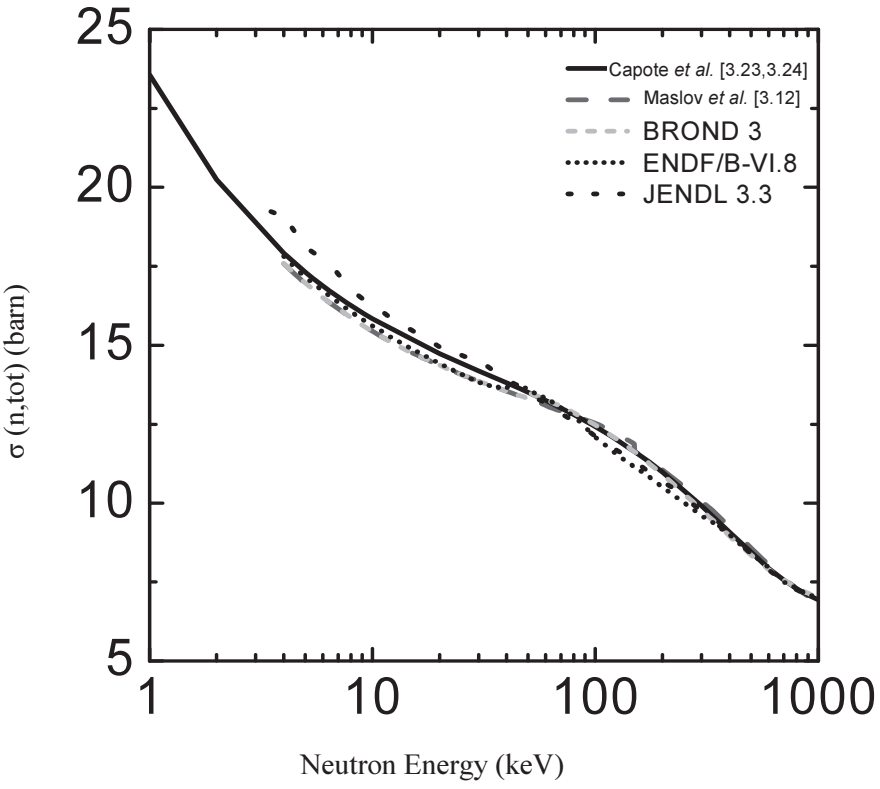

FIG. 3.2. Comparison of the total cross-section data evaluated by Soukhovitskii et al. [3.23] and Capote [3.24] with the evaluated data of Maslov et al. [3.12] and the cross-sections recommended in the ENDF/B-VI.8, JENDL 3.3 and BROND 3 libraries.

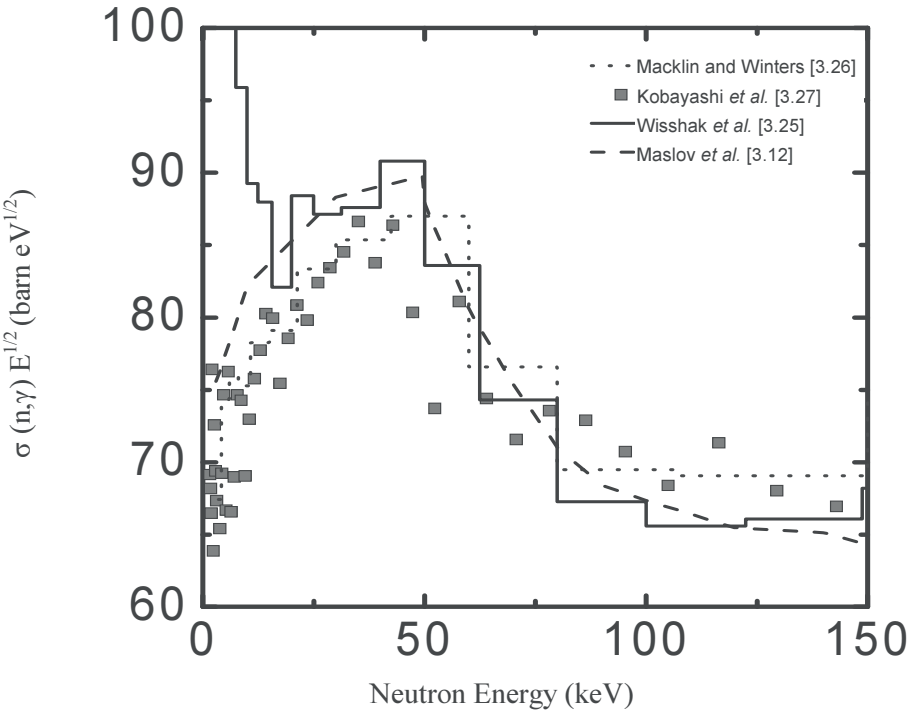

FIG. 3.3. Comparison of the capture cross-section data obtained by Macklin and Winters [3.26], Kobayashi et al. [3.27] and Wisshak et al. [3.25] with the cross-sections recommended by Maslov et al. [3.12].

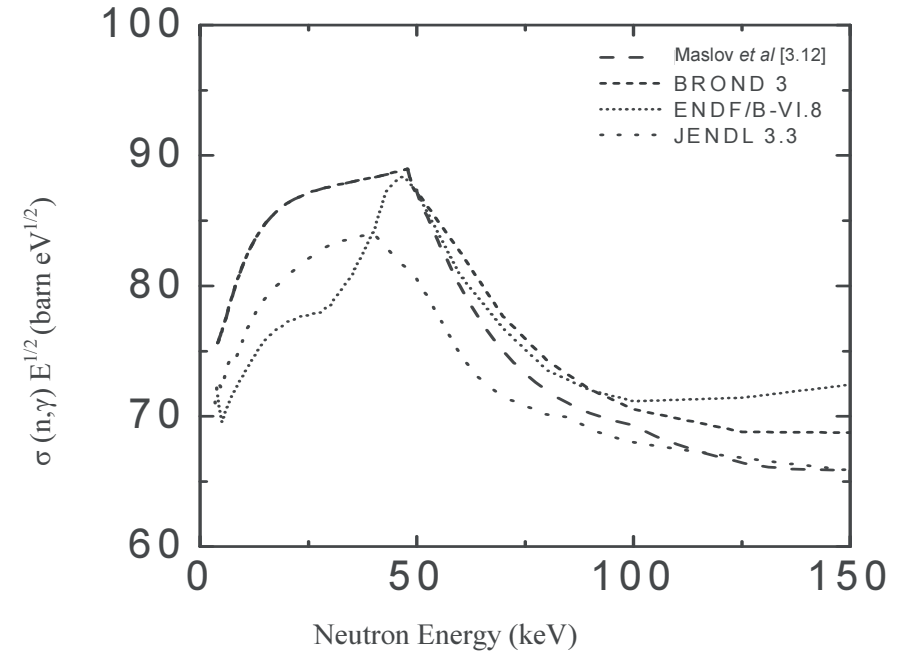

FIG. 3.4. Comparison of the capture cross-sections recommended by Maslov et al. [3.12] with the evaluated data in the BROND 3, ENDF/B-VI and JENDL 3.3 libraries.

New measurements of the ^{232}Th(n, γ) reaction were performed at the GELINA facility of IRMM at Geel and the n_TOF facility at CERN, by Borella et al. [3.30] and Aerts et al. [3.31, 3.32], respectively. A collaborative effort was established between IRMM and the CEA at Saclay to improve the data analysis and avoid systematic bias effects due to the normalization procedure and applied weighting function [3.33]. Both experiments were based on the total energy detection principle and the use of C_6D_6 detectors to apply the pulse height weighting technique. Weighting functions were deduced by Monte Carlo simulations to account for the neutron transport in the sample and the impact of the resonance strength, as described in Ref. [3.33]. The energy dependence of the neutron flux for the n_TOF data below 1 keV was deduced from measurements with a ^{6}Li deposit viewed by four silicon detectors, and above 1 keV by a ^{235}U-loaded parallel plate chamber. At GELINA the energy dependence of the neutron flux is continuously monitored by means of a ^{10}B ionization chamber placed in the neutron beam 1 m closer to the neutron source than the capture sample. Absolute normalization of the data of Borella et al. [3.30] and Aerts et al. [3.31, 3.32] was obtained from the well isolated saturated resonance at 23.5 eV. Results of the experiments performed at GELINA and n_TOF are compared in Fig. 3.5, and show that there is very good agreement between the data with respect to shape and absolute value. Borella et al. [3.30] have noted that the GELINA data are consistent with the data of Macklin and Winters [3.26] and Kobayashi et al. [3.27], within a systematic difference of 6.5% and 9% arising from the weighting functions used and normalization procedures applied by Borella et al. and Aerts et al. The data of Borella et al. are also in good agreement with the capture cross-sections determined by Poenitz et al. [3.34] from activation measurements. Good agreement between the data of Aerts et al., Borella et al. and Poenitz et al. and the renormalized cross-sections of Macklin and Winters and Kobayashi et al. is also confirmed in Fig. 3.5.

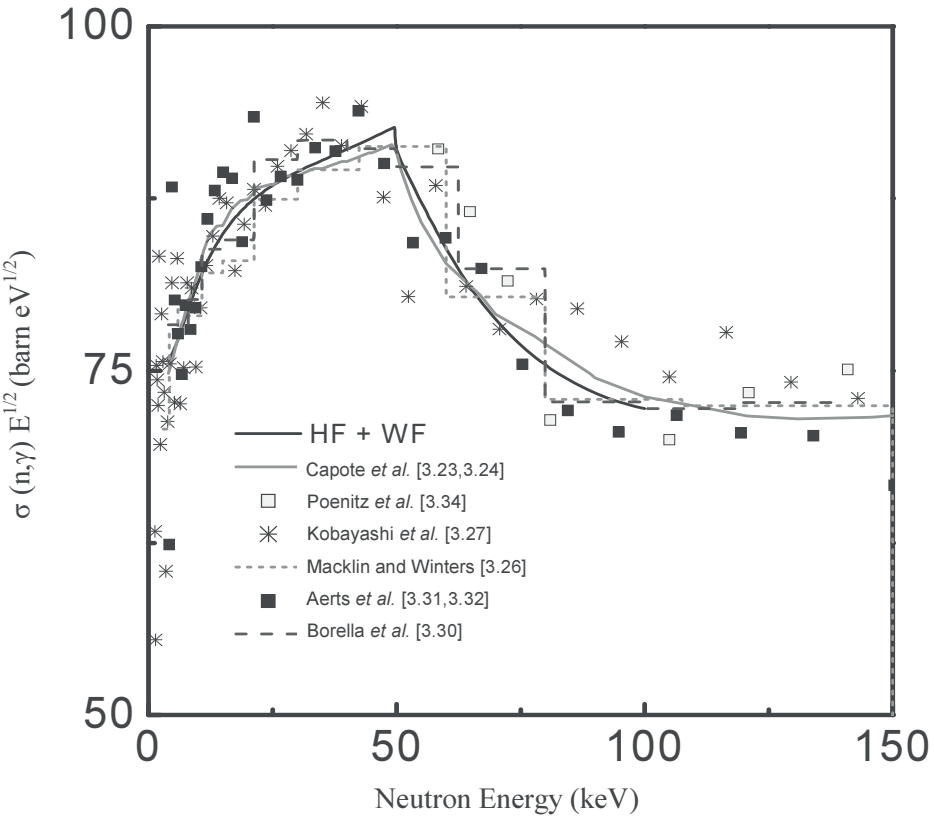

FIG. 3.5. Capture cross-sections of ^{232}Th obtained from an evaluation of the experimental data of Aerts et al. [3.31, 3.32], Borella et al. [3.30], Kobayashi et al. [3.27], Macklin and Winters [3.26] and Poenitz et al. [3.34] compared with the results obtained by Soukhovitskii et al. [3.23] and Capote [3.24] (the results of Macklin and Winters [3.26] and Kobayashi et al. [3.27] have been renormalized on the basis of the values of Borella et al. [3.30]).

3.2.2. An ENDF-6 compatible representation of the cross-sections in the URR

A generalized single level representation has been used by following the approach of Fröhner [3.35, 3.36], with minimum approximations to ensure compatibility with the energy dependent options of the ENDF-6 single level Breit–Wigner (SLBW) formula [3.37]. The contribution of the distant levels has been accommodated according to the standard description scheme, but with distant level parameters (R_c^{∞}) and hard sphere (potential) scattering radius ($R_c' = R'$) defined as energy dependent by deduction from the shape elastic cross-section and neutron transmission coefficients obtained from Capote et al. optical model calculations [3.23, 3.24].

The average partial cross-section ($\bar{\sigma}_c$) for a given spin and parity (J^{π}) with entrance channel c and exit channel c' in the URR can be expressed as a sum of a compound cross-section contribution (in terms of the Hauser–Feshbach theory with fluctuations) and a direct elastic contribution:

$$\bar{\sigma}_{cc'} = \bar{\sigma}_c^{\mathrm{se}}\delta_{cc'} + \frac{\pi}{k_c^2} g_c \frac{T_c T_{c'}}{T} F_{cc'} \tag{3.1}$$

where $\bar{\sigma}_c^{\mathrm{se}}$ is the direct (shape) elastic scattering cross-section, k_c is the wavenumber of the incoming neutron in the centre-of-mass system, g_c is the statistical factor, T_c is the neutron transmission coefficient for an entrance channel c, $T_{c'}$ is the transmission coefficient for exit channel c', T is the total transmission coefficient (the sum of all channel transmission coefficients for the J^{π} sequence under consideration) and $F_{cc'}$ is the fluctuation factor, which shows elastic enhancement in the case of elastic scattering. The total cross-section in the ENDF-6 prescription is calculated as a sum of the partial cross-sections, and the fluctuation factors $F_{cc'}$ are calculated by statistical integration with ten point Gaussian quadratures [3.38], assuming a narrow width (vanishing overlap) approximation with a chi-square distribution for the effective partial widths.

The shape elastic cross-section ($\bar{\sigma}_c^{\mathrm{se}}$) can be presented [3.39] in ENDF-6 terms as:

$$\bar{\sigma}_c^{\mathrm{se}} = 2\pi k_c^{-2} g_c \left[1 - \cos\left(2\varphi_c\right)\right]\left(1 - T_c/2\right) \tag{3.2}$$

where $\varphi_c(R') = \phi_c\left(k_c R'\right)$ is the hard sphere phase-shift expressed in terms of the hard sphere phase-shift function ϕ_c. Without any direct reactions, the neutron transmission coefficient T_c is given by means of the neutron strength function S_c and distant level parameters R_c^{∞} [3.36, 3.40] based on the analytical averaging of the collision matrix:

$$T_c(E) = \frac{2\pi\sqrt{E}\, P_c S_c / k_c a_c}{\left(1 + \pi\sqrt{E}\, P_c S_c / 2 k_c a_c\right)^2 + \left(P_c R_c^{\infty}\right)^2} \tag{3.3}$$

where P_c is the neutron penetrability factor, a_c is the channel radius and E is the incoming neutron energy in the laboratory system. The distant level parameter R_c^{∞} is related to the scattering radius R' as follows [3.39]:

$$R_c^{\infty} = \tan\left[\phi_c\left(k_c a_c\right) - \phi_c\left(k_c R'\right)\right]/P_c \tag{3.4}$$

Both Eqs (3.3) and (3.4) are valid for 'standard' boundary conditions, which are also the conditions of the ENDF-6 Reich–Moore (RM) representation in the resolved resonance region.

The transmission coefficient for an inelastic scattering channel through the ith excited level $T_{c'(i)}$ is equal to that for an elastic neutron channel T_c, if c has the same orbital momentum and kinetic channel energy as c'. Since only the first inelastic level is considered in the ENDF-6 prescription, the following equation can be derived:

$$T_{c'(l')}(E) = T_{c(l=l')}\left(E - E_{\mathrm{t}}\right) \tag{3.5}$$

where E_{t} signifies the threshold energy.

The lumped transmission coefficient for the capture channel $T_{\gamma}^{J^{\pi}}$ can be parameterized by the following expression:

$$T_{\gamma}^{J^{\pi}}(E) = T_{\gamma^0}^{J^{\pi}} f_{T_\gamma}^{J^{\pi}}(E) \tag{3.6}$$

where $T_{\gamma^0}^{J\pi}$ is the transmission coefficient for the capture channel at zero neutron energy, and the energy dependence $f_{T_\gamma}^{J^{\pi}}(E)$ can be determined from the $T_{\gamma}^{J^{\pi}}(E)$ definition as the sum of single channel photon transmission coefficients $T_{XL}(\varepsilon_\gamma)$. Summation (integration) occurs over the transition types X, multipolarities L and photon energies ε_γ of the primary γ quanta that de-excite the compound nucleus to lower lying states of density $\rho^{J'^{\pi'}}$. Thus, for the electric dipole approximation:

$$f_{T_\gamma}^{J}(E) = \frac{\sum_{\pi'} \frac{1-\pi\pi'}{2} \sum_{J'=|J-1|}^{J+1} \int_0^{B+E^{\mathrm{cm}}} T_{E1}\left(\varepsilon_\gamma\right) \rho^{J'^{\pi'}}\left(B+E^{\mathrm{cm}}-\varepsilon_\gamma\right) \mathrm{d}\varepsilon_\gamma}{\sum_{\pi'} \frac{1-\pi\pi'}{2} \sum_{J'=|J-1|}^{J+1} \int_0^{B} T_{E1}\left(\varepsilon_\gamma\right) \rho^{J'^{\pi'}}\left(B-\varepsilon_\gamma\right) \mathrm{d}\varepsilon_\gamma} \tag{3.7}$$

where B is the neutron binding energy and E^{cm} is the centre-of-mass energy. $T_{E1}\left(\varepsilon_\gamma\right)$ is mostly represented by a giant dipole resonance (GDR) in a single Lorentzian approximation of the photoabsorption cross-section.

The independent parameters describing the total and partial cross-sections are the neutron strength function S_ℓ (where ℓ is the momentum of the incoming neutron), the scattering radius R' and the capture transmission coefficients at zero energy $T_{\gamma^0}^{J^{\pi}}$. The J dependence of $T_{\gamma^0}^{J^{\pi}}$ is most commonly determined from the known J dependence of the level density. Thus, independent parameters for the capture channel might be any two $T_{\gamma^0}^{J^{\pi}}$ values that belong to different parities, for example, $T_{\gamma^0}^{(I+1/2)^+}$ and $T_{\gamma^0}^{(I+1/2)^-}$, where I is the target spin.

3.2.3. The resulting ENDF file as prepared by the CRP

The energy dependence of the potential scattering radius $R'(E)$ has been determined from the implicit Eq. (3.2) after summation over the entrance channels and total spin, where both the shape elastic cross-section and neutron transmission coefficients have been obtained from DCCOM calculations performed by Capote et al. [3.23, 3.24]. A parabolic fit to $R'(E)$ obtained in this way is shown in Fig. 3.6, with boundary values R' of 9.80 fm at 4 keV and 9.53 fm at 100 keV.

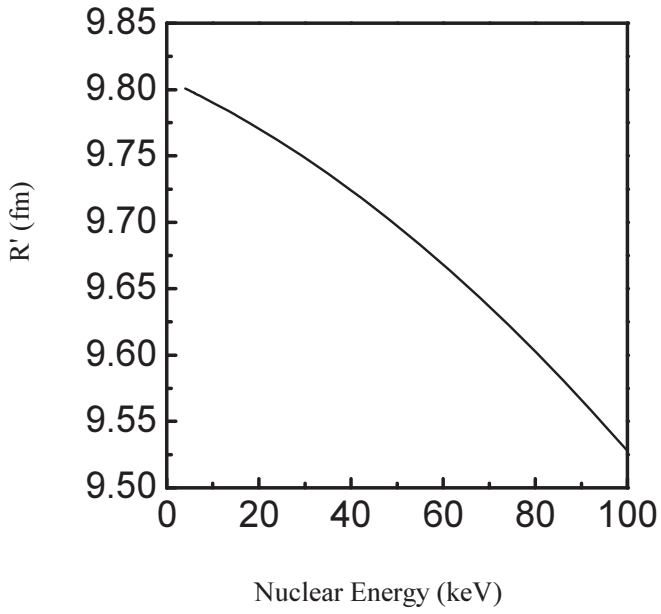

FIG. 3.6. Energy dependence of the scattering radius R'(E) determined from the shape elastic cross-section and transmission coefficients obtained from DCCOM calculations performed by Capote et al. [3.23, 3.24].

Average resonance parameters have been deduced from a simultaneous least squares fit to the experimental data: the total cross-section data of Uttley et al. [3.17], Iwasaki et al. [3.19] and Poenitz and Smith [3.20], the capture cross-section data of Gunsing [3.3], Borella et al. [3.33] and Poenitz et al. [3.34], and the renormalized capture cross-section data of Macklin and Winters [3.26] and Kobayashi et al. [3.27] with the constraint to be consistent with the total cross-section data determined by Soukhovitskii et al. [3.23] and Capote [3.24]. The average parameters which have been determined are the neutron strength functions for the s, p and d waves (S_0, S_1 and S_2) and the capture channel transmission coefficients $T_{\gamma^0}^{1/2^+}$ and $T_{\gamma^0}^{1/2^-}$ for the s and p waves, respectively. Capture channel transmission coefficients for d wave neutrons were deduced from the coefficient $T_{\gamma^0}^{1/2^+}$ for the s wave. The Gilbert–Cameron composite formula has been used for the level density, and single Lorentzian GDR parameters for the compound nucleus of ^{233}Th have been adopted from Holmes et al. [3.41]. Average resonance parameters are given in Table 3.2. Total and partial cross-sections have been calculated from the average resonance parameters by means of the RECENT code [3.42].

Evaluated average capture, total and inelastic cross-sections (denoted HF + WF) [3.43] are compared with experimental data in Figs 3.5, 3.7 and 3.8, respectively, as well as with Capote et al. evaluation [3.23, 3.24] based on the EMPIRE code [3.44].

TABLE 3.2. EVALUATED AVERAGE RESONANCE PARAMETERS AND RELATIVE UNCERTAINTIES FOR THE URR OF ^{232}Th

Wave	S_ℓ (10^{-4})	Relative uncertainty (%)	$T_{\gamma^0}^{1/2}$ (10^{-3})	Relative uncertainty (%)
s	0.878	0.2	8.505	4.2
p	1.902	4.1	8.182	3.7
d	1.266	20.5		

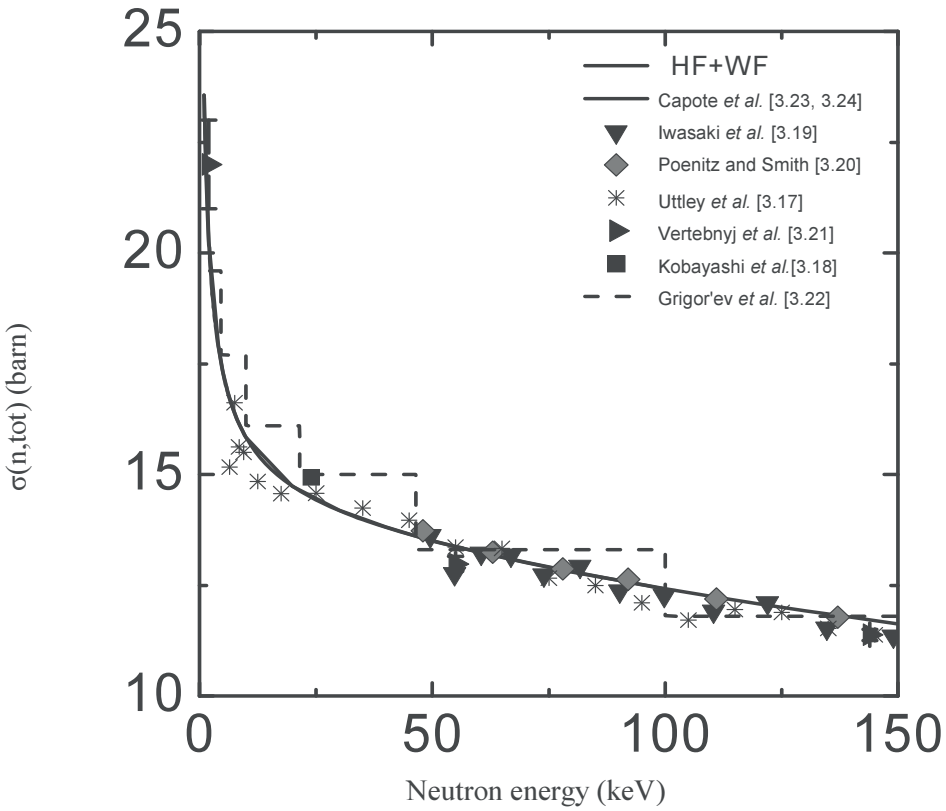

FIG. 3.7. Total cross-sections obtained from an evaluation of the experimental data in the URR compared with the results of Capote et al. [3.23, 3.24].

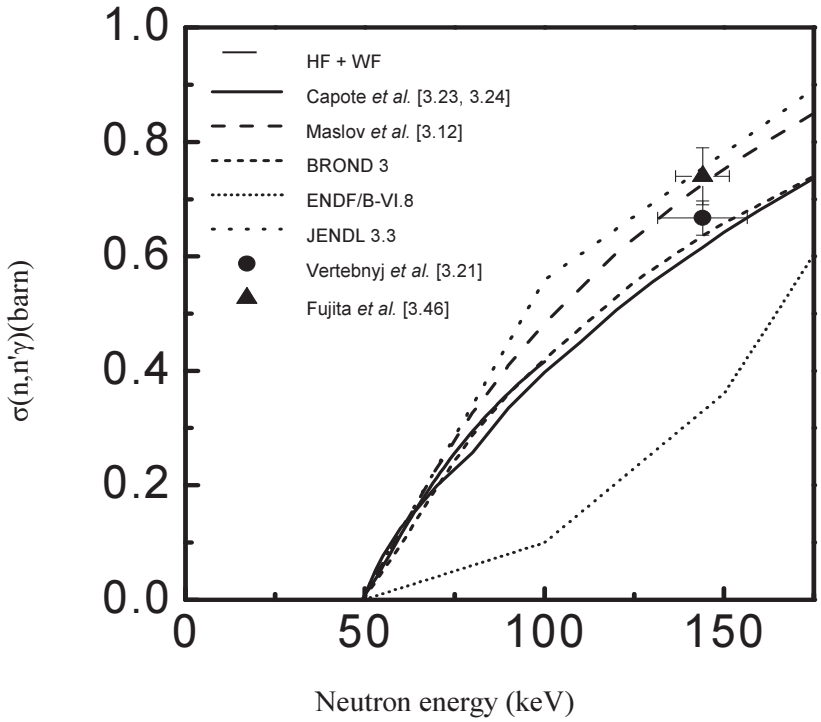

FIG. 3.8. Inelastic cross-section obtained from an evaluation of the experimental data (including the results of Fujita et al. [3.46]) in the URR compared with the result of Capote et al. [3.23, 3.24].

Conversion into the ENDF-6 format requires the transmission coefficients to be translated into energy dependent effective widths $\overline{\Gamma}_c$ by means of the following relationship:

$$T_c^{J\pi} = 2\pi \overline{\Gamma}_c^{J\pi} \rho^J \tag{3.8}$$

where c may be any entrance or exit, single or lumped, channel, and ρ^J is the level density. The s wave level spacing at zero neutron energy D_0 is usually used to determine the level density parameter, and hence the energy dependence in the level density formula. However, the sensitivity of $f_{T_\gamma}(E)$ with respect to D_0 is very low in the URR. Even for ^{232}Th, a nucleus with a low effective binding energy, the above sensitivity is approximately 0.1% at 10 keV, and 1% at 100 keV. Consequently, the average level spacing D_0 cannot be determined from an optimization of D_0 to average capture cross-section data in the URR. Therefore, the ^{232}Th s wave level spacing at zero energy (D_0 = 17.40 eV) has been adopted from the latest results obtained on the n_TOF facility for the resolved resonance region [3.3].

The above description refers to the basic evaluation. However, most of the existing processing codes (e.g. NJOY [3.45]) could not handle the energy dependent scattering radius and consequently the resulting basic evaluation. Therefore, a best NJOY-compatible approximation was adopted by introducing pointwise infinitely dilute cross-section data into File-3 (ENDF terminology). Thus, the unresolved resonance parameters (with approximate R' representation) were only used to calculate self-shielding. With the LSSF flag set to 1 in File-2, the infinitely dilute cross-sections have been preserved in the same form as in the basic evaluation, and File-2 was only used for NJOY calculations of self-shielding factors that vary slowly with energy.

Two consecutive approximations have been made within the R' representation of File-2 in order to ensure sufficient accuracy for the self-shielding calculations. First, a staircase energy dependence of R' has been used as a File-2 approximation compatible with the NJOY subroutines RECONR, BROADR and UNRESR. The URR has been divided into eleven ranges, each one possessing a constant R'. Small deviations of the potential scattering (less than 25 mb) do not influence the self-shielding factors, and cause either a negligible effect in the self-shielded capture cross-section or occur in both the numerator (shielded) and denominator (unshielded total or elastic cross-section computed from File-2). Therefore, the multiple range evaluation (with a range-wise constant R' in File-2) has been shown to introduce bias effects of less than 0.06% for the self-shielding factors even at the multiple boundaries and for a dilution cross-section σ_0 of 1 b.

The multiple range ENDF-6 option was found to be inadequately handled by the NJOY subroutine PURR, which is used for probabilistic calculations in Monte Carlo codes such as MCNP. Thus, a further approximation has been made in the R' representation of File-2 in order to reach compatibility with PURR. Considering that self-shielding effects are strongest at the lower end of the energy range, the constant scattering radius approximation with the R' value at a neutron energy of 4 keV has been shown to retain the self-shielding factors practically intact. This approximation has been justified by a comparison with the multiple range evaluation (UNRESR) and by integral benchmark calculations of reactor multiplication factors k_{eff} in which the PURR module of NJOY was used [3.47].

Figure 3.9 compares both approximations in terms of the most sensitive current-weighted total self-shielding factor at different energies, T of 300 K and σ_0 values of 1, 10 and 100 b. The maximum deviation introduced by the constant radius approximation at 100 keV is 0.1% for a σ_0 of 10 b and 0.32% for a σ_0 of 1 b. The maximum deviation in the less sensitive capture self-shielding factor amounts to 0.026% for a σ_0 of 10 b and 0.2% for a σ_0 of 1 b.

Thus, the consistency of both the cross-sections and self-shielding factors of the NJOY-compatible evaluation has been checked against the basic evaluation with an energy dependent scattering radius. Furthermore, the evaluated total, capture and inelastic cross-sections are fully consistent with the values obtained with the EMPIRE code, justifying the unified use of the EMPIRE results in File-3 (infinitely dilute cross-sections) and File-4 (angular distributions of secondary neutrons) of current evaluation from 4 to 100 keV.

3.2.4. The covariance matrix of unresolved resonance parameters

The covariances of the average resonance parameters have been calculated, and are presented in File-32. A short description of the procedure is given below. If $\boldsymbol{\theta}$, $\mathbf{z}$ and $\mathbf{y}$ are vectors of the average resonance parameters, experimental cross-section data and evaluated (modelled) cross-sections, respectively, the covariance matrix of the parameters, $\mathbf{C}_{\boldsymbol{\theta}}$, can be expressed in terms of the covariance matrix of the experimental data, $\mathbf{C}_{\mathbf{z}}$, by the following relationship:

$$\mathbf{C}_{\boldsymbol{\theta}} = \left(\mathbf{D}_{\boldsymbol{\theta}}^{T} \mathbf{C}_{\mathbf{z}}^{-1} \mathbf{D}_{\boldsymbol{\theta}} \right)^{-1} \tag{3.9}$$

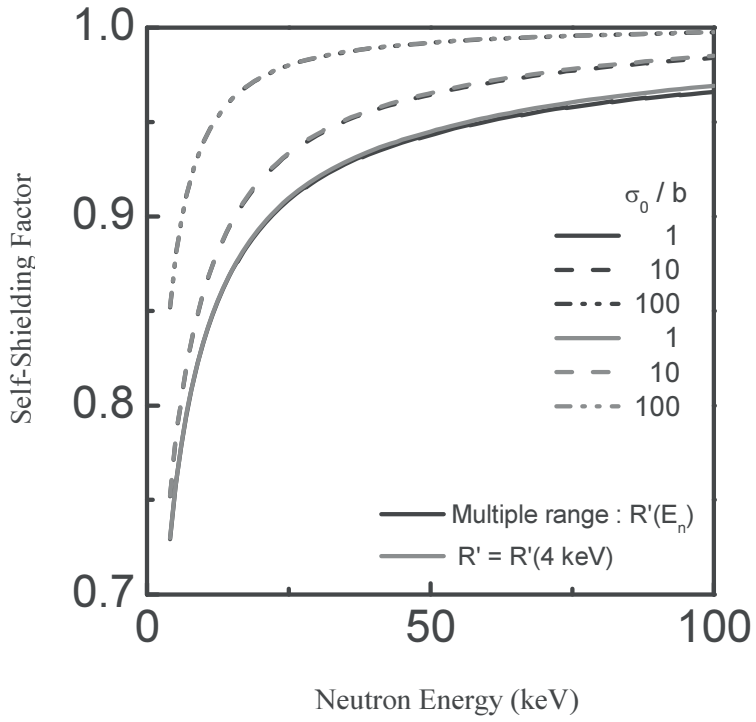

FIG. 3.9. Self-shielding factor for the current-weighted total cross-section: the multiple range evaluation is compared with the constant radius approximation at T = 300 K and σ_0 of 1, 10 and 100 b.

where $\mathbf{D}_{\theta}$ is the design matrix composed of the first partial derivatives of the theoretical cross-sections with respect to the parameters:

$$\mathbf{D}_{\theta} = \frac{\partial \mathbf{y}}{\partial \boldsymbol{\theta}} \tag{3.10}$$

The covariance matrix $\mathbf{C}_{z}$ has been constructed by assuming 1% correlated and 0.5% uncorrelated uncertainties for the total cross-section, and 1.5% correlated and 1.5% uncorrelated uncertainty for the capture cross-section. The design matrix $\mathbf{D}_{\theta}$ has been deduced by means of the RECENT code and the adoption of the final average resonance parameters (Table 3.2). Since the neutron strength functions $S_{\ell = 0,1,2}$ and the capture transmission coefficients at zero energy $T_{\gamma^0}^{(1/2)^+}$ and $T_{\gamma^0}^{(1/2)^-}$ have been adjusted in the fitting procedure, only the partial derivatives with respect to these parameters have been considered.

The final results are summarized in Table 3.3, and these data have been used to construct File-32. A very small relative uncertainty for the level distance has been introduced, assuming that the relative covariance elements for the reduced neutron widths can be approximated by the relative covariance elements of the neutron strength functions.

The covariance matrix of the calculated cross-section, $\mathbf{C}_{y}$, has been determined from the covariance matrix of the average parameters, $\mathbf{C}_{\theta}$, by means of the following equation:

$$\mathbf{C}_{y} = \mathbf{D}_{\theta}\mathbf{C}_{\theta}\mathbf{D}_{\theta}^{T} \tag{3.11}$$

The results for the total and capture cross-sections are given in Table 3.4.

3.2.5. An independent evaluation based on the ‘characteristic function’ approach from 4 to 150 keV

A new version of the HARFOR code includes an improved understanding of the external level contribution [3.48], and has been used to perform an independent evaluation of the average resonance parameters at INRNE, Sofia, Bulgaria. This method offers analytical expressions even for non-linear functionals (observables) of the cross-sections, such as transmission and self-indication ratios. Unfortunately, this approach is not supported by the ENDF-6 format. The resulting partial and total cross-sections are consistent with the cross-sections of the ENDF-compatible evaluation presented in Section 3.2.3. The average parameters based on the characteristic function approach are given in Table 3.5.

TABLE 3.3. RELATIVE UNCERTAINTY Σ OF THE AVERAGE RESONANCE PARAMETERS AND THE CORRELATION MATRIX

Resonance parameter		Σ (%)	Correlation matrix				
S_0	0.878×10^{-4}	2.0	1.00	–0.61	0.87	–0.54	0.73
$T_{\gamma^0}^{(1/2)^+}$	8.51×10^{-3}	4.2		1.00	–0.64	0.69	–0.58
S_1	1.90×10^{-4}	4.1			1.00	–0.53	0.74
$T_{\gamma^0}^{(1/2)^-}$	8.18×10^{-3}	3.7				1.00	–0.86
S_2	1.27×10^{-4}	20.5					1.00

TABLE 3.4. EVALUATED TOTAL (σ_t) AND CAPTURE (σ_c) CROSS-SECTIONS, TOGETHER WITH THE RELATIVE UNCERTAINTY (Σ) AND THE CORRELATION MATRIX

E (keV)	σ_t (b)	Σ (%)	Correlation matrix									
5	17.22	0.7	1.00	0.98	0.95	0.94	0.93	0.08	0.11	0.17	–0.03	0.22
25	14.52	0.5		1.00	0.99	0.99	0.98	0.10	0.14	0.20	–0.02	0.23
50	13.44	0.6			1.00	1.00	0.99	0.10	0.13	0.20	–0.02	0.24
70	12.95	0.6				1.00	1.00	0.09	0.12	0.19	–0.03	0.24
100	12.40	0.7					1.00	0.07	0.10	0.17	–0.04	0.24
E (keV)	σ_c (b)	Σ (%)	Correlation matrix									
5	1.085	1.6						1.00	0.92	0.91	0.92	0.86
25	0.559	1.5							1.00	0.98	0.95	0.80
50	0.408	1.5								1.00	0.97	0.89
70	0.299	1.6									1.00	0.89
100	0.229	1.6										1.00

TABLE 3.5. EVALUATED AVERAGE RESONANCE PARAMETERS BASED ON THE CHARACTERISTIC FUNCTION APPROACH IN THE URR OF ^{232}Th

Average	S ($\times 10^{-4}$)	D (eV)	Γγ (meV)	R' (fm)
s wave	0.868 ± 0.05	17.28	24	9.63 ± 2.67
p wave	1.93 ± 0.03	5.76	24.4	9.63 ± 2.67
d wave	1.17	3.456	24	9.63 ± 2.67

3.3. EVALUATION IN THE FAST ENERGY RANGE

Starting values for nuclear model parameters were taken from the RIPL-2 database [3.49], and the coupled-channel optical model potential (OMP) developed by Soukhovitskii et al. [3.23] was selected for the analysis. The major features of this study included: systematic accumulation of all relevant experimental data, renormalization, assessment of the applicability of the optical model to the triple humped fission barrier, and interpretation of the experimental results in terms of nuclear theory to allow interpolation and extrapolation of the data into unmeasured regions.

All nuclear data calculations were based primarily on a theoretical analysis with the EMPIRE 2.19 modular code [3.44, 3.50]. The EMPIRE code accounts for all of the nuclear reaction models needed to evaluate the nuclear reactions that occur over the energy range of interest. This range starts just above the resonance region (~0.001 MeV) and extends up to 60.0 MeV. On the basis of a large suite of implemented nuclear reaction models, the EMPIRE system produced a nuclear data file comprising a complete set of cross-sections. The resulting file conforms to the ENDF-6 format rules, satisfies internal consistency constraints and represents fully the experimental data on which the evaluation was based.

The nuclei of greatest interest within the thorium region are ^{232}Th and ^{231,233}Pa, for which second order shell effects split the outer fission barrier to produce a triple humped structure. Triple humped barriers are believed to encourage the formation of exotic hyper-deformed class III vibrational states, and could explain the significant structure observed near the barrier in the fission cross-section of light actinides. Over recent years, several studies have been published of neutron induced reactions on thorium and protactinium, based on the triple humped fission barrier [3.51, 3.52]. However, uncoupled fission barriers were employed, whereby the resonant structure present in the experimental data was only being reproduced on average and the energy range studied was very limited.

The fission formalism based on the optical model was extended in the present evaluation to include triple humped barriers [3.53–3.56], integrated in a consistent way within the statistical model of nuclear reactions [3.57] and implemented in the EMPIRE 2.19 code [3.44]. This formalism provides information on the fission barrier parameters. Accurate predictions of fission cross-sections were obtained for all three nuclei in the energy range studied.

3.3.1. A compound nucleus formalism based on decay probabilities deduced in the optical model for fission

All of the calculations are based on a theoretical analysis that utilizes the optical and direct reaction models, the pre-equilibrium exciton model and the fully featured Hauser–Feshbach (HF) model. The coupled-channel ECIS03 code incorporated into the EMPIRE-2.19 system was used for optical model calculations [3.58], and pre-equilibrium emission was taken into account by the PCROSS module featuring a one component exciton model with gamma, nucleon and cluster emissions. Hauser–Feshbach [3.59] and Hoffmann–Richert–Tepel–Weidenmüller (HRTW) [3.60] versions of the statistical model were used for the compound nucleus cross-section calculations. Both approaches include the decay probabilities deduced in the optical model for fission [3.53, 3.54], and account for the multiple particle emission and the full gamma cascade.

The compound cross-section for fission (*f*) and the competing outgoing channels ($d = \{\gamma, \mathrm{n}, \mathrm{p}, \alpha\}$) at incident energy E are calculated by means of the following equation:

$$\sigma_k(E) = \sum_{J\pi} \sigma(EJ\pi) P_k(EJ\pi),\ k = f, d \tag{3.12}$$

where $\sigma(EJ\pi)$ is the population cross-section of the compound nucleus states with spin J and parity π, and $P_k(EJ\pi)$ is the corresponding decay probability.

The decay probabilities for fission and competing channels are calculated according to the following expressions in which gamma decay in the isomeric well was neglected [3.57]:

$$P_d(EJ\pi) = \frac{T_d(EJ\pi)}{T_{\mathrm{dir}}(E^*J\pi) + \sum_d T_d(EJ\pi)} \left(1 - \frac{1}{a}\right) \tag{3.13}$$

$$P_f(EJ\pi) = P_{\mathrm{dir}}(EJ\pi) + P_{\mathrm{ind}}(EJ\pi) = \frac{T_{\mathrm{dir}}(E^*J\pi)}{T_{\mathrm{dir}}(E^*J\pi) + \sum_d T_d(EJ\pi)} \left(1 - \frac{1}{a}\right) + \frac{1}{a} \tag{3.14}$$

where

$$a = \left(1 + b^2 + 2b \coth\left[\frac{1}{2}(T_A(E^*J\pi) + T_{B,(C)}(E^*J\pi))\right]\right)^{1/2} \tag{3.15}$$

$$b = \frac{T_{\mathrm{dir}}(E^*J\pi) + \sum_d T_d(EJ\pi)}{T_{\mathrm{abs}}(E^*J\pi)} \frac{T_A(E^*J\pi) + T_{B,(C)}(E^*J\pi)}{T_{B,(C)}(E^*J\pi)} \tag{3.16}$$

E^* is the excitation energy in the decaying nucleus, T_A, $T_{B(C)}$, T_{dir} and T_{ind} are fission coefficients defined in Section 3.3.4, and T_d are the transmission coefficients for the competing channels. These general expressions are valid for the partial damping of class II vibrational states, and can be applied at any excitation energy below or above the fission barrier. Consider fission by direct transmission of the flux across the barrier: the quantity $1/a$ is taken from the flux, and re-emitted in the fission channel after being absorbed in the isomeric well. At very low excitation energies where the class II vibrational states preserve their individuality, fission occurs entirely by direct transmission across the barrier, and the second term in the above equation disappears. The opposite case of complete damping involves the entire flux transmitted through the inner hump being absorbed in the isomeric well, and the following familiar expression for decay probabilities being derived:

$$P_k(EJ\pi) = \frac{T_k(EJ\pi)}{\sum_{k'} T_{k'}(EJ\pi)}, \quad k = f, d \tag{3.17}$$

3.3.2. Fission barriers

The optical model for fission involves consideration of the possible transmission mechanisms based on a complex potential:

$$V_f = V + \mathrm{i}W \tag{3.18}$$

to describe the one dimensional multi-humped fission barrier, as can be seen in Fig. 3.10.

The real part of the barriers associated with the discrete transition states are parameterized as a function of the quadrupole deformation β by smoothly joined parabolas of the form:

$$V_i(\beta) = E_{fi} + (-1)^i \frac{1}{2}\mu\hbar^2\omega_i^2(\beta - \beta_i)^2 \tag{3.19}$$

where i extends from 1 to 5 for a triple humped barrier. The energies E_{fi} represent maxima of V_i in odd regions (humps) and minima in even regions (wells), β_i are the corresponding abscissas, the harmonic oscillator frequencies

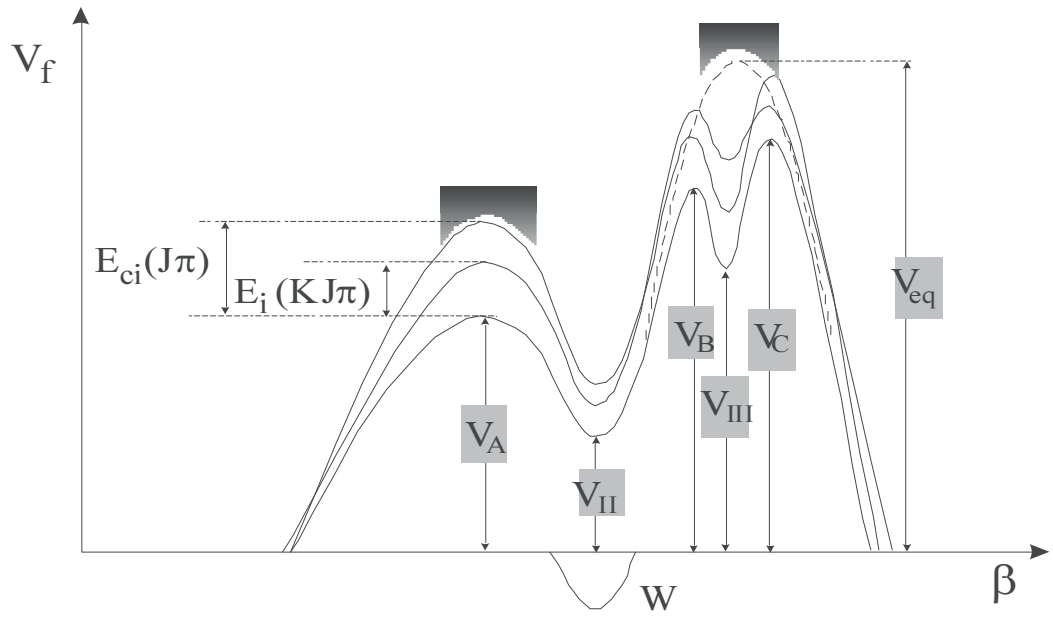

FIG. 3.10. Parameterization of the triple humped fission barrier. Humps are denoted with capital letters A, B, C (i = 1, 3, 5), and wells with Roman numerals II (i = 2) and III (i = 4).

ω_i define the curvature of each parabola, and μ is the inertial mass parameter assumed to be independent of deformation and approximated by the semi-empirical expression $\mu \approx 0.054A^{5/3}$ MeV^{-1} [3.61], where A is the mass number.

The discrete transition states are rotational levels built on vibrational or non-collective band-heads characterized by a given set of quantum numbers (angular momentum J, parity π and angular momentum projection on the nuclear symmetry axis K) with the following excitation energies:

$$E_i(KJ\pi) = E_{fi} + \varepsilon_i(K\pi) + \frac{\hbar^2}{2\Im_i}\left\{\begin{array}{l} J(J+1) - K(K+1) \\ \quad + s\left[1+(-1)^{J+1/2}\left(J+1/2\right)\right]\delta_{K,1/2} \end{array}\right\} \tag{3.20}$$

where $\varepsilon_i(K\pi)$ are the band-head energies, $\Im_i$ are the inertial parameters, and s is the decoupling parameter for $K = 1/2$ bands — a parabolic barrier with height $E_i(KJ\pi)$ and curvature $\hbar\omega_i$ is identified with each transition state. This relationship is obtained in the strong coupling limit of the particle rotor model for odd-mass nuclei, and is also valid for even–even nuclei since K is an integer and the Kronecker symbol delta on the right hand side of Eq. (3.20) is obviously zero. The equation is similarly applied to odd–odd nuclei by neglecting any residual proton–neutron interaction.

The transition state spectrum has a discrete component up to a certain energy E_{ci}, above which the spectrum is continuous and described by the level density functions $\rho_i(EJ\pi)$, accounting for collective enhancements specific to the nuclear shape asymmetry at each saddle point. When a triple humped barrier is considered, the reasonable assumption can be made that the shell effects will decrease with increasing excitation energy and the outer barriers will collapse into a single hump. Therefore, triple humped barriers are associated with discrete transition states only in the present formalism. Accordingly, the continuum contribution to the fission coefficient is calculated in terms of a double humped barrier, with the second peak representing a single barrier V_{eq} equivalent to the two outer humps (Fig. 3.10). The parameters of the equivalent barrier are determined on the basis of equal transmission.

After the present evaluation had been completed and microscopic level densities for all three saddle points became available [3.62], the optical model for fission through a multi-humped barrier was revised by eliminating the approximation of the equivalent outer barrier. Preliminary calculations support the removal of this approximation.

The negative imaginary potential, iW, is introduced into the deformation range, corresponding to the second well in order to simulate damping of the class II vibrational states. This approach causes absorption of the incoming flux in this well, while the tertiary well is supposed to be shallow enough to neglect damping of class III vibrational states, and therefore no absorption occurs there.

The strength W is assumed to be a quadratic function of deformation akin to the real part V, and to be energy dependent:

$$W(\beta) = \alpha(E)[E - V(\beta)] \tag{3.21}$$

in which the $\alpha(E)$ parameter, which controls the strength of the imaginary part of the fission potential, should be chosen to fit the width of the resonances in the sub-barrier fission cross-section and to be consistent with physical values for the transmission coefficients at higher energies.

A fission formalism based on the optical model with triple humped barriers [3.53–3.56] has been integrated in a consistent way within the statistical model of nuclear reactions [3.57] and implemented in the EMPIRE 2.19 code. The derived fission barriers and employed transitional and class II and III states are tabulated in Ref. [3.57].

3.3.3. Level densities at saddle points

Among the various models describing level densities, the EMPIRE-specific level density model was chosen for the present calculations [3.44, 3.50]. The formalism uses the superfluid model below the critical excitation energy and the Fermi gas model above the critical excitation energy. Account is taken of the deformation dependent collective effects on the level densities due to nuclear vibration and rotation (rotational and vibrational enhancements and their temperature dependent damping). This approach was used to describe the continuum spectra for equilibrium and saddle point deformations. A consistent description of the shell, pairing and collective

effects can only be achieved by means of generalized superfluid model parameters derived on the basis of the systematics, with corresponding modifications to the pairing, asymptotic level density parameters and moments of inertia at the saddle states.

Nuclear shape was assumed to be axial and mass symmetric at the deformation corresponding to the first saddle, and axial symmetric and mass asymmetric at the deformation corresponding to the equivalent outer saddle, which brings an additional enhancement factor of 2 relative to the normal states.

The shell correction, pairing and asymptotic values of the level density parameter at each saddle have been calculated using the RIPL-2 recommendations as starting values [3.48]:

(a) The recommended values for the pairing parameter within the saddle points are $\Delta_A = \Delta_{B,\mathrm{eq}} = 14A^{-1/2}$; data description required values of approximately $13A^{-1/2}$.
(b) On the basis of the semiclassical approach and microscopic calculations, the RIPL-2 recommendation for the ratio a_f/a_n is approximately 1.05–1.07 for the asymptotic level density parameters of the fission and neutron channels; the present level density model required values for this ratio to be in the range 0.85–1.02 to achieve suitable fits of the fission data.
(c) Shell corrections at saddle points required values derived from an analysis of the fission cross-section in the first plateau region (2–5 MeV over the fission barrier) using the phenomenological version of the generalized superfluid model proposed in the RIPL-2 recommendations:

$$\delta W_A = 2.6 \text{ MeV}$$
$$\delta W_{B,\mathrm{eq}} = 0.6 + 0.1(Z - 97) + 0.04(N - 143) \text{ MeV} \quad (3.22)$$

Detailed information about level density parameterizations and systematics can be found in the comprehensive description given by the EMPIRE code [3.50].

3.3.4. Fission coefficients

The fission coefficient through one discrete barrier is the sum of two terms:

(1) $T_\mathrm{dir}(EKJ\pi)$ represents the direct transmission;
(2) $T_\mathrm{ind}(EKJ\pi)$ represents the indirect transmission;

and is given by the product of the absorption coefficient $T_\mathrm{abs}(EKJ\pi)$ and the branching ratio for prompt and delayed fission. Neglecting gamma decay in the isomeric well, the delayed fission can be expressed in terms of the following equation:

$$\begin{aligned} T_f(EKJ\pi) &= T_\mathrm{dir}(E^*KJ\pi) + T_\mathrm{ind}(E^*KJ\pi) \\ &= T_\mathrm{dir}(E^*KJ\pi) + T_\mathrm{abs}(E^*KJ\pi)\frac{T_{B(C)}(E^*KJ\pi)}{T_A(E^*KJ\pi) + T_{B(C)}(E^*KJ\pi)} \end{aligned} \quad (3.23)$$

where E^* is the excitation energy, $T_A(EKJ\pi)$ is the transmission coefficient through the first peak, and

$$T_{B(C)}(EKJ\pi) = T_B(EKJ\pi)$$

is the transmission coefficient through the outer peak of a double humped fission barrier, or

$$T_{B(C)}(EKJ\pi) = T_{BC}(EKJ\pi)$$

is the direct transmission through the outer peaks of a triple humped fission barrier.

Single humped transmission coefficients (T_j) are expressed in terms of the momentum integrals K_j in the Wentzel–Kramers–Brillouin (WKB) approximation [3.63, 3.64]:

$$T_j = \frac{1}{1+\exp(2K_j)}, \qquad j = A, B, C \tag{3.24}$$

with

$$K_j = \pm \left| \int_{a_j}^{b_j} \left(2\mu[E - V_j(\beta)]/\hbar^2\right)^{1/2} \mathrm{d}\beta \right|, \qquad j = A, B, C \tag{3.25}$$

where ± represents the sub-barrier and over-barrier excitation energies, and a_j, b_j are the deformation intercepts. The momentum integrals of the wells of the real part of the fission potential are approximated as follows:

$$\nu_j = \int_{a_i}^{b_i} \left(2\mu[E - V_i(\beta)]/\hbar^2\right)^{1/2} \mathrm{d}\beta \tag{3.26}$$

where $j = 1$ for i = II, and $j = 2$ for i = III, while the imaginary potential in the isomeric well is given by the equation:

$$\delta = -\left(\frac{\mu}{2\hbar^2}\right)^{1/2} \int_{a_{\mathrm{II}}}^{b_{\mathrm{II}}} \frac{W(\beta)}{[E - V_{\mathrm{II}}(\beta)]^{1/2}} \mathrm{d}\beta \tag{3.27}$$

The general expression for the direct transmission coefficient through a double or triple humped fission barrier with an imaginary potential in the second well is given by the following equation:

$$T_{\mathrm{dir}} = \frac{T_A T_{B(C)}}{\mathrm{e}^{2\delta} + 2\left[(1-T_A)(1-T_{B(C)})\right]^{1/2} \cos(2\nu_{\mathrm{II}}) + (1-T_A)(1-T_{B(C)})\mathrm{e}^{-2\delta}} \tag{3.28}$$

A similar expression in the limit $\delta = 0$ is obtained for a triple humped barrier — direct transmission through the outer peaks is given by the following equation:

$$T_{BC} = \frac{T_B T_C}{1 + 2\left[(1-T_B)(1-T_C)\right]^{1/2} \cos(2\nu_{\mathrm{III}}) + (1-T_B)(1-T_C)} \tag{3.29}$$

Since the fission barrier is complex, there is a non-zero absorption coefficient:

$$T_{\mathrm{abs}} = T_{\mathrm{dir}} \left(\frac{\mathrm{e}^{2\delta}}{T_{B(C)}} - \frac{1-T_{B(C)}}{T_{B(C)}} \mathrm{e}^{-2\delta} - 1 \right) \tag{3.30}$$

The dependence of the transmission coefficients on $EKJ\pi$ has not been shown explicitly in Eqs (3.28)–(3.30) for the sake of simplicity.

The total fission coefficient for a certain spin and parity as included in the statistical model of nuclear reactions is the sum of the contributions of all bands containing levels with the same spin and parity. As adopted in the present evaluations involving the full K-mixing approximation, the excitation of the internal degrees of freedom in the second well permits the nucleus to change its K value during the time associated with internal motions.

Formally, this behaviour is described by adding the absorption from different transition states irrespective of the associated K value into a quantity preserving spin and parity. Consequently, the term describing prompt indirect fission is given by the following equation:

$$T_{\text{ind}}(E^*KJ\pi) = \sum_{K''\leq J} T_{\text{abs}}(E^*K''J\pi)\frac{T_{B(C)}(E^*KJ\pi)}{\sum_{K''\leq J}[T_A(E^*K''J\pi)+T_{B(C)}(E^*K''J\pi)]} \tag{3.31}$$

The total fission coefficient for a specified spin and parity can be defined by the following equation:

$$T_f(EJ\pi) = \sum_{K\leq J} T_f(EKJ\pi) = T_{\text{dir}}(E^*J\pi) + T_{\text{abs}}(E^*J\pi)\frac{T_{B(C)}(E^*J\pi)}{T_A(E^*J\pi)+T_{B(C)}(E^*J\pi)} \tag{3.32}$$

and the total transmission coefficient across one hump is the sum of the contributions corresponding to the discrete and continuous parts of the transition state spectrum:

$$T_{A,B}(E^*J\pi) = \sum_{K\leq J} T_{A,B}(E^*KJ\pi) + \int_{E_c(A,B)}^{\infty} \frac{\rho_{A,B}(\varepsilon J\pi)\mathrm{d}\varepsilon}{1+\exp\left[-\dfrac{2\pi(E^*-V_{A,B}-\varepsilon)}{\hbar\omega_{A,B}}\right]} \tag{3.33}$$

When a triple humped barrier is modelled, the total direct transmission coefficient through the outer peaks is the sum of the transmission through the discrete barriers and the continuum above the equivalent barrier:

$$T_{BC}(E^*J\pi) = \sum_{K\leq J} T_{BC}(E^*KJ\pi) + \int_{E_c(\text{eq})}^{\infty} \frac{\rho_{\text{eq}}(\varepsilon J\pi)\mathrm{d}\varepsilon}{1+\exp\left[-\dfrac{2\pi(E^*-V_{\text{eq}}-\varepsilon)}{\hbar\omega_{\text{eq}}}\right]} \tag{3.34}$$

By increasing the excitation energy, the strength of the imaginary potential increases, the entire flux transmitted through the inner hump is absorbed in the isomeric well ($T_{\text{abs}} \rightarrow T_A$) and the direct transmission disappears ($T_{\text{dir}} \rightarrow 0$). Therefore, direct transmission is considered to occur only for sub-barrier excitation energies and through discrete channels as defined by the following equation:

$$T_{\text{dir}}(E^*J\pi) = \sum_{K\leq J} T_{\text{dir}}(E^*KJ\pi) \tag{3.35}$$

while absorption in the isomeric well occurs through all fission channels:

$$T_{\text{abs}}(E^*J\pi) = \sum_{K\leq J} T_{\text{abs}}(E^*KJ\pi) + \int_{E_{cA}}^{\infty} \frac{\rho_A(\varepsilon J\pi)\mathrm{d}\varepsilon}{1+\exp\left[-\dfrac{2\pi(E^*-V_A-\varepsilon)}{\hbar\omega_A}\right]} \tag{3.36}$$

3.3.5. Results and discussion: Neutron emission and fission cross-sections

3.3.5.1. Neutron emission

The ^{232}Th(n, f) fission cross-section is relatively small, and therefore is very sensitive to any change in the contribution of the other outgoing channels, especially neutron emission. Hence, the overall description of the

experimental data was a major constraint for the fission parameters. The direct interaction cross-sections and transmission coefficients for the incident and outgoing neutron channels on ^{232}Th were obtained in these calculations from the derived RIPL-608 dispersive coupled-channel optical model given in Refs [3.23, 3.24]. These same optical potential parameters of Soukhovitskii et al. [3.23] were also used for the transmission coefficients of the outgoing proton channel (RIPL-4608) because this potential describes both neutron and proton scattering simultaneously. The optical model potential RIPL-9600 as derived by Avrigeanu et al. [3.65] was employed for the inverse alpha channel.

Calculations of the neutron elastic and inelastic angular distributions on ^{232}Th were shown to be in excellent agreement with the available experimental data (see Fig. 2 of Ref. [3.23]). A comparison of the calculated neutron total cross-section with selected experimental data up to 200 MeV is shown in Fig. 3.11.

Another important quantity obtained from the optical model calculations is the total inelastic cross-section. A comparison of calculated inelastic cross-sections with available experimental data is shown in Fig. 3.12. Below ≈800 keV, the total inelastic cross-section is dominated by contributions of direct reaction cross-sections on the ground state rotational band calculated by the coupled channel method (CCM). On the other hand, the maximum of the total inelastic cross-section around 3 MeV is dominated by the equilibrium emission. Proper consideration of the width fluctuations is critical in order to achieve a good description of this emission channel. The excitation function of the first inelastic level is also shown in Fig. 3.12 (dashed curve), which coincides with the total inelastic cross-section up to about 200 keV. Agreement with experimental data is very good over the full energy range if three of the points measured by Smith [3.69] above 1 MeV are excluded, which are clearly outliers when compared with the other measurements as well as the calculated cross-sections.

The experimental data for the ^{232}Th(n, 2n) reaction have been measured in different laboratories [3.71–3.77]. The results calculated using the EMPIRE code are in good agreement with selected experimental data, as shown in

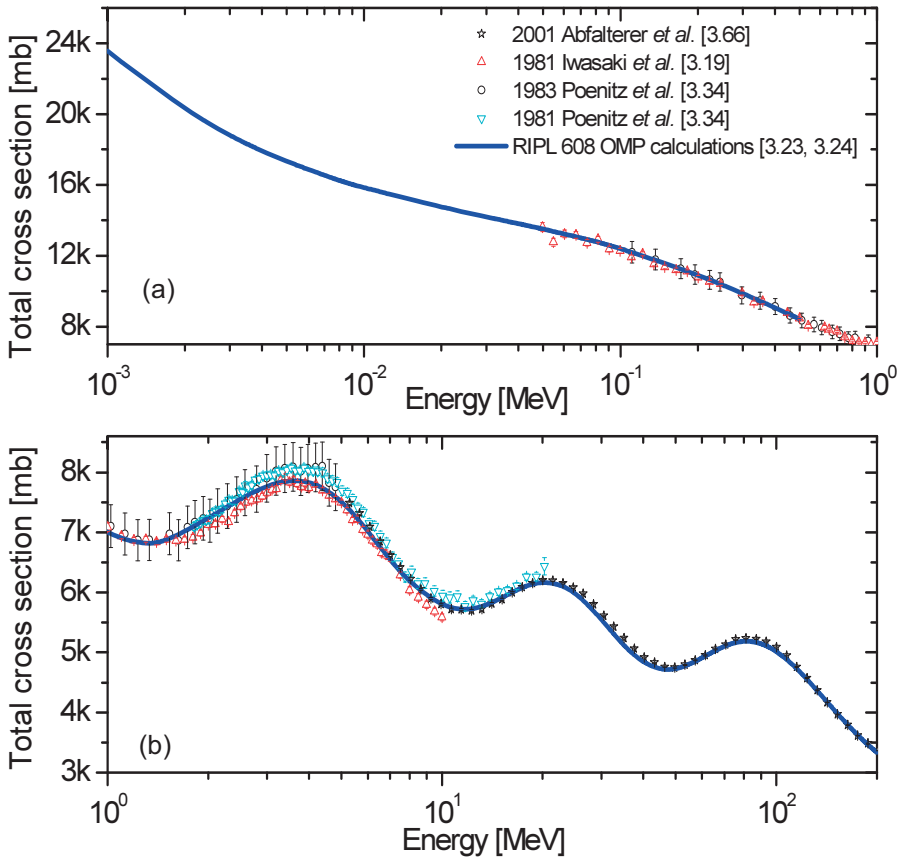

FIG. 3.11. Neutron total cross-sections for ^{232}Th at neutron energies from (a) 0.001 to 1 MeV and (b) 1 to 200 MeV.

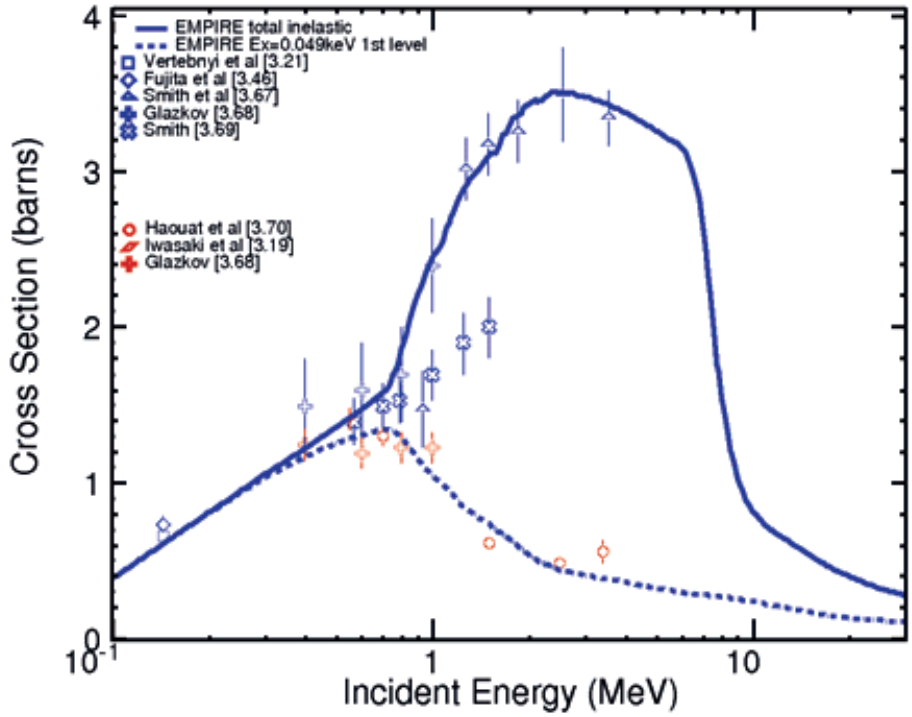

FIG. 3.12. Neutron inelastic cross-sections for ^{232}Th at neutron energies from 0.1 to 30 MeV.

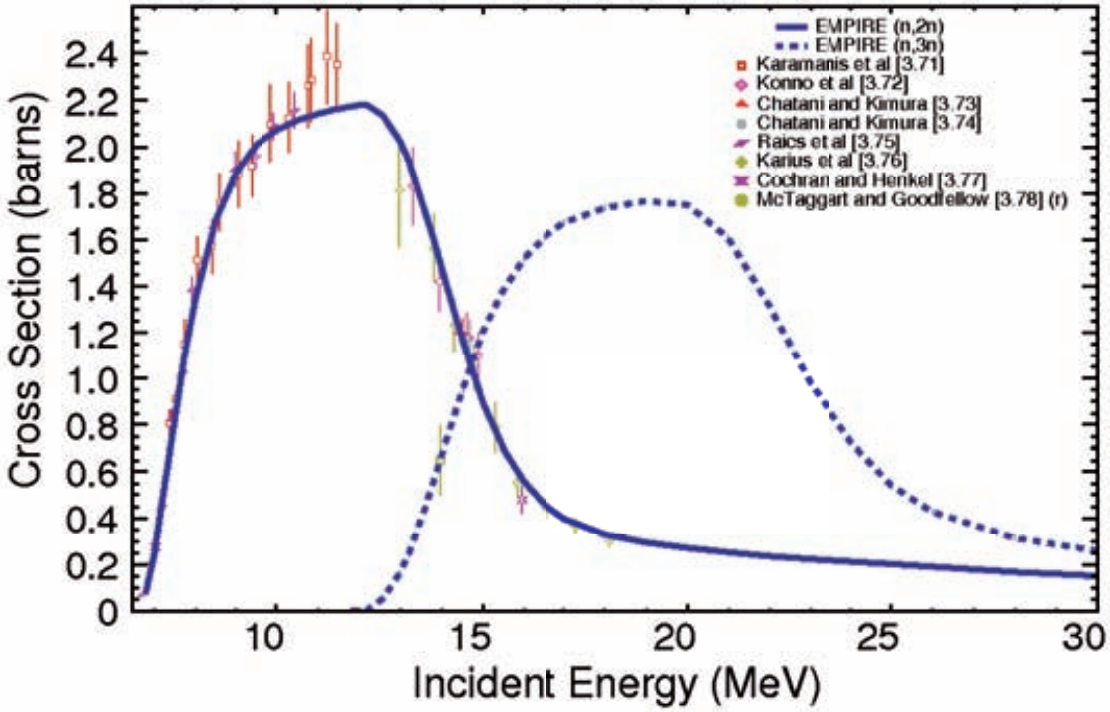

FIG. 3.13. Excitation function for ^{232}Th(n, 2n) and ^{232}Th(n, 3n) reactions up to 30 MeV.

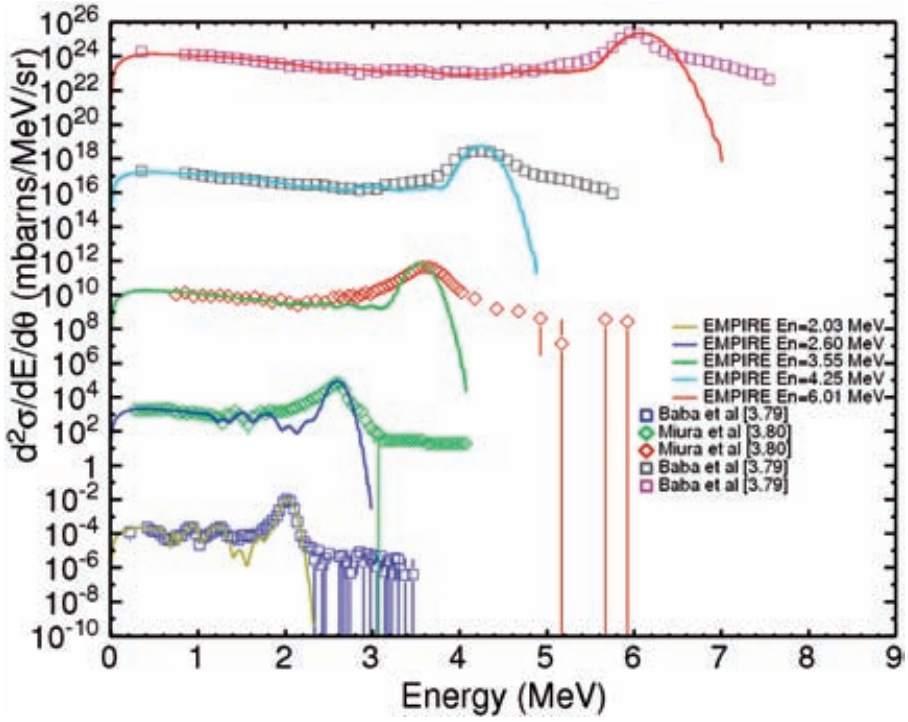

FIG. 3.14. Calculated double differential cross-sections for neutron emission (solid curves) at 30° compared with experimental data [3.79, 3.80] at 2.03, 2.60, 3.55, 4.25 and 6.01 MeV incident neutron energy: all the plots but the lowest are shifted by 10^7 units in the vertical axis for better visibility.

Fig. 3.13. A minor disagreement is observed in the region around the maximum where the EMPIRE calculations were not able to describe the two highest energy points measured by Karamanis et al. [3.71]. Several data sets for this reaction that showed discrepancies were discarded. Only one point at 14 MeV has been measured for the ^{232}Th(n, 3n) reaction by McTaggart and Goodfellow [3.78] relative to the quoted ^{232}Th(n, 2n) value of 1.2 ± 0.05 b (denoted as (r)) [3.78]. We used our evaluated (n, 2n) reaction to renormalize the McTaggart and Goodfellow measurement [3.78]. A derived (n, 3n) cross-section value for the reaction at 14.0 MeV is in excellent agreement with the EMPIRE calculation, as can be seen in Fig. 3.13.

A Japanese group led by Baba has measured double differential cross-sections of the neutron emission of thorium at eight incident neutron energies: 2.03, 2.60, 3.55, 4.25, 6.01, 11.9, 14.1 and 18 MeV [3.79–3.81]. Measured data include contributions from elastic and inelastic neutron scattering, multiple neutron emission and prompt fission neutrons. EMPIRE calculations at all incident energies and emission angles are in good agreement with the measured data. As an example of this agreement, the measured distributions at 30° for incident neutron energies lower than 7 MeV can be considered compared with theoretical calculations (Fig. 3.14). There is a small disagreement between the calculated results and the measured data in the elastic peak as the energy resolution used to broaden the calculated elastic cross-section does not always correspond to the experimental resolution. Additionally, the contribution of prompt fission neutrons to the experimental spectra can be seen in the form of the flat neutron background at emission energies higher than the corresponding incident energies: the calculated prompt fission neutron contribution was not included in Fig. 3.14. The lowest plot in Fig. 3.14 (corresponding to 2.03 MeV incident neutron energy) shows that the structure of the double differential cross-sections below the elastic peak is well reproduced and comes from the contributions of inelastic scattering cross-sections of 40 discrete levels of the target ^{232}Th nucleus included up to 1.4 MeV excitation energy.

Direct reaction cross-sections have been calculated in the present evaluation by the CCM for coupled levels of the ground state rotational band (0^+, 2^+, 4^+, 6^+ and 8^+) and by the distorted wave Born approximation (DWBA) theory for the remaining discrete levels up to 1.4 MeV. The ground state rotational band deformation parameters were adopted from the optical model fit [3.24], and were 0.213, 0.0660 and 0.0015 for the β_2, β_4 and β_6 parameters, respectively. Calculated direct cross-sections have been incoherently added to the statistical cross-sections.

Following the suggestions of Young et al. [3.81], consideration was taken of the DWBA direct cross-section contributions arising from the inelastic neutron scattering on quasi-discrete levels embedded into the continuum up to excitation energies of approximately 10 MeV. The calculated cross-section for each of those quasi-discrete levels is smeared by a Gaussian function with an energy resolution of 50 keV. Dynamic deformations for the DWBA calculations were fitted to adjust the emission spectra, and were based on the corresponding energy weighted sum rules. All the discrete and quasi-discrete levels (80) of the ^{232}Th nucleus considered are listed in Table 3.6, including the level number N_{lev}, excitation energy E_x, J, π and the corresponding dynamical deformation used in the DWBA cross-section calculation for each level. The energy continuum started at E_x = 1.4 MeV, and therefore all the levels below this energy were treated as discrete levels in the calculations; levels above this energy were considered as quasi-discrete. The level number also contains information about whether DWBA or CCM was used: namely, all levels with numbers greater than 20 were calculated by the DWBA method.

A recent publication by Wienke et al. [3.82] provides strong arguments justifying the inclusion in the evaluation of quasi-discrete levels embedded into the continuum. Such a contribution is numerically equivalent to the multi-step direct (MSD) quantum mechanical calculation of the cross-section to the continuum for a deformed nucleus (see Fig. 1 of Ref. [3.82] — the ENDF/B-VII results in the right hand column correspond to this evaluation compared with the MSD results in the left hand column).

The empirical inclusion of DWBA calculations to treat the scattering into the continuum allowed for an excellent description of the hard part of the neutron emission spectra starting at low neutron incident energies, where the contribution of the pre-equilibrium mechanism is still very small. This statement is validated in Fig. 3.15, in which measurements at 30° of double differential cross-sections of the neutron emission of thorium for 6.02 MeV neutron incident energy [3.79] are compared with two different sets of EMPIRE calculations: consideration of the CCM and DWBA contributions (solid curve: current evaluation) and inclusion of only the CCM contribution from the ground state rotational band (dashed curve). The DWBA contribution of the neutron scattering on discrete and quasi-discrete levels is clearly seen from the difference between the two curves from 2.5 to 5 MeV neutron emission energies.

There is a remaining discrepancy between the experimental data and this evaluation (solid curve) around a neutron emission energy of 5.3 MeV. This difference is related to the DWBA treatment of beta and gamma rotational band-heads in the target nucleus. Such levels are strongly excited in neutron scattering, especially the octupole rotational band-head at 0.7 MeV excitation energy (≈6–0.7 = 5.3 MeV emission energy). A full treatment of band-head excitation requires a coupled channel calculation, including the ground state rotational band coupled

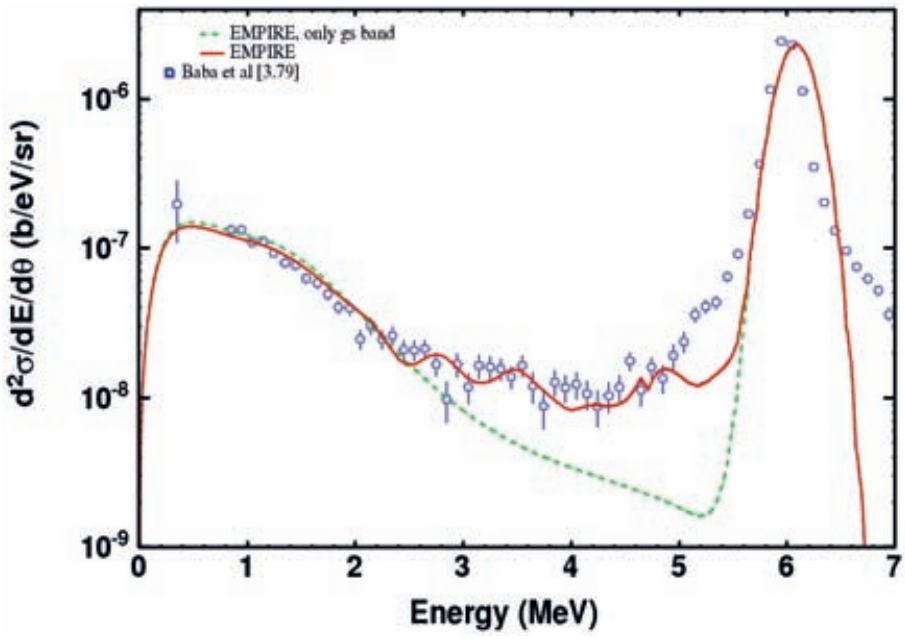

FIG. 3.15. Measured double differential cross-sections of neutron emission at 30° and 6.01 MeV incident neutron energy [3.79] compared with EMPIRE calculations: the solid curve corresponds to the full evaluation (see text); the dashed curve includes only the direct contribution from the five coupled levels (0^+, 2^+, 4^+, 6^+ and 8^+) of the ground state rotational band.

TABLE 3.6. DISCRETE AND QUASI-DISCRETE LEVELS OF ^{232}Th AND DEFORMATION PARAMETERS FOR DWBA CALCULATIONS

N_{lev}	E_x (MeV)	J	π	Dyn. def.	N_{lev}	E_x (MeV)	J	π	Dyn. def.
1	0.0000	0	+	(gs band)	41	1.0729	2	+	0.0130
2	0.0494	2	+	(gs band)	42	1.0775	1	–	0.0130
3	0.1621	4	+	(gs band)	43	1.0787	0	+	0.0130
4	0.3322	6	+	(gs band)	44	1.0944	3	–	0.0130
5	0.5560	8	+	(gs band)	45	1.1057	3	–	0.0120
25	0.5569	8	+	0.0090	46	1.1218	2	+	0.0120
26	0.7143	1	–	0.0133	47	1.1371	12	+	0.2152
27	0.7304	0	+	0.0180	48	1.1433	4	–	0.0170
28	0.7741	2	+	0.0130	49	1.1460	7	+	0.0200
29	0.7744	3	–	0.0123	50	1.1483	4	+	0.0170
30	0.7853	2	+	0.0160	51	1.1825	3	–	0.0170
31	0.8270	10	+	0.0252	52	1.2089	5	–	0.0260
32	0.8296	3	+	0.0180	53	1.2181	4	–	0.0330
33	0.8730	4	+	0.0200	54	1.2221	8	+	0.0350
34	0.8836	5	–	0.0113	55	1.2496	9	–	0.0350
35	0.8901	4	+	0.0200	56	1.2587	8	+	0.0330
36	0.9604	5	+	0.0200	57	1.2932	2	+	0.0210
37	1.0231	6	+	0.0200	58	1.3294	6	+	0.0250
38	1.0429	7	–	0.0155	59	1.3700	6	+	0.0250
39	1.0499	6	+	0.0140	60	1.3872	6	+	0.0250
40	1.0536	2	+	0.0130					

QUASI-DISCRETE LEVELS EMBEDDED INTO THE CONTINUUM

N_{lev}	E_x (MeV)	J	π	Dyn. def.	N_{lev}	E_x (MeV)	J	π	Dyn. def.
61	1.4140	2	+	0.020	81	4.6160	4	+	0.036
62	1.5290	3	–	0.022	82	4.8160	4	+	0.035
63	1.6500	2	+	0.025	83	5.0160	4	+	0.044
64	1.7800	3	–	0.030	84	5.2160	4	+	0.046
65	1.8800	4	+	0.034	85	5.4160	2	+	0.030
66	2.0800	3	–	0.032	86	5.6160	4	+	0.045
67	2.2500	4	+	0.034	87	5.8160	4	+	0.046
68	2.4000	3	–	0.032	88	6.0160	3	–	0.045
69	2.5060	2	+	0.031	89	6.3160	2	+	0.030
70	2.5560	3	–	0.035	90	6.6160	3	–	0.042
71	2.6960	2	+	0.027	91	6.9160	4	+	0.042
72	2.8960	4	+	0.035	92	7.2160	2	+	0.030
73	3.0960	3	–	0.030	93	7.5160	3	–	0.042
74	3.1960	4	+	0.035	94	7.8160	4	+	0.042
75	3.2960	4	+	0.035	95	8.1160	2	+	0.030
76	3.3960	4	+	0.033	96	8.2560	4	+	0.042
77	3.8960	2	+	0.027	97	8.6560	2	+	0.032

TABLE 3.6. DISCRETE AND QUASI-DISCRETE LEVELS OF ^{232}Th AND DEFORMATION PARAMETERS FOR DWBA CALCULATIONS (cont.)

N_{lev}	E_x (MeV)	J	π	Dyn. def.	N_{lev}	E_x (MeV)	J	π	Dyn. def.
78	4.0160	4	+	0.034	98	9.0060	3	–	0.042
79	4.2160	4	+	0.033	99	9.5060	2	+	0.030
80	4.4160	2	+	0.028					

to the beta and gamma band-heads as suggested by Maslov [3.52]. Such an improvement is warranted in future updates.

EMPIRE calculations at incident neutron energies higher than 10 MeV for double differential neutron emission cross-sections both at forward (30°) and at backward (120°) emission angles are shown in Fig. 3.16. Higher neutron incident energies increase the anisotropy of distributions, but the agreement between experimental data and EMPIRE calculations is still very good. Discrepancies that can be seen below the 5 MeV emission energy for the 14.1 and 18 MeV data disappear when the prompt fission neutron spectra are added to the theoretical calculations.

3.3.5.2. Fission cross-sections

Over the energy range from 0.001 to 60 MeV, the total fission cross-section for the nuclei under study is the sum of the cross-sections of the following processes: (n, *xnf*), (n, p*xnf*) and (n, *αxnf*), where *x* extends from 0 to 8 over the energy range considered. The optical model for fission and the complex triple humped fission barrier have been considered for first chance fission. Double humped barriers have been used, and complete damping has been assumed for the other fission chances.

The main ingredients of the fission model are the fission barrier parameters consisting of the heights and widths of the parabolas describing the fundamental barriers, the discrete transition states at saddle points and intermediate wells, and the level densities at saddle points. These parameters have been empirically determined from an analysis of the measured fission cross-sections, considering the values reported in the literature and assessing the overall fit of the available experimental data for competing channels.

Attention was focused on first chance fission, not only because of the important contribution of this process to the total fission cross-section but also in order to test the capability of the optical model to describe the resonant structure. A minimum number of input parameters should be adopted for evaluation purposes, but these inputs need to be sophisticated enough to describe the experimental data with the accuracy required for applications. Therefore, we concentrated on reproducing the gross vibrational resonant structure of the fission cross-section for first chance fission, without attempting to describe the fine structure related to the rotational levels.

The analysis of the experimental data for the ^{232}Th first chance fission cross-section reveals the following features (Figs 3.17 and 3.18):

(a) Resonant structure is noted above the fission threshold, indicating the existence of a third shallow well that accommodates undamped hyperdeformed vibrational states.
(b) The first change of slope is observed around a neutron incident energy of 1.1 MeV, suggesting a height of the inner barrier of 5.9 ± 0.2 MeV (the neutron separation energy in ^{233}Th is 4.78 MeV).
(c) Wide resonances appear below 1.1 MeV, which could be associated with partially damped vibrational states in the second well.
(d) The fission threshold around the neutron incident energy of 1.5 MeV suggests a height of the outer barriers of 6.3 ± 0.2 MeV.
(e) The positions of the resonances is assumed to be related to class II and III states (Fig. 3.18), with a smooth rise between them (from 1.1 to 1.5 MeV) indicating that there is no overlap between the excitation energy ranges of the vibrational states in the two wells.

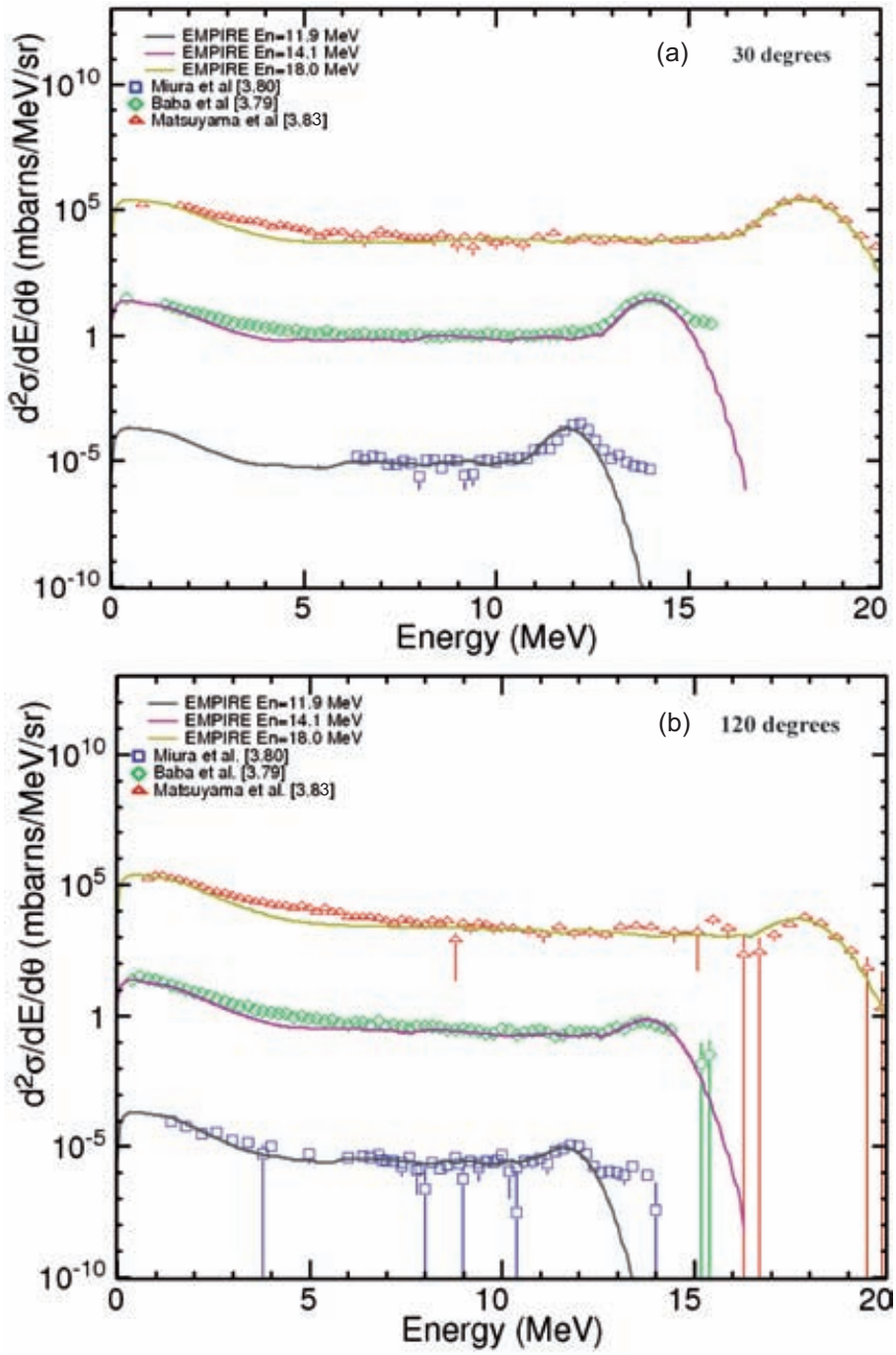

FIG. 3.16. Calculated double differential cross-sections of neutron emission (solid lines) at (a) 30° and (b) 120° compared with experimental data at 11.9 [3.80], 14.1 [3.79] and 18 MeV [3.83] incident neutron energy: all the plots but the lowest in each panel are shifted by 10^5 units along the vertical axis for better visibility.

The best description of the experimental data was obtained by using fission barrier parameters in agreement with these assumptions. Inner barrier parameters (V_A = 5.82 MeV, $\hbar\omega_A$ = 1.00 MeV) are supported by some recent calculations [3.84] and differ from earlier predictions [3.54, 3.85], indicating a lower and wider inner hump. The parameters for the second well were deduced from the position of the wide resonances at low energies related to class II vibrational states: experimental data are scarce in this energy range, so values have been adopted that are typical for actinides: V_{II} = 2.12 MeV for the depth (defined with respect to the ground state) and $\hbar\omega_{II}$ = 1.00 MeV for the width. The heights of the second and third humps were defined as V_B = 6.23 MeV and V_C = 6.45 MeV, while their widths were deduced from the slope of the fission barrier at excitation energies above the inner barrier ($\hbar\omega_{B,C}$ = 1.30 MeV).

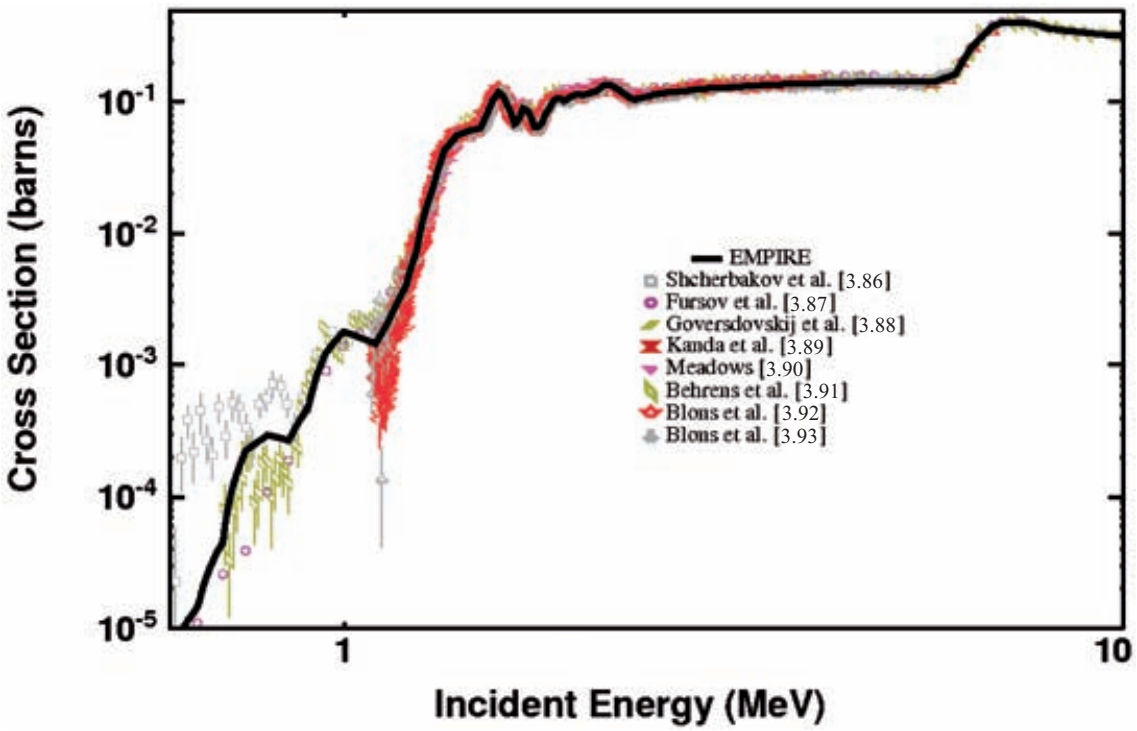

FIG. 3.17. The neutron induced fission cross-section of ^{232}Th up to 10 MeV.

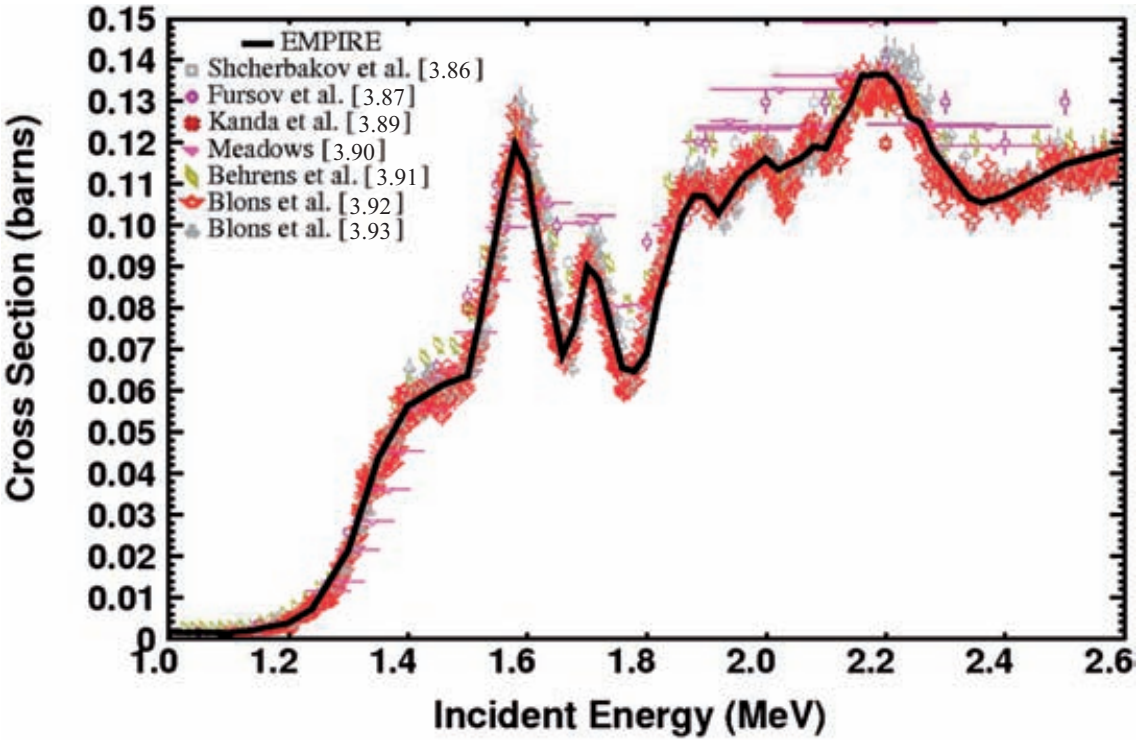

FIG. 3.18. The neutron induced fission cross-section of ^{232}Th near the fission threshold.

The parameters for the third well are controversial: early calculations predicted a shallow well with a depth of 0.2–0.5 MeV for the accommodation of undamped class III vibrational states, but more recent theoretical [3.85] and experimental [3.94] studies (albeit focused on even–even fissioning nuclei) support a much deeper well of up to 3 MeV, which may require partial damping. However, independent of the depth of the third well, it is expected that class III resonances should be less damped than class II resonances — the main microscopic source of damping is the coupling to class I compound states, which is much less likely in the third well, where the nucleus is reflection asymmetric and more strongly elongated than in the second well, where the nucleus is reflection symmetric and less deformed and therefore closer to the characteristics of the first well where class I states are excited. While the present formalism does not allow for the damping of class III vibrational states and might have an impact on the shape, the positions of the resonances will not be affected. These calculations show that a deep third well gives rise to a resonant structure (especially at energies below the threshold), while a shallower well produces resonances in the plateau region.

Measured fission cross-sections indicate a rather shallow third well, although resonances below 1.1 MeV could also be related to partially damped class III vibrational states in a deeper third well. The best description of the data was obtained using a depth of approximately 0.7 MeV (V_{III} = 5.65 MeV) and width $\hbar\omega_{III}$ = 1.00 MeV. Under these conditions, the bottom of the third well is close to the top of the first hump, indicating that the positions of the class III vibrational states correspond to excitation energies for which the class II vibrational states are almost completely damped. Therefore, there is no interference among the resonances due to the states in the two wells, confirming our initial hypothesis.

The parameters of the barriers associated with the discrete transition states have mainly been deduced from a fitting procedure and consideration of the asymmetry of the third well. Very similar widths to those of the fundamental barrier have been used, and the strength of the imaginary potential in the isomeric well was chosen to fit the width of the resonances at sub-barrier energies (0.8 and 1.0 MeV, see Fig. 3.17) and to ensure complete damping close to the top of the inner barrier. The contribution of the continuum to the fission coefficients is calculated using an equivalent double humped fission barrier, of which the outer barrier parameters are V_{eq} = 6.35 MeV and $\hbar\omega_{eq}$ = 0.60 MeV.

Fission competes with radiative capture and with elastic and inelastic scattering in the energy region from 0.8 to 1 MeV. The largest influence comes from inelastic scattering (Fig. 3.12) and depends on the reaction mechanism. Direct inelastic scattering affects the entire range above the threshold, while compound inelastic scattering and the level density of the residual influences mainly the second half of the plateau, and pre-equilibrium emission has a role only above 5 MeV.

As demonstrated in Figs 3.17 and 3.18, the optical model for fission with the barrier parameters discussed above provides a very good description of the available experimental data for first chance fission of ^{232}Th.

The next three fission chances were modelled for fission and a complex triple humped fission barrier. As mentioned at the beginning of this section, double humped barriers have been used for the other chances, and complete damping was assumed.

After fixing first chance fission and the (n, 2n) cross-section, ^{232}Th fission barrier parameters were deduced mainly from an analysis of the experimental data. They agree with the parameters used in Ref. [3.95] to describe photon induced fission on ^{232}Th. A similar procedure was applied in treating third chance fission. The starting values for the fission barrier parameters for ^{231}Th were those of ^{233}Th, adjusted slightly to describe the fission, (n, 2n) and (n, 3n) experimental data. Final values are in agreement with those deduced from fitting neutron induced fission on ^{231}Th [3.95].

The thresholds of the higher chance fissions are visible in the profile of the fission experimental data (Fig. 3.19), and provide information about the highest hump. All of the other parameters for barriers and level densities are deduced from the fit and constraints imposed by systematics. Above 35–40 MeV, the contribution of (n, p*x*n*f*) processes becomes visible, while the contribution of (n, α*x*n*f*) remains very small in the whole energy range below 60 MeV.

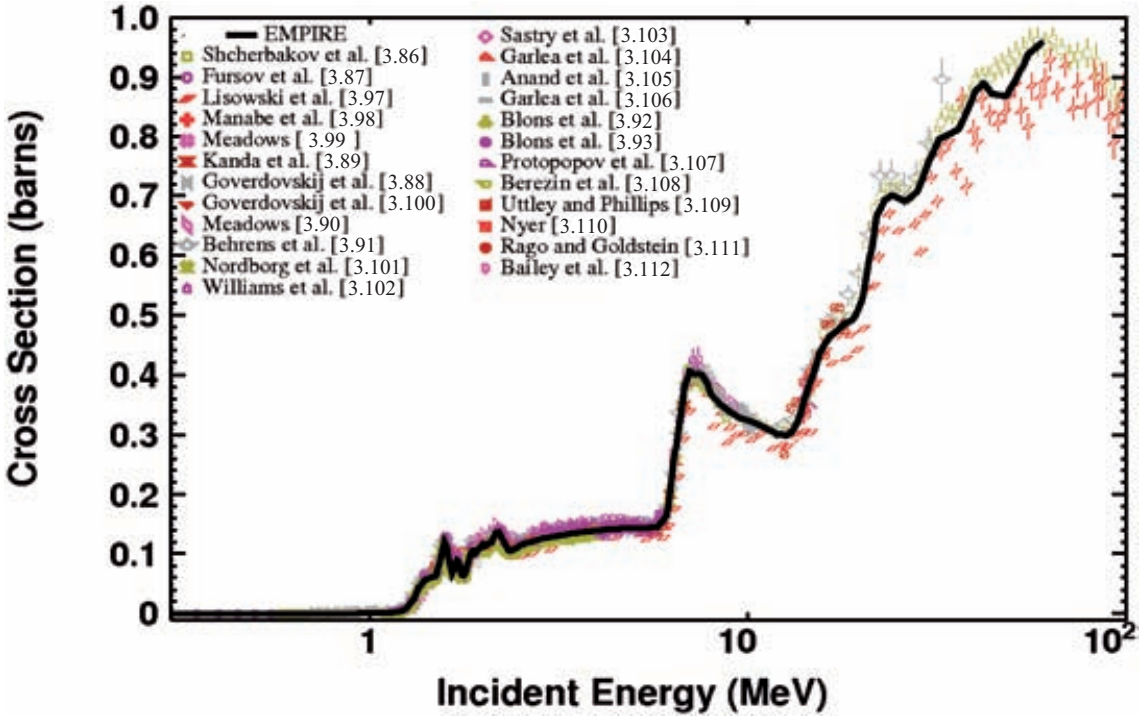

FIG. 3.19. Neutron induced fission cross-section of ^{232}Th: multiple chance fission. Fission cross-sections measured as a ratio to ^{235}U(n, f) are listed in the left hand column and those directly measured are listed in the right hand column.

3.3.5.3. Fission spectra and average number of neutrons per fission

The prompt neutron fission spectrum was obtained directly using the EMPIRE code. The spectra of neutrons emitted from the fission fragments were based on the empirical parameterization proposed by Kornilov et al. [3.96]. The emissive contribution of (n, *x*n*f*) neutrons in second and higher chance fission were calculated using the EMPIRE neutron (n, *x*n) spectra, which include direct and pre-equilibrium components. Because of these contributions, the fission spectra became anisotropic and were coded in File-6 format in ENDF terminology, which allows storage of such data without loss of information.

The delayed neutron data were not evaluated. They were adopted from the BROND-3 evaluation.

The average number of prompt and delayed neutrons per fission (nubar) was adopted from the BROND-3 evaluation, which is based on a careful analysis of all available experimental data and includes the covariances for the total number of neutrons per fission.

3.3.6. Covariance matrices

The covariance matrices were generated by the Monte Carlo technique within the EMPIRE code, according to the procedure proposed by Smith [3.113]. Calculated covariances were used as a prior in a subsequent analysis introducing experimental data by the generalized least squares method as implemented in the GANDR system [3.114]. An example of the prior uncertainty for the first discrete-level inelastic cross-section (MF3, MT51 in ENDF notation) is shown in Fig. 3.20: the resulting data exhibit a large uncertainty, which is greatly constrained when experimental data are introduced.

GANDR generates covariance matrices on a fixed energy grid, including cross-covariances between different reaction channels. The selected experimental data used in the analysis were normally taken from the EXFOR database. The EXFOR entries, authors and years of publication are given in Tables 3.7–3.10 for the total, fission, (n, 2n) and radiative capture, respectively.

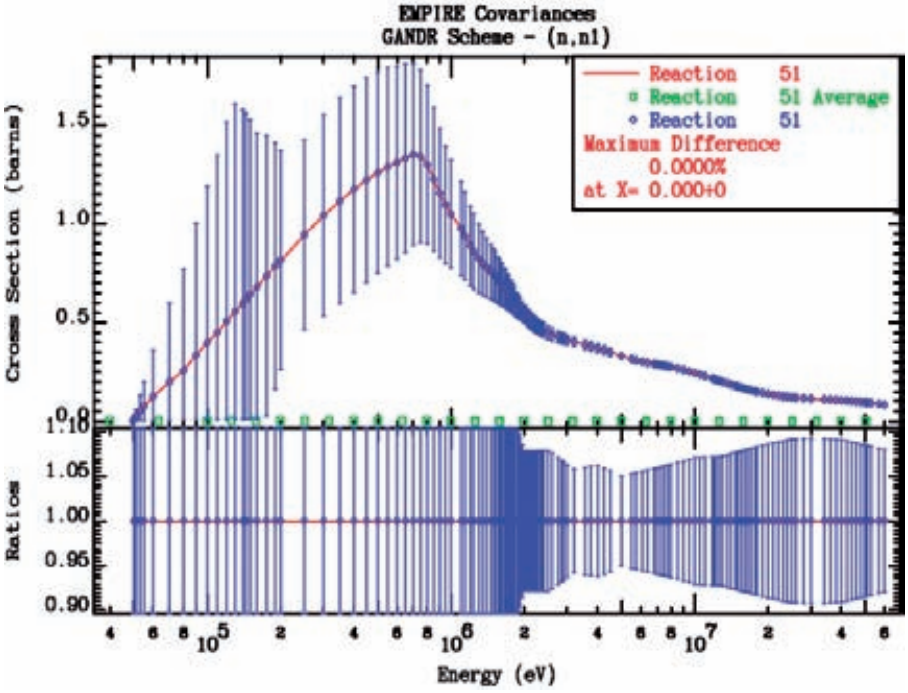

FIG. 3.20. Example of the uncertainty in the prior for the first discrete-level inelastic cross-section.

TABLE 3.7. EXPERIMENTAL DATA USED IN THE FITTING OF TOTAL CROSS-SECTIONS

EXFOR entry	Authors	Year
21088003	Uttley et al. [3.17]	1966
21766002	Iwasaki et al. [3.19]	1981
10935004	Poenitz et al. [3.34]	1981
12853052	Poenitz et al. [3.34]	1983
10047094	Foster and Glasgow [3.115]	1971
13753029	Abfalterer et al. [3.66]	2001

TABLE 3.8. EXPERIMENTAL DATA USED IN THE FITTING OF THE FISSION CROSS-SECTION

EXFOR entry	Authors	Year	Comment
41430006	Shcherbakov et al. [3.86]	2001	Ratio
31424002	Sastry et al. [3.103]	1992	
31459025	Garlea et al. [3.104]	1992	
41111002	Fursov et al. [3.87]	1991	Ratio
14176002	Lisowski et al. [3.97]	1988	Ratio
40888002	Goverdovskij et al. [3.88]	1986	Ratio
22014002	Kanda et al. [3.89]	1985	Ratio
30813007	Garlea et al. [3.106]	1984	
10843003	Meadows [3.90]	1983	Ratio
10658002	Behrens et al. [3.91]	1982	Ratio
20796002	Blons et al. [3.93]	1975	

TABLE 3.9. EXPERIMENTAL DATA USED IN THE FITTING OF THE (n, 2n) CROSS-SECTIONS

EXFOR entry	Authors	Year
22845002	Karamanis et al. [3.71]	2003
22637089	Konno et al. [3.72]	1993
22235002	Chatani and Kimura [3.73]	1992
22203002	Chatani and Kimura [3.74]	1991
30816002	Raics et al. [3.75]	1985
20499003	Karius et al. [3.76]	1979
12305002	Cochran and Henkel [3.77]	1958

TABLE 3.10. EXPERIMENTAL DATA USED IN THE FITTING OF THE RADIATIVE CAPTURE CROSS-SECTIONS

EXFOR entry	Authors	Year
20871002	Kobayashi et al. [3.27]	1979
10554003	Macklin and Halperin [3.29]	1977
22931002	Aerts et al. [3.31, 3.32]	2006
22875002	Borella et al. [3.30]	2004
22654003	Wisshak et al. [3.25]	2001
10735002	Poenitz and Smith [3.20]	1978
22663002	Karamanis et al. [3.116]	2001
41183003	Davletshin et al. [3.117]	1993

Although the uncertainties are quoted as total, a systematic uncertainty of 1% was acknowledged by Abfalterer et al. [3.66]. By analogy, the same systematic uncertainty is adopted for all measurements. Furthermore, a fully correlated uncertainty of 0.2% was assumed between all measurements.

Since practically all measurements were defined as ratios to a chosen standard, a fully correlated uncertainty of 2% was added to all the resulting data.

Examples of the covariance matrices are presented in Fig. 3.21. The uncertainty of the fission cross-section decreases as the absolute magnitude of the cross-section increases above the pseudo-threshold. The uncertainty above the pseudo-threshold is strongly correlated, which implies that the shape of the cross-section is known fairly well, although the absolute cross-section has an uncertainty of about 2%. The uncertainty of the capture cross-section above the RRR up to about 300 keV is also approximately 2%. Both of these evaluated uncertainties are consistent with the uncertainty estimated by Ignatyuk [3.118].

The uncertainty of the two-neutron emission cross-sections (represented by MT851 in the ENDF file and in Fig. 3.21) resulting from the least squares analysis is about 2%, compared with the uncertainty of 5% estimated by Ignatyuk [3.118]. The uncertainty of the inelastic cross-section is about 5–10% at energies where the cross-section is significant. A reduction in the uncertainty occurs compared with the prior, even although no measured inelastic cross-section data were available for the least squares fitting. This reduction in the uncertainties comes from the correlations in the prior with other reactions, and originates from the physical constraints imposed by the nuclear models.

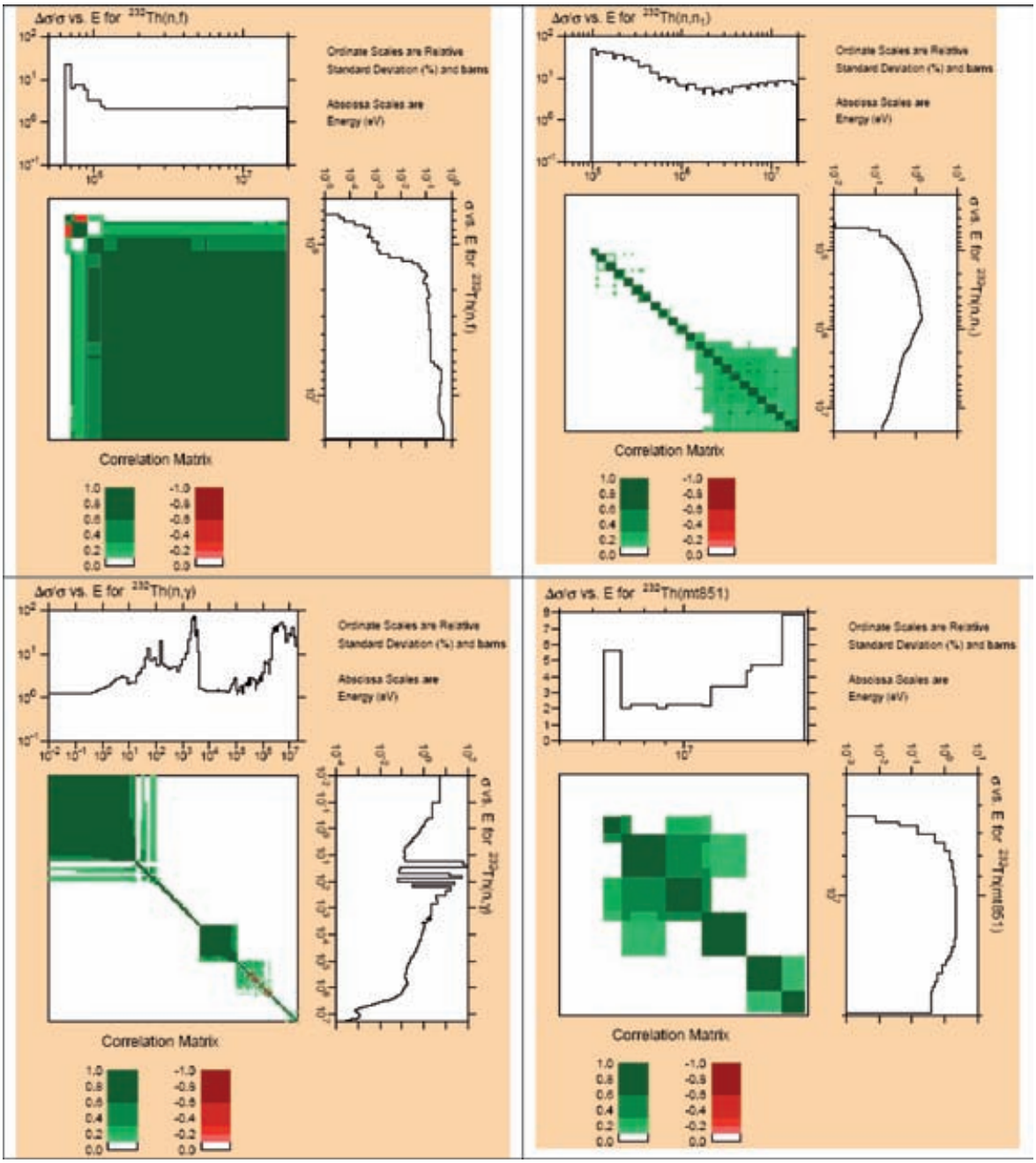

FIG. 3.21. Examples of covariance matrices for the fission, inelastic, radiative capture and two-neutron emission (label mt851) cross-sections.

REFERENCES TO SECTION 3

[3.1] OLSEN, D.K., INGLE, R.W., Measurement of Neutron-Transmission Spectra through ^{232}Th from 8 MeV to 4 keV, Rep. ORNL/TM-7661 (ENDF-307), Oak Ridge Natl Lab., TN (1981).

[3.2] SCHILLEBEECKX, P., Institute for Reference Materials and Measurements, Geel, Belgium, personal communication, 2005.

[3.3] GUNSING, F., Commissariat à l'énergie atomique, Centre de Saclay, Gif-sur-Yvette, France, personal communication, 2005.

[3.4] CHRIEN, R.E., LIOU, H.I., KENNY, M.J., STELTS, M.L., Neutron cross sections of thorium-232, Nucl. Sci. Eng. **72** (1979) 202–215.
[3.5] LUNDGREN, G., A study of the energy dependence of the Th-232 capture cross section in the energy range 0.1 to 3.4 eV, Nukleonik **11** (1968) 61–67.
[3.6] TRKOV, A., Jožef Stefan Institute, Ljubljana, Slovenia, personal communication, 2005.
[3.7] OLSEN, D.K., An Evaluation of the Resolved-Resonance-Region Cross Sections of ^{232}Th, Rep. ORNL/TM-8056 (ENDF-319), Oak Ridge Natl Lab., TN (1981).
[3.8] PELLONI, S., YOUINOU, G., WYDLER, P., "Impact of different nuclear data on the performance of fast spectrum systems based on the thorium–uranium fuel cycle", Nuclear Data for Science and Technology (Proc. Int. Conf. Trieste, 1997), Vol. 59, Part II (REFFO, G., VENTURA, A., GRANDI, C., Eds), Italian Physical Society, Bologna (1997) 1172–1176.
[3.9] CHENG, E.T., MATHEWS, R.D., "The influence of nuclear data on thorium fusion–fission hybrid blanket nucleonic performance", Nuclear Cross Sections for Technology (Proc. Int. Conf. Knoxville, 1979), Rep. NBS–SP 594 (FOWLER, J.L., JOHNSON, C.H., BOWMAN, C.D., Eds), United States Department of Commerce, Washington, DC (1980) 834–838.
[3.10] BARTINE, D.E., "The use of thorium in fast breeder reactors", ibid., pp. 119–121.
[3.11] SALVATORES, M., "Experimental facilities, training and expertise in the nuclear data field: Needs and gaps for reactor physics applications", Nuclear Data for Science and Technology (Proc. Int. Conf. Trieste, 1997), Vol. 59, Part I (REFFO, G., VENTURA, A., GRANDI, C., Eds), Italian Physical Society, Bologna (1997) 3–17.
[3.12] MASLOV, V.M., et al., Neutron Data Evaluation of ^{232}Th, Rep. INDC(BLR)-016, IAEA, Vienna (2003).
MASLOV, V.M., PORODZINSKIJ, Yu.V., BABA, M., HASEGAWA, A., Neutron capture cross section of ^{232}Th, Nucl. Sci. Eng. **143** (2003) 177–187.
[3.13] DE SAUSSURE, G., MACKLIN, R.L., Evaluation of the ^{232}Th Neutron Capture Cross Section above 3 keV, Rep. ORNL/TM-6161, Oak Ridge Natl Lab., TN (1977).
[3.14] MEADOWS, J., et al., Evaluated Nuclear Data File of Th-232, Rep. ANL/NDM–35, Argonne Natl Lab., IL (1978).
[3.15] OHSAWA, T., OHTA, M., Neutron nuclear data evaluation for thorium-232, J. Nucl. Sci. Technol. **18** (1981) 408–426.
[3.16] OHSAWA, T., INOUE, M., "Nuclear data evaluation of actinides relevant to thorium fuel cycle", Nuclear Data for Science and Technology (Proc. Int. Conf. Mito, 1988), (IGARASI, S., Ed.), Saikon, Tokyo (1988) 565–569.
[3.17] UTTLEY, C.A., NEWSTEAD, C.M., DIMENT, K.M., "Neutron strength function measurements in the medium and heavy nuclei", Nuclear Data for Reactors (Proc. Conf. Paris, 1966), Vol. 1, IAEA, Vienna (1967) 165–174.
[3.18] KOBAYASHI, K., FUJITA, Y., OOSAKI, T., BLOCK, R.C., Neutron total cross-section measurement of thorium near 24 keV with an iron-filtered neutron beam, Nucl. Sci. Eng. **65** (1978) 347–353.
[3.19] IWASAKI, T., et al., "Measurements of neutron total cross section for Th-232", Fast Neutron Scattering on Actinide Nuclei (Proc. Specialists' Mtg Paris, 1981), Rep. NEANDC(J)-75, Organisation for Economic Co-operation and Development, Paris (1981).
[3.20] POENITZ, W.P., SMITH, D.L., Fast Neutron Radiative Capture Cross Section of ^{232}Th, Rep. ANL/NDM-42, Argonne Natl Lab., IL (1978).
[3.21] VERTEBNYJ, V.P., MURZIN, A.V., PSHENICHNYJ, V.A., LITVINSKIJ, L.L., PAK, En Men, "Medium and thermal neutron beams and their use", Properties of Neutron Sources (Proc. Adv. Group Mtg Leningrad, 1986), IAEA-TECDOC-410, IAEA, Vienna (1987) 257–270.
[3.22] GRIGOR'EV, Yu.V., et al., Investigation of neutron cross-section for ^{232}Th and ^{237}Np in energy range 2 eV–100 keV, Yad. Konst. **1** (1998) 9–16.
[3.23] SOUKHOVITSKII, E.Sh., CAPOTE, R., QUESADA, J.M., CHIBA, S., Dispersive coupled-channel analysis of nucleon scattering for ^{232}Th up to 200 MeV, Phys. Rev. C **72** (2005) 024604.
[3.24] CAPOTE, R., IAEA, Vienna, personal communication.
[3.25] WISSHAK, K., VOSS, F., KÄPPELER, F., Neutron capture cross section of ^{232}Th, Nucl. Sci. Eng. **137** (2001) 183–193.
[3.26] MACKLIN, R.L., WINTERS, R.R., Stable isotope capture cross sections from the Oak Ridge electron linear accelerator, Nucl. Sci. Eng. **78** (1981) 110–112.
MACKLIN, R.L., Thorium resonance neutron capture (2.6 to 10 keV), Nucl. Sci. Eng. **79** (1981) 118–122.
[3.27] KOBAYASHI, K., FUJITA, Y., YAMAMURO, N., Measurement of neutron capture cross section of thorium-232 from 1 keV to 480 keV, J. Nucl. Sci. Technol. **18** (1981) 823–834.
KOBAYASHI, K., FUJITA, Y., YAMAMURO, N., Kyoto Univ., personal communication, 1979.
[3.28] HAN, Y., SHEN, Q., ZHANG, J., ZHANG, Z., Calculation and analysis of n + ^{232}Th reaction cross sections, Nucl. Sci. Eng. **143** (2003) 202–210.
[3.29] MACKLIN, R.L., HALPERIN, J., ^{232}Th(n, γ) cross section from 2.6 to 800 keV, Nucl. Sci. Eng. **64** (1977) 849–858.
[3.30] BORELLA, A., et al., Determination of the ^{232}Th (n, γ) cross section from 4 to 140 keV at GELINA, Nucl. Sci. Eng. **152** (2006) 1–14.
[3.31] AERTS, G., et al., Neutron capture cross section of ^{232}Th measured at the n_TOF facility at CERN in the unresolved resonance region up to 1 MeV, Phys. Rev. C **73** (2006) 054610.
AERTS, G., et al., "Measurement of the ^{232}Th neutron capture cross section at the CERN n_TOF facility", Nuclear Data for Science and Technology (Proc. Int. Conf. Santa Fe, 2004), AIP Conf. Proc. **769** Part 2 (2005) 1470–1473.

[3.32] AERTS, G., "Mesure de la section efficace de capture neutronique du Th-232 à n_TOF au CERN", Thèse-09/05, Rep. DAPNIA-05-12-T, CERN, Geneva (2005).
[3.33] BORELLA, A., AERTS, G., GUNSING, F., MOXON, M., SCHILLEBEECKX, P., The use of C_6D_6 detectors for neutron induced capture cross-section measurements in the resonance region, Nucl. Instrum. Methods Phys. Res. A **577** (2007) 626–640.
[3.34] POENITZ, W.P., WHALEN, J.F., SMITH, A.B., Total neutron cross sections of heavy nuclei, Nucl. Sci. Eng. **78** (1981) 333–341.
POENITZ, W.P., WHALEN, J.F., Neutron Total Cross Section Measurements in the Energy Range from 47 keV to 20 MeV, Rep. ANL/NDM-80, Argonne Natl Lab., IL (1983).
[3.35] FRÖHNER, F.H., Evaluation of the unresolved resonance range of ^{238}U, Nucl. Sci. Eng. **103** (1989) 119–128.
[3.36] FRÖHNER, F.H., Evaluation and Analysis of Nuclear Resonance Data, JEFF Rep. 18, OECD Nuclear Energy Agency, Paris (2000).
[3.37] CROSS SECTION EVALUATION WORKING GROUP, ENDF-6 Formats Manual: Data Formats and Procedures for the Evaluated Nuclear Data File ENDF/B-VI and ENDF/B-VII, Rep. BNL-NCS-44945-05-Rev. (ENDF-102), (HERMAN, M., Ed.), Brookhaven Natl Lab., Upton, NY (2005).
[3.38] HENRYSON, H., TOPPEL, B.J., STENBERG, C.G., MC-2: A Code to Calculate Fast Neutron Spectra and Multigroup Cross Sections, Rep. ANL-8144 (ENDF-239), Argonne Natl Lab., IL (1976).
[3.39] SIRAKOV, I., SCHILLEBEECKX, P., CAPOTE, R., "Evaluation of neutron cross section data in the unresolved resonance region with a link to the optical model", Nuclear Data Evaluation for Reactor Applications (Proc. Workshop Cadarache, 2006), (SEROT, O., Ed.), OECD Nuclear Energy Agency, Paris (2006) CD-ROM.
[3.40] LARSON, N.M., Updated Users' Guide for SAMMY: Multilevel R-Matrix Fits to Neutron Data Using Bayes' Equation, Rep. ORNL/TM-9179/R6 (ENDF-364), Oak Ridge Natl Lab., TN (2003).
[3.41] HOLMES, J.A., WOOSLEY, S.E., FOWLER., W.A., ZIMMERMAN, B.A., Tables of thermonuclear-reaction-rate data for neutron-induced reactions on heavy nuclei, At. Data Nucl. Data Tables **18** (1976) 305–412.
[3.42] CULLEN, D.E., ENDF/B Pre-processing Codes, Version 2005-1, http://www-nds.iaea.org/ndspub/endf/prepro/
[3.43] SIRAKOV, I., CAPOTE, R., GUNSING, F., SCHILLEBEECKX, P., TRKOV, A., An ENDF-6 compatible evaluation for neutron induced reactions of ^{232}Th in the unresolved resonance region, Ann. Nucl. Energy **35** (2008) 1223–1231.
[3.44] HERMAN, M., et al., EMPIRE Nuclear Reaction Model Code, Version 2.19, http://www-nds.iaea.org/empire/
HERMAN, M., "EMPIRE-II statistical model code for nuclear reaction calculations", Nuclear Data and Nuclear Reactors: Physics, Design and Safety (Proc. Workshop Trieste, 2000), (PAVER, N., HERMAN, M., GANDINI, A., Eds), International Centre for Theoretical Physics, Trieste (2001) 137–230.
[3.45] MacFARLANE, R., et al., NJOY 99 Nuclear Data Processing System,www.nea.fr/abs/html/psr-0480.html
[3.46] FUJITA, Y., et al., Measurement of nuclear inelastic scattering cross section of thorium-232 for 144 keV Si-filtered neutrons, J. Nucl. Sci. Technol. **20** (1983) 983–990.
[3.47] TRKOV, A., CAPOTE NOY, R., "Highlights from the CRP on the thorium–uranium fuel cycle", Neutron Measurements, Evaluations and Applications (Proc. 3rd Workshop Borovets, Bulgaria, 2006), (PLOMPEN, A.J.M., Ed.), Rep. 22794 EN, Institute for Reference Materials and Measurements, Geel, Belgium (2007) 43–48.
[3.48] JANEVA, N.B., Bulgarian Academy of Sciences, Sofia, personal communication, 2006.
[3.49] BELGYA, T., et al., Handbook for Calculations of Nuclear Reaction Data: RIPL-2, IAEA-TECDOC-1506, IAEA, Vienna (2006), http://www-nds.iaea.org/RIPL-2/
[3.50] HERMAN, M., et al., EMPIRE: Nuclear reaction model code system for data evaluation, Nucl. Data Sheets **108** (2007) 2655–2715.
[3.51] HAN, Yinlu, ZHANG, Zhengjun, Double differential neutron emission cross sections for n + ^{230,231,232,233,234}Th reactions, Nucl. Phys. A **753** (2005) 53–82.
[3.52] MASLOV, V.M., Analysis of n + ^{232}Th interaction up to 200 MeV, Nucl. Phys. A **757** (2005) 390–410.
[3.53] BACK, B.B., HANSEN, O., BRITT, H.C., GARRETT, J.D., Fission of doubly even actinide nuclei induced by direct reactions, Phys. Rev. C **9** (1974) 1924–1947.
[3.54] BHANDARI, B.S., Three-hump fission barrier in ^{232}Th, Phys. Rev. C **19** (1979) 1820–1826.
[3.55] SIN, M., VLĂDUCĂ, G., "STATIS — A statistical model code including sub-barrier fission resonances", Nuclear Data for Science and Technology (Proc. Int. Conf. Trieste, 1997), Vol. 59, Part II (REFFO, G., VENTURA, A., GRANDI, C., Eds), Italian Physical Society, Bologna (1997) 976–978.
[3.56] VLDUCA, G., SIN, M., NEGOITA, C.C., Neutron cross-sections of ^{238}U in the energy range 0.01 ± 5.5 MeV, Ann. Nucl. Energy **27** (2000) 995–1010.
[3.57] SIN, M., CAPOTE, R., VENTURA, A., HERMAN, M., OBLOZINSKY, P., Fission of light actinides: ^{232}Th(n, f) and ^{231}Pa(n, f) reactions, Phys. Rev. C **74** (2006) 014608.
[3.58] RAYNAL, J., "Optical-model and coupled-channel calculations in nuclear physics", Computing as a Language of Physics (Proc. Int. Sem. Course Trieste, 1971), IAEA, Vienna (1972) 281–322.
[3.59] HAUSER, W., FESHBACH, H., The inelastic scattering of neutrons, Phys. Rev. **87** (1952) 366–373.
[3.60] HOFFMANN, H.M., RICHERT, J., TEPEL, J.W., WEIDENMÜLLER, H.A., Direct reactions and Hauser–Feschbach theory, Ann. Phys. (N.Y.) **90** (1975) 403–435.

[3.61] NILSSON, S.G., et al., On the spontaneous fission of nuclei with *Z* near 114 and *N* near 184, Nucl. Phys. A **115** (1968) 545–562.
[3.62] HILAIRE, S., GORIELY, S., Global microscopic nuclear level densities within the HFB plus combinatorial method for practical applications, Nucl. Phys. A **779** (2006) 63–81.
[3.63] FRÖMAN, N., FRÖMAN, P.O., JWKB Approximation, Contributions to the Theory, North-Holland, Amsterdam (1965).
[3.64] FRÖMAN, N., DAMMERT, Ö., Tunnelling and super-barrier transmission through a system of two real potential barriers, Nucl. Phys. A **147** (1970) 627–649.
[3.65] AVRIGEANU, V., HODGSON, P.E., AVRIGEANU, M., Global optical potentials for emitted alpha particles, Phys. Rev. C **49** (1994) 2136–2141.
[3.66] ABFALTERER, W.P., et al., Measurement of neutron total cross sections up to 560 MeV, Phys. Rev. C **63** (2001) 044608.
[3.67] SMITH, A.B., GUENTHER, P.T., McKNIGHT, R.D., "On the neutron inelastic-scattering cross sections of ^{232}Th, ^{233}U, ^{235}U, ^{238}U, ^{239}Pu and ^{240}Pu", Nuclear Data for Science and Technology (Proc. Int. Conf. Antwerp, 1982), (BÖCKHOFF, K.H., Ed.), Central Bureau for Nuclear Measurements, Geel, Belgium (1983) 39–44.
[3.68] GLAZKOV, N.P., Spectra and cross-sections of the neutron inelastic scattering in the energy range of 0.4–1.2 MeV on the nuclei U, Th, Hg, W, Sb, Cd, Mo, Nb and Fe, Sov. At. Energy **14** (1964) 405–407.
[3.69] SMITH, A.B., Elastic and inelastic scattering of fast neutrons from ^{232}Th, Phys. Rev. **126** (1962) 718–725.
[3.70] HAOUAT, G., et al., Neutron scattering cross sections for Th-232, U-233, U-235, U-238, Pu-239 and Pu-242 between 0.6 and 3.4 MeV, Nucl. Sci. Eng. **81** (1982) 491–511.
[3.71] KARAMANIS, D., et al., Neutron cross-section measurements in the Th–U cycle by the activation method, Nucl. Instrum. Methods Phys. Res. A **505** (2003) 381–384.
[3.72] KONNO, C., et al., Activation Cross Section Measurements at Neutron Energy from 13.3 to 14.9 MeV, Rep. JAERI-1329, Japan Atomic Energy Research Inst., Tokai-mura (1993).
[3.73] CHATANI, H., KIMURA, I., Measurement of Th-232(n, 2n)Th-231 reaction cross section with 14.5-MeV neutrons, Ann. Nucl. Energy **19** (1992) 425–429.
[3.74] CHATANI, H., KIMURA, I., Measurement of Th-232(n, 2n)Th-231 Reaction Cross Section with 14-MeV Neutrons, Rep. JAERI-M-91-032, Japan Atomic Energy Research Inst., Tokai-mura (1991) 245–254.
[3.75] RAICS, P., et al., Measurement of the cross sections for the Th-232(n, 2n) reaction in the 6.745 to 10.450 MeV energy range, Phys. Rev. C **32** (1985) 87–91.
[3.76] KARIUS, H., ACKERMANN, A., SCOBEL, W., The pre-equilibrium contribution to the (n, 2n) reactions of Th-232 and U-238, J. Phys. G **5** (1979) 715–721.
[3.77] COHRAN, D.R.F., HENKEL, R.L., "^{232}Th(n, 2n)", Reports to the AEC Nuclear Cross Sections Advisory Group, Oak Ridge National Laboratory, Rep. WASH-1013, Brookhaven Natl Lab., Upton, NY (1958) 34.
[3.78] McTAGGART, M.H., GOODFELLOW, H., Measurements at 14 MeV neutron energy of the (n, 2n) cross section of beryllium and the (n, 3n) cross section of thorium, J. Nucl. Energy A/B **17** (1963) 437–439.
[3.79] BABA, M., WAKABAYASHI, H., ITOH, N., MAEDA, K., HIRAKAWA, N., Measurements of Prompt Fission Neutron Spectra and Double-Differential Neutron Inelastic Scattering Cross Sections for U-238 and Th-232, Rep. JAERI-M-89-143, Japan Atomic Energy Research Inst., Tokai-mura (1989) (in Japanese).
[3.80] MIURA, T., et al., Measurements of the double-differential neutron emission cross-sections of ^{238}U and ^{232}Th for 2.6, 3.6 and 11.8 MeV neutrons, Ann. Nucl. Energy **28** (2001) 937–951.
[3.81] YOUNG, P.G., Los Alamos Natl Lab., NM, personal communication, 2005.
YOUNG, P.G., et al., Evaluation of neutron reactions for ENDF/B-VII: $^{232–241}$U and ^{239}Pu, Nucl. Data Sheets **108** (2007) 2589–2654.
[3.82] WIENKE, H., CAPOTE, R., HERMAN, M., SIN, M., Deformation-dependent Tamura–Udagawa–Lenske multistep direct model, Phys. Rev. C **78** (2008) 064611.
[3.83] MATSUYAMA, S., et al., Measurement of Double-Differential Neutron Emission Spectra of ^{238}U and ^{232}Th at Neutron Energy 18.0 MeV, Rep. JAERI-M-91-032, Japan Atomic Energy Research Inst., Tokai-mura (1990) 219–226.
[3.84] THIROLF, P.G., HABS, D., Spectroscopy in the second and third minimum of actinide nuclei, Prog. Part. Nucl. Phys. **49** (2002) 325–402.
[3.85] ĆWIOK, S., et al., Hyperdeformations and clustering in the actinide nuclei, Phys. Lett. B **322** (1994) 304–310.
[3.86] SHCHERBAKOV, O.A., et al., "Neutron-induced fission of ^{233}U, ^{238}U, ^{237}Np, ^{239}Pu and ^{232}Th in the energy range 1–200 MeV", Interaction of Neutrons with Nuclei (Proc. Conf. Dubna, 2001), Joint Inst. for Nuclear Research, Dubna (2001) 257–270.
[3.87] FURSOV, B.I., et al., Cross-section ratios Th-232 to U-235 and U-234 to U-235 measurements in the neutron energy range 0.13–7.4 MeV, Sov. At. Energy **71** (1991) 827–831.
[3.88] GOVERDOVSKIJ, A.A., et al., Fission cross-section ratio of Th-232 to U-235 measurement in the neutron energy range 5–10 MeV, Sov. At. Energy **61** (1986) 958–960.

[3.89] KANDA, K., IMARUOKA, H., YOSHIDA, K., SATO, O., HIRAKAWA, N., "Measurements of fast neutron induced fission cross sections of Th-232, U-233 and U-234 relative to U-235", Nuclear Data for Basic and Applied Science (Proc. Int. Conf. Santa Fe, 1985), Vol. 1 (YOUNG, P.G., BROWN, R.E., AUCHAMPAUGH, G.F., LISOWSKI, P.W., Eds), Gordon and Breach, New York (1986) 569–572.
KANDA, K., IMARUOKA, H., YOSHIDA, K., SATO, O., HIRAKAWA, N., Measurement of fast neutron induced fission cross sections of ^{232}Th, ^{233}U and ^{234}U relative to ^{235}U, Radiat. Eff. **93** (1986) 233–236.
[3.90] MEADOWS, J.W., The fission cross sections of some thorium, uranium, neptunium and plutonium isotopes relative to ^{235}U, Nucl. Sci. Eng. **85** (1983) 271–279.
[3.91] BEHRENS, J.W., BROWNE, J.C., ABLES, E., Measurements of the neutron-induced fission cross section of ^{232}Th relative to ^{235}U from 0.7 to 30 MeV, Nucl. Sci. Eng. **81** (1982) 512–519.
[3.92] BLONS, J., MAZUR, C., PAYA, D., RIBRAG, M., WEIGMANN, H.,Institute for Reference Materials and Measurements, Geel, Belgium, personal communication, 1980.
BLONS, J., MAZUR, C., PAYA, D., RIBRAG, M., WEIGMANN, H., On the existence of triple-humped barriers in ^{231,233}Th, Nucl. Phys. A **414** (1984) 1–41.
[3.93] BLONS, J., MAZUR, C., PAYA, D., Fission cross sections for Th-232 and U-238, Phys. Rev. Lett. **35** (1975) 1749–1751.
[3.94] CSATLÓS, M., et al., Resonant tunnelling through the triple-humped fission barrier of ^{236}U, Phys. Lett. B **615** (2005) 175–185.
[3.95] SIN, M., et al., Improvement of the fission channel in the EMPIRE code, AIP Conf. Proc. **769** (2005) 1249–1252.
SIN, M., et al., "Fission of thorium isotopes", Neutron Measurements, Evaluations and Applications (Proc. 2nd Conf. Bucharest, 2004), (PLOMPEN, A.J.M., Ed.), Inst. for Reference Materials and Measurements, Geel, Belgium (2005) 153–156.
[3.96] KORNILOV, N.V., KAGALENKO, A.B., HAMBSCH, F.-J., Computing the spectra of prompt fission neutrons on the basis of a new systematics of experimental data, Phys. Atom. Nucl. **62 (**1999) 173–185.
[3.97] LISOWSKI, P.W., et al., "Neutron induced fission cross section ratios for ^{232}Th, ^{235,238}U, ^{237}Np and ^{239}Pu from 1 to 400 MeV", Nuclear Data for Science and Technology (Proc. Int. Conf. Mito, 1988), (IGARASI, S., Ed.), Saikon, Tokyo (1988) 97–99.
[3.98] MANABE, F., et al., Measurements of neutron induced fission cross section ratios of ^{232}Th, ^{233}U, ^{234}U, ^{236}U, ^{238}U, ^{237}Np, ^{242}Pu and ^{243}Am relative to ^{235}U around 14 MeV, Technol. Rep. Tohoku Univ. **52** (1988) 97–126.
[3.99] MEADOWS, J.W., The fission cross sections of ^{230}Th, ^{232}Th, ^{233}U, ^{234}U, ^{236}U, ^{238}U, ^{237}Np, ^{239}Pu and ^{242}Pu relative to ^{235}U at 14.74 MeV neutron energy, Ann. Nucl. Energy **15** (1988) 421–429.
[3.100] GOVERDOVSKIJ, A.A., et al., Fission cross-section measurement for heavy nuclei by the neutrons at energy sixteen MeV, Sov. At. Energy **60** (1986) 494–496.
[3.101] NORDBORG, C., CONDE, H., STROEMBERG, L.G., "Fission cross section ratio measurements of ^{232}Th/^{235}U and ^{236}U/^{235}U", Neutron Physics and Nuclear Data (Proc. Int. Conf. Harwell, 1978), OECD Nuclear Energy Agency, Paris (1978) 910–913.
[3.102] WILLIAMS, J.H., et al., Fission Cross Sections of 02, 23, 25, 28, 49, B^{10} and Li^{6}, Rep. LA-520, Los Alamos Natl Lab., NM (1946) 1–12.
[3.103] SASTRY, C.V., JAIN, R.K., SINGH, S.K., BOSE, S.K., RAMA RAO, J., Fast neutron induced fission cross section of thorium, Nucl. Phys. B **35** (1992) 288–289.
[3.104] GARLEA, I., MIRON-GARLEA, C., ROSU, H.N., FODOR, G., RADUCU, V., Integral neutron cross sections measured around 14 MeV, Rev. Roum. Phys. **37** (1992) 19–25.
[3.105] ANAND, R.P., IYENGAR, K.N., AJITANAND, N.N., "Measurement of fast neutron induced fission cross section of Th-232 relative to U-238", Nuclear Physics (Proc. Symp. Jaipur, India, 1985), Vol. 2, Bhaba Atomic Research Centre, Bombay (1985) 350–351.
[3.106] GARLEA, I., et al., Measuring of the integral cross sections at 14 MeV for reactions In-115(n, n′), Au-197(n, 2n), Nb-93(n, 2n), Al-27(n, a), Fe-56(n, p), Pu-239(n, f), U-238(n, f), Th-232(n, f) and Np-237(n, f), Rev. Roum. Phys. **29** (1984) 421–426.
[3.107] PROTOPOPOV, A.N., SELITSKII, Y.A., SOLOV'EV, S.M., Fission cross sections of ^{232}Th and ^{237}Np for 14.6 MeV neutrons, Sov. J. At. Energy **4** (1958) 256–258.
[3.108] BEREZIN, A.A., STOLIAROV, G.A., NIKOL'SKII, Yu.V., CHELNOKOV, I.E., Cross section for fission of ^{235}U and ^{232}Th by 14.6 MeV neutrons, Sov. J. At. Energy **5** (1958) 1604–1605.
[3.109] UTTLEY, C.A., PHILLIPS, J.A., Fission Cross Sections of U-238, U-235, U-233, Pu-239 and Th-232 for 14 MeV Neutrons, Rep. AERE-NP/R-1996, Atomic Energy Research Establishment, Harwell, UK (1956).
[3.110] NYER, W., Fission Cross Section of Thorium 232, Uranium 233, 235 and 236 and Plutonium 239 Relative to Uranium 238 for 14 MeV Neutrons, Rep. LAMS-938, Los Alamos Natl Lab., NM (1950).
[3.111] RAGO, P.F., GOLDSTEIN, N., Thorium fission cross section for neutrons between 12.5 and 18 MeV using fission fragment damage tracks in Lexan, Health Phys. **13** (1967) 654.
[3.112] BAILEY, C.J., et al., Measurements of Sigma(f)(02)/Sigma(f)(28) and the Value of Sigma(f)(02) as a Function of Neutron Energy, Rep. 39, Los Alamos Sci. Lab., NM (1942) 1–12.
[3.113] SMITH, D.L., Covariance Matrices for Nuclear Cross-sections Derived from Nuclear Model Calculations, Rep. ANL/NDM-159, Argonne Natl Lab., IL (2004).
[3.114] MUIR, D.W., KODELI, I., CAPOTE, R., ZERKIN, V., "The global assessment of nuclear data — GANDR", Nuclear Data for Science and Technology (Proc. Int. Conf. Nice, 2007), (BERSILLON, O., GUNSING, F., BAUGE, E., JACQMIN, R., LERAY, S., Eds), EDP Sciences, Les Ulis (2008), http://dx.doi.org/10.1051/ndata:07635

[3.115] FOSTER, D.G., GLASGOW, D.W., Neutron total cross sections, 2.5–15 MeV, I: Experimental, Phys. Rev. C **3** (1974) 576–603.
[3.116] KARAMANIS, D., et al., Neutron radiative capture cross section of ^{232}Th in the energy range from 0.06 to 2 MeV, Nucl. Sci. Eng. **139** (2001) 282–292.
[3.117] DAVLETSHIN, A.N., TEPLOV, E.V., TIPUNKOV, A.O., TIKHONOV, S.V., TOLSTIKOV, V.A., Neutron radiation cross-sections by the Th-232 and Au-197 nuclei in the energy range 0.37–1 MeV, Yad. Konst. **1** (1993) 13–16.
[3.118] IGNATYUK, A.V., HAMBUSH, F.J., "Nu-bar and fission spectra", paper presented at the 3rd Research Coordination Mtg on Evaluated Nuclear Data for Th–U Fuel Cycle, Vienna, 2006.

4. NEUTRON CROSS-SECTIONS OF PROTACTINIUM-231, -233

4.1. EVALUATION IN THE RESONANCE RANGE

4.1.1. The ^{231}Pa resonance parameters

The RRR spans from 10^{-5} to 117 eV. Multilevel Breit–Wigner resonance parameters were taken from the evaluation by Mughabghab [4.1]. A bound level was postulated to fit the thermal constants [4.1], and a potential scattering radius of 10.4 fm was required to fit a bound coherent scattering amplitude of 9.3 fm, which is larger than the systematics in this mass region. However, after adopting these parameters, the following thermal constants were obtained:

(a) A capture constant of 200.7 b;
(b) A scattering constant of 11.2 b;
(c) A fission constant of 0.020 b;
(d) A capture resonance integral of 536 b, including the contribution from the unresolved region.

Fission widths above 60 eV that were zero in the original evaluation were assigned a width of 5×10^{-6} eV. An additional reformulation of the parameters was undertaken: resonance parameters were converted into the RM formalism, and a covariance matrix was generated from the quoted uncertainties of the resonance parameters.

The unresolved resonance parameter range extends up to 78.0242 keV. Average resonance parameters were taken from the Minsk file [4.2] and used only to calculate self-shielding, while the smooth cross-section curve was taken from the nuclear model calculation [4.3].

4.1.2. The ^{233}Pa resonance parameters

Resolved resonance parameters were available from the ENDF/B-VI, JENDL-3.3, JEFF-3.1 and Mughabghab evaluations. A resonance parameter file was also submitted by Morogovskij and Bakhanovich [4.4], which extended up to 106.6 eV. A statistical analysis was undertaken by Leal within the scope of the present project to split the spin states and transform the multilevel Breit–Wigner formalism into the RM formalism, while ensuring consistency with the total thermal and capture cross-sections. The covariance matrix was also produced from the estimated uncertainties of the resonance parameters.

The average resonance parameters in the URR were taken from the Maslov file [4.2] and applied to the calculation of the self-shielding factors from 106.6 to 70 keV, while the smooth cross-sections at infinite dilution were derived from the nuclear model calculation [4.3].

4.2. EVALUATION IN THE FAST ENERGY RANGE

The nuclear models for ^{231,233}Pa (except fission) were the same as those adopted for ^{232}Th. The optical model deformations were adjusted to reproduce the measured neutron strength functions.

4.2.1. The ^{231}Pa(n, *f*) cross-section

The measured neutron induced fission cross-section of ^{231}Pa has a complicated structure in first chance fission (Fig. 4.1). Fission barrier parameters are defined by the following features:

(a) As with ^{232}Th, a pronounced resonant structure above the fission threshold indicates a triple humped barrier.
(b) Unlike ^{232}Th, a superposition of wide (E = 0.185, 0.315 MeV) and sharp resonances (E = 0.155, 0.173, 0.370 MeV) in the sub-threshold region implies the coexistence of class II and III vibrational states in this excitation energy range (Fig. 4.2).

(c) There is no obvious change of slope, but above a neutron incident energy of 0.4 MeV (Fig. 4.2) there are no more wide resonances (presumably related to the partially damped class II vibrational states), revealing that the height of the inner barrier would be 5.9 ± 0.2 MeV (the neutron separation energy in ^{232}Pa is 5.55 MeV).

(d) The fission threshold around a neutron incident energy of 0.5 MeV suggests heights for the outer barriers of 6.1 ± 0.2 MeV.

(e) Sharp resonances below the threshold are assumed to be related to class III vibrational states, and indicate a deeper third well.

The best description of the fission cross-section was obtained by adopting fundamental barrier parameters similar to those obtained for thorium, with two exceptions:

(1) A larger width was needed for the first hump, to reproduce the small value of the fission cross-section at low energies.

(2) A lower value for the bottom of the third well (V_{III} = 5.20 MeV), to describe the sharp resonances at sub-threshold energies.

The parameters for the barriers to discrete transition states have been deduced to fit the resonances. Calculations for protactinium show that resonances produced by vibrational states in the isomeric well are strongly influenced by the positions of the corresponding transition states in the third well. This behaviour could explain why the fissioning compound nucleus of ^{232}Pa has such spectacular resonant structure, as observed in Fig. 4.1, arising partially from the vibrational states in the isomeric well, despite being doubly odd. Neutron induced fission cross-sections of odd–even targets are normally smooth without any resonant structure (e.g. the ^{241}Am(n, f) cross-section). This behaviour is related to the complete damping of the vibrational states in the isomeric well, and is explained in terms of the small distance among the class II vibrational and non-vibrational states compared with their widths, specific for doubly odd nuclei. The atypical behaviour of the ^{231}Pa(n, f) cross-section could be explained by the coexistence of the second and third wells in the fission barrier: the penetrability through the class II vibrational states is being 'triggered' by the class III vibrational states. However, the possibility that all the resonances are related to class III vibrational states cannot be completely rejected, and further studies of the spectra

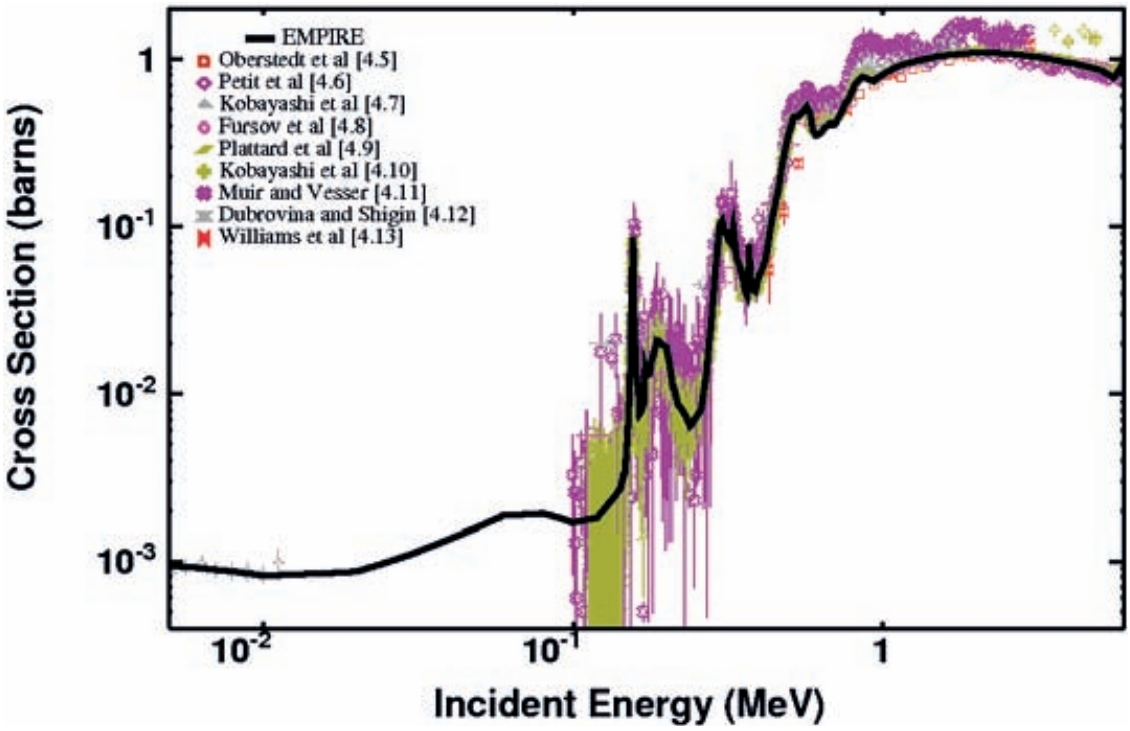

FIG. 4.1. The neutron induced fission cross-section of ^{231}Pa: first chance fission.

of the fission transition states are needed to explore these effects. The strength of the imaginary potential in the isomeric well was chosen to fit the width of the wide resonances at sub-barrier energies and to ensure complete damping close to the top of the inner barrier. The contributions of the transition states in the continuum to the fission coefficients were calculated on the basis of the same procedure as for ^{232}Th. The parameters of the equivalent outer barrier used in these calculations were V_{eq} = 6.05 MeV and $\hbar\omega_{eq}$ = 50 MeV.

Good agreement of the calculated ^{231}Pa(n, *f*) cross-section with the experimental data was obtained for first chance fission, confirming the validity of the fission model and the hypothesis concerning the barrier parameters (Fig. 4.1). It should be noted that evaluators in the EMPIRE calculations followed the most recent measurements by Oberstedt et al. [4.5] in the region from 2 to 3 MeV incident neutron energy. Discrepant experimental data occur from 8 to 14 MeV incident neutron energy (Fig. 4.3), and there is a complete lack of data at energies above 14 MeV. Under these unsatisfactory circumstances, the predicted fission cross-sections could deviate significantly from the real values. Following what is considered to be a reasonable trend in the fission parameters, values were obtained that were lower than the other evaluations for second and third chance fission. This prediction is supported by the experimental point at 14 MeV measured by Birgul and Lyle [4.14], and preliminary unpublished IRMM data between 15 and 21 MeV.

At even higher energies there are no experimental constraints, and the fission cross-section of ^{237}Np was followed, the closest neighbour nucleus of the same type (odd–even) for which experimental data are available. The final fission cross-section calculated for an incident neutron energy range of 1 keV to 60 MeV is shown in Fig. 4.4.

4.2.2. The ^{233}Pa(n, *f*) cross-section

With a short half-life of 27.0 d, only two sets of experimental data are available for the neutron induced fission of ^{233}Pa. The fission probability of ^{234}Pa was obtained by Petit et al. [4.6] in a study of the surrogate ^{232}Th(^{3}He, p)^{234}Pa reaction. Energy resolved fission cross-section data have been directly measured by Tovesson et al. [4.15], and are lower than those obtained from the substitution reaction. A possible explanation for this discrepancy has been given by Vlăducă et al. [4.16]. The starting fission parameters in the present evaluation were those deduced from fitting the ^{231}Pa(n, *f*) experimental data and adjusted to describe the data of Tovesson et al. for first chance fission. Calculations in the second chance region followed the observed trend in ^{231}Pa(n, n*f*), slightly

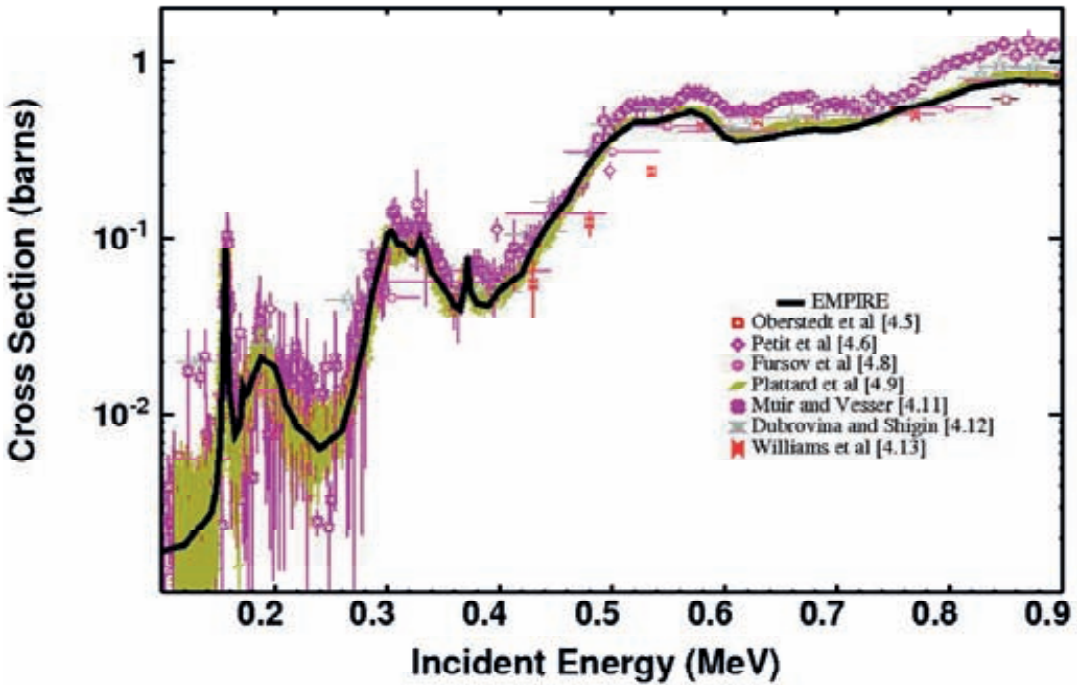

FIG. 4.2. The resonant structure of the neutron induced fission cross-section of ^{231}Pa near the fission threshold.

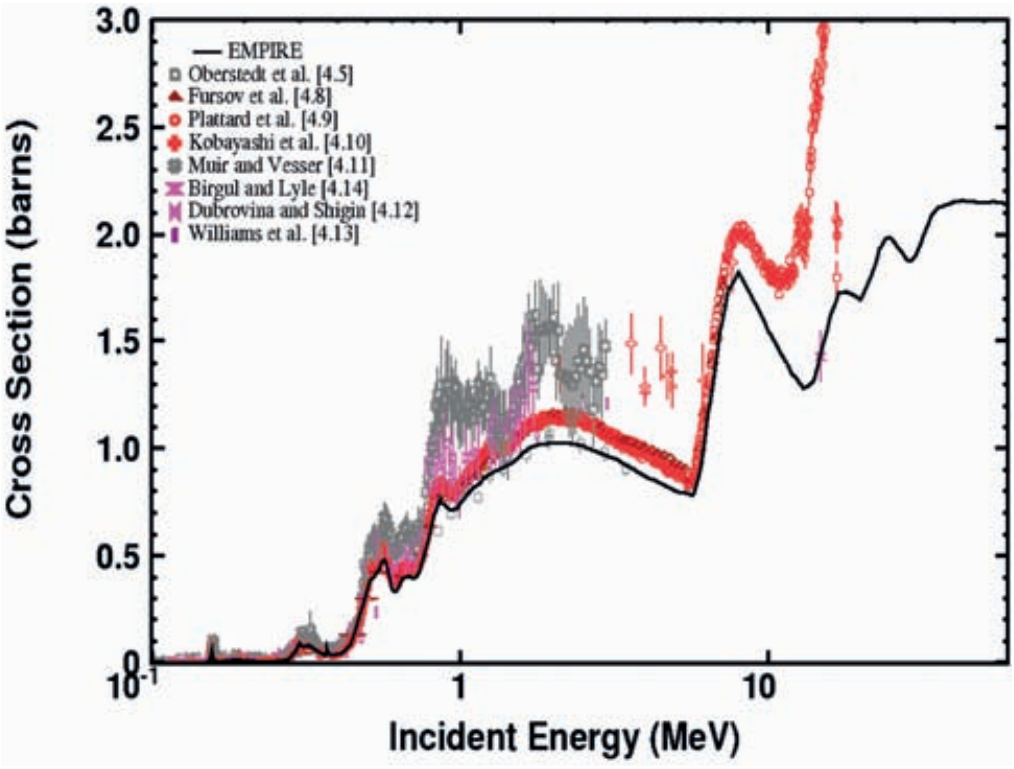

FIG. 4.3. The neutron induced fission cross-section of ^{231}Pa: multiple chance fission.

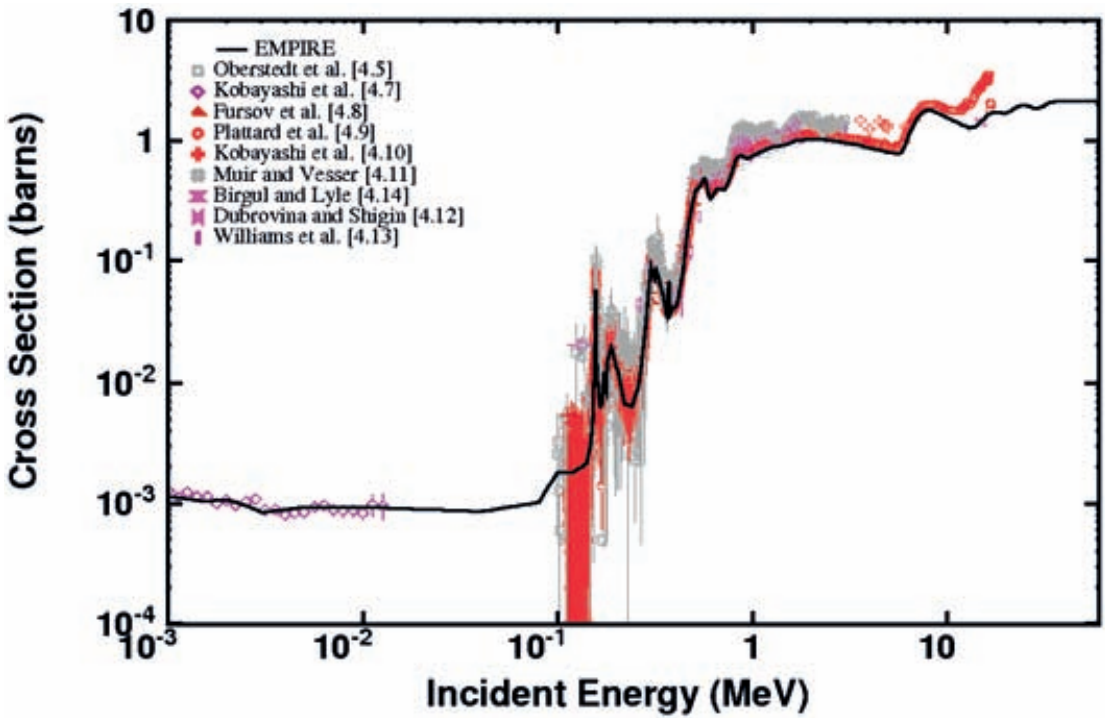

FIG. 4.4. The neutron induced fission cross-section of ^{231}Pa at neutron energies from 1 keV to 60 MeV.

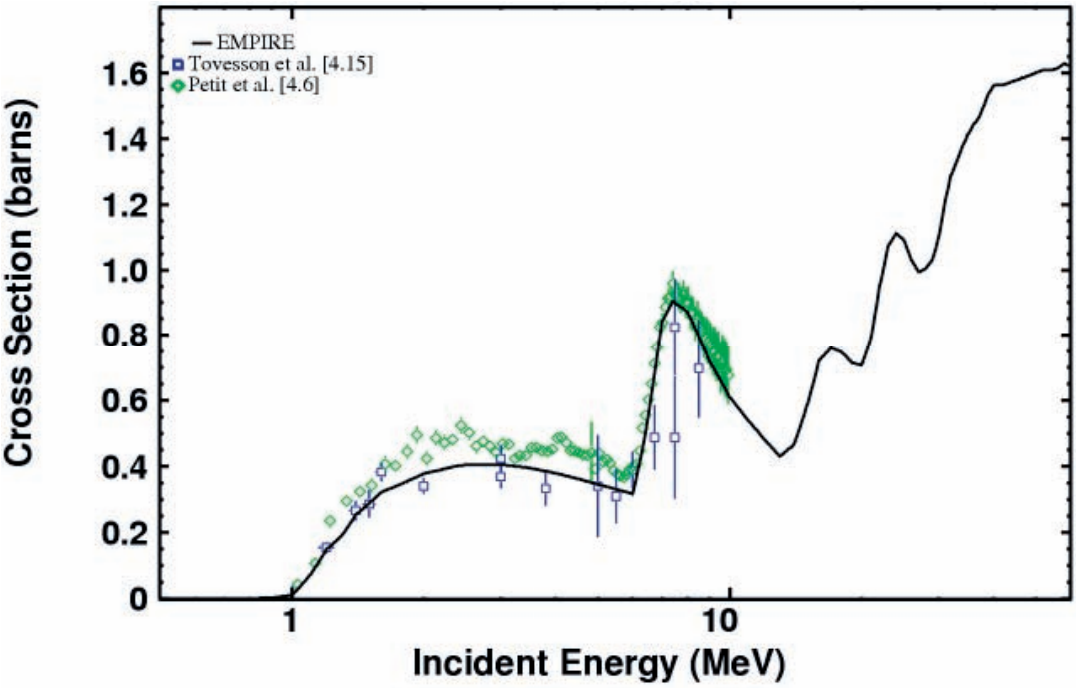

FIG. 4.5. The neutron induced fission cross-section of ^{233}Pa at neutron energies from 1 keV to 60 MeV.

overestimating the experimental data but producing lower values than other evaluations. The same procedure and parameters as for ^{231}Pa have been used for higher chance fissions. Final results are shown in Fig. 4.5.

4.2.3. Fission spectra and average number of neutrons per fission

The prompt neutron fission spectra for both protactinium isotopes were obtained directly from the EMPIRE calculations, as for ^{232}Th. The spectra of neutrons emitted from the fission fragments were based on the empirical parameterization proposed by Kornilov et al. [4.17]. The emissive contribution of (n, *xnf*) neutrons in the second and higher chance fission were calculated using EMPIRE neutron (n, *x*n) spectra, which include direct and pre-equilibrium components. Because of these contributions, the fission spectra became anisotropic and were coded in File-6 format in ENDF terminology, which allows storage of such data without loss of information. The average number of neutrons per fission was also taken from the EMPIRE calculation.

The delayed neutron data were not evaluated. They were adopted from the BROND-3 evaluation.

REFERENCES TO SECTION 4

[4.1] MUGHABGHAB, S.F., Atlas of Neutron Resonances: Resonance Parameters and Thermal Cross Sections Z = 1–100, 5th edn, Elsevier, Amsterdam (2006).

[4.2] MASLOV, V.M., et al., Evaluated Neutron Nuclear Data for Pu, Am and Cm Isotopes, Rep. INDC(BLR)-2-11, IAEA, Vienna (1995–1998), http://www-nds.iaea.org/minskact/

[4.3] CAPOTE, R., IAEA, Vienna, personal communication based on optical model as given in the following reference: SOUKHOVITSKII, E.Sh., CAPOTE, R., QUESADA, J.M., CHIBA, S., Dispersive coupled-channel analysis of nucleon scattering for ^{232}Th up to 200 MeV, Phys. Rev. C **72** (2005) 024604.

[4.4] MOROGOVSKIJ, G.B., BAKHANOVICH, L.A., Evaluation of the resolved resonance region for ^{233}Pa, Yad. Konst. **1–2** (2003) (in Russian) [English translation: INDC(CCP)-440, IAEA, Vienna (2004) 7–16], http://www.ippe.obninsk.ru/podr/cjd/indc(ccp)/indc-ccp-440.pdf

[4.5] OBERSTEDT, S., et al., New results on the neutron-induced fission cross-section of ^{231}Pa for incident neutron energies E_n = 0.8–3.5 MeV, Ann. Nucl. Energy **32** (2005) 1867–1874.

[4.6] PETIT, M., et al., Determination of the ^{233}Pa(n, f) reaction cross section from 0.5 to 10 MeV neutron energy using the transfer reaction ^{232}Th(^{3}He, p)^{234}Pa, Nucl. Phys. A **735** (2004) 345–371;
PETIT, M., Mesure de al section efficace de fission du ^{233}Pa, PhD Thesis, Univ. of Bordeaux (2002).
[4.7] KOBAYASHI, K., et al., Measurement of neutron-induced fission cross sections of ^{229}Th and ^{231}Pa using linac-driven lead slowing-down spectrometer, Nucl. Sci. Eng. **139** (2001) 273–281.
[4.8] FURSOV, B.I., et al., Measurement of the fast-neutron cross sections of ^{231}Pa and ^{243}Am, At. Ehnerg. **59** (1985) 339–343.
[4.9] PLATTARD, S., et al., Some spectroscopic properties of fine structures observed near the ^{231}Pa(n, f) threshold, Phys. Rev. Lett. **46** (1981) 633–636.
[4.10] KOBAYASHI, K., KIMURA, I., GOTOH, H., YAGI, H., Cross Section Measurement for the Pa-231(n, f) Reaction, Rep. KURRI-TR-8, Kyoto Univ. Research Reactor Institute (1975) 10–16.
[4.11] MUIR, D., VESSER, L.R., Neutron-induced Fission Cross Sections of ^{230}Th and ^{231}Pa, Rep. LA-4648-MS, Los Alamos Natl Lab., NM (1971).
[4.12] DUBROVINA, S.M., SHIGIN, V.A., Fission cross section for ^{231}Pa and ^{239}Pu with neutrons in the energy interval 1.5 to 1500 keV, Sov. Phys. Dokl. **9** (1965) 579–580.
[4.13] WILLIAMS, J.H., et al., The Cross Sections for Fission of 25, 49, 28, 11, 37, 00, 02, B and Li, Rep. LA-150**,** Los Alamos Natl Lab., NM (1944).
[4.14] BIRGUL, O., LYLE, S.J., Radiochemical studies of 3 and 14 MeV neutron induced fission of Pa-231, Radiochim. Acta **11** (1969) 108–112.
[4.15] TOVESSON, F., et al., ^{233}Pa(n, f) cross section up to E_n = 8.5 MeV, Nucl. Phys. A **733** (2004) 3–19.
[4.16] VLĂDUCĂ, G., et al., Calculation of the neutron induced fission cross-section of ^{233}Pa up to 20 MeV, Nucl. Phys. A **740** (2004) 3–19.
[4.17] KORNILOV, N.V., KAGALENKO, A.B., HAMBSCH, F.-J., Computing the spectra of prompt fission neutrons on the basis of a new systematics of experimental data, Phys. At. Nucl. **62 (**1999) 173–185.

5. NEUTRON CROSS-SECTIONS OF URANIUM ISOTOPES

5.1. EVALUATION OF ^{232}U

The neutron induced cross-section of ^{232}U was directly adopted from the Minsk file [5.1]. When compared with equivalent data in the ENDF/B-VII file, specific advantages include the RM resonance parameters and better neutron emission spectra. No covariance data are included for ^{232}U.

5.2. EVALUATION OF ^{233}U

Significant effort was expended on the ENDF/B-VII evaluation and validation of ^{233}U data, and therefore this file was adopted for the project in order to avoid duplication of work. However, equivalent data in the Minsk file [5.1] include a better theoretical foundation for the evaluation of the prompt fission neutron emission spectra (PFNS). Since the evaluation process for ^{233}U was not based on a single model calculation, no serious additional inconsistency was introduced by adopting the fission spectra from the Minsk file. No covariance data are included for ^{233}U.

5.3. EVALUATION OF ^{234}U

There is a problem with the existing ^{234}U resonance evaluations due to an incorrect interpretation of the experimental data. One of the authors of the experimental data recommends adopting the parameters that are listed in the publication together with 25 meV as an average radiation width [5.2]. Within the scope of the project, Leal transformed the resonance parameters into the RM format representation, and adjusted the bound state to the thermal cross-section values.

Kawano noted that the preliminary results of capture measurements at the DANCE/LANSCE installation can only be described with an extremely small radiation width of 15 meV. Preference is given to the Minsk evaluation for the fast region rather than to ENDF/B-VII because of a better description of PFNS (unless a re-evaluation would indicate contradictions).

The corrected resonance parameters and cross-sections in the fast energy range from the Minsk evaluation were merged into a self-consistent file to produce the final evaluation for ^{234}U.

5.4. EVALUATION OF ^{236}U

The neutron induced cross-sections of ^{236}U were directly adopted from the ENDF/B-VII.β2 evaluation without any changes.

REFERENCES TO SECTION 5

[5.1] MASLOV, V.M., et al., Evaluated Neutron Nuclear Data for Pu, Am and Cm Isotopes, Rep. INDC(BLR)-2-11, IAEA, Vienna (1995–1998), http://www-nds.iaea.org/minskact/

[5.2] HARVEY, J.A., HUGHES, D.J., Spacing of nuclear energy levels, Phys. Rev. **109** (1958) 471–479.

6. VALIDATION OF CROSS-SECTION DATA

6.1. SCOPE OF BENCHMARK STUDIES

Benchmarks from the handbook of the International Criticality Safety Benchmark Evaluation Project (ICSBEP) [6.1] were considered in the validation exercise, and are shown in Table 6.1. The benchmark from the SINBAD database [6.2] on the leakage spectrum measurement from a thorium sphere with a D–T source at the Institute for Physics and Power Engineering, Obninsk, Russian Federation, was also considered. RBMK benchmarks were not analysed because their sensitivity to thorium data was judged to be low, and benchmarks in which thorium appeared only as an impurity were also excluded.

The MCNP5 Monte Carlo code was used in the analysis with various data libraries. Inputs for MCNP5 were taken from the ICSBEP handbook or the SINBAD specifications, but the number of particle histories and batches for the determination of the multiplication factor k_{eff} was increased so that the statistical uncertainty in the calculations was negligible compared with the experimental uncertainties. Material composition data were changed when necessary to replace elemental number densities with the corresponding isotopic data. A sensitivity analysis of the source data libraries was also performed. Most of the libraries were available from the MCNPDATA package distribution. ACE files from the ENDF/B-VII.β2 library were obtained from the National Nuclear Data Center (NNDC), Brookhaven National Laboratory, USA: adjustments to the average number of neutrons per fission at thermal energies for ^{233}U as recommended for ENDF/B-VII.β3 were made locally. Additional libraries and ^{232}Th and ^{233}U files in ACE format were generated at the IAEA and at the Jožef Stefan Institute, Ljubljana, Slovenia.

TABLE 6.1. THORIUM-BEARING LATTICES IN ICSBEP

Identifier	Cases	Benchmark	Description
HEU-MET-FAST-068	1	KBR22	KBR22 (U/Th metal, PE*)
HEU-MET-INTER-008	1	KBR23	KBR23 (U/Th metal, PE)
IEU-COMP-FAST-002	1	KBR18	KBR18 (90% $^{235}UO_2$ + Th metal + 36% $^{235}UO_2$)
IEU-COMP-INTER-001	1	KBR19	KBR19 (90% $^{235}UO_2$ + Th metal + 36% $^{235}UO_2$, PE)
	1	KBR20	KBR20 (90% $^{235}UO_2$ + Th metal, PE)
IEU-COMP-THERM-005	1	KBR21	KBR21 (36% $^{235}UO_2$ + Th metal, PE)
PU-MET-FAST-008	1	THOR	THOR Pu sphere/Th reflector
HEU-COMP-THERM-015	1	LWBR SB-1	LWBR SB-1 (93% $^{235}UO_2$ + ZrO_2, ThO_2 blanket)
	1	LWBR SB-5	LWBR SB-5 (93% $^{235}UO_2$ + ZrO_2, ThO_2 blanket)
U233-COMP-THERM-001	1	LWBR SB-2	LWBR SB-2 (97% $^{233}UO_2$ + ZrO_2, ThO_2 blanket)
	1	LWBR SB-2½	LWBR SB-2½ (97% $^{233}UO_2$ + ZrO_2, no blanket)
	1	LWBR SB-3	LWBR SB-3 (97% $^{233}UO_2$ + ZrO_2, UO_2 + ThO_2 blanket)
	1	LWBR SB-4	LWBR SB-4 (97% $^{233}UO_2$ + ZrO_2, UO_2 + ThO_2 blanket)
	1	LWBR SB-6	LWBR SB-6 (97% $^{233}UO_2$ + ZrO_2, ThO_2 blanket)
	1	LWBR SB-7	LWBR SB-7 (97% $^{233}UO_2$ + ZrO_2, UO_2 + ThO_2 blanket)
LEU-COMP-THERM-060	10	RBMK	RBMK (Th absorbers, cases 19–28)
U233-SOL-THERM-006	1	ORCEF	ORCEF (Th as impurity only)
U233-SOL-THERM-008	1	ORNL	ORNL (Th as impurity only)
U233-SOL-THERM-009	1	ORNL	ORNL (Th as impurity only)
U233-SOL-THERM-012	1	ORCEF	ORCEF (Th as impurity only)
U233-SOL-THERM-013	1	ORCEF	ORCEF (Th as impurity only)

* PE: polyethylene.

The following libraries were considered in the analysis:

(a) ENDF/B-VI.8: The '.62c' series of materials in the ACTI files of the MCNPDATA set.
(b) ENDF/B-VII.β2+: The ENDF/B-VII.β2 library generated at NNDC, corrected for the neutron yield flag in the TYR block. The only change for ENDF/B-VII.β2+ is the average number of neutrons per fission of ^{233}U (implemented at the IAEA).
(c) JEFF-3.1: The library generated at the NEA databank based on JEFF-3.1.
(d) ADS-1.0: The reference library for ADS (version 1.0) from the IAEA is based on JEFF-3.1 data, but contains a limited number of materials (the remainder are taken from the default ACE library based on ENDF/B-VI data).

6.2. RESULTS

All the results of the validation study are presented as the differences between the calculated multiplication factor k_c and the measured multiplication factor k_m in units of parts per 100 000 (pcm). Separate plots for each set of benchmarks are presented.

6.2.1. KBR benchmarks

Cases 22 and 23 are critical configurations; cases 18–21 are k_∞ measurements with progressively softer spectra and are highly sensitive to ^{232}Th data. Figure 6.1 shows the sensitivity of the results to the different libraries. The maximum spread in the results with ENDF/B-VI.8 data is around 7000 pcm. KBR18 and KBR21 are the most significant outliers, with the hardest and softest spectra, respectively. Adoption of JEFF-3.1 data does not improve the agreement between measurements and calculations, whereas a significant improvement occurs when the ENDF/B-VII.β2+ data are used: the maximum spread of the results is reduced to about 3000 pcm, although the two outliers are still beyond the 2σ uncertainty interval. The influence of the new ^{232}Th data alone is shown in Fig. 6.2, confirming the fact that these data are primarily responsible for the observed improvement.

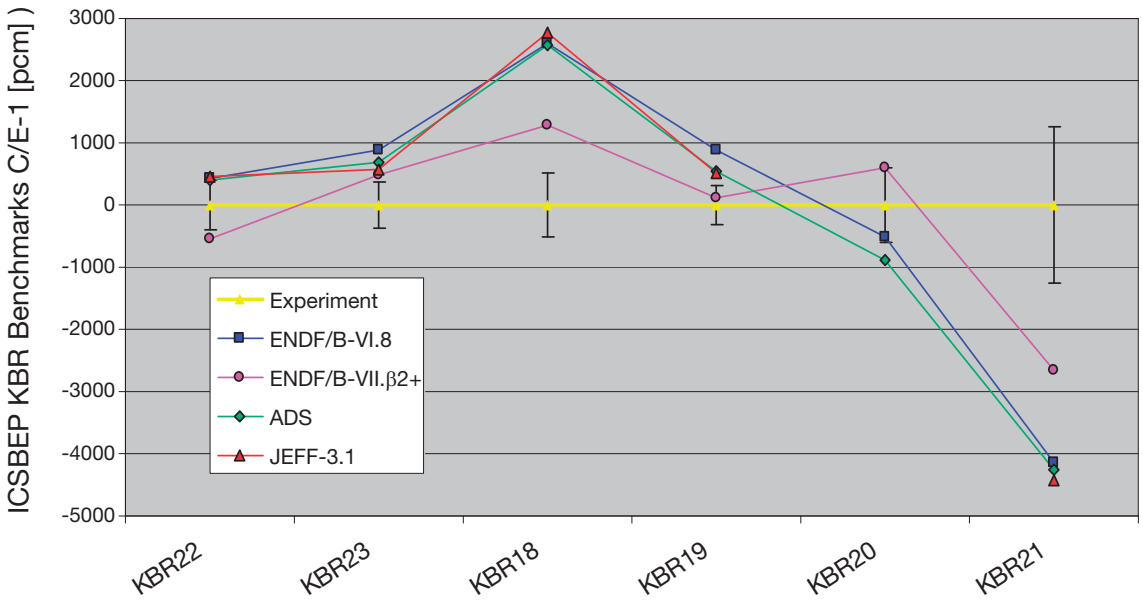

FIG. 6.1. Results of calculations for the KBR series of benchmarks with different libraries.

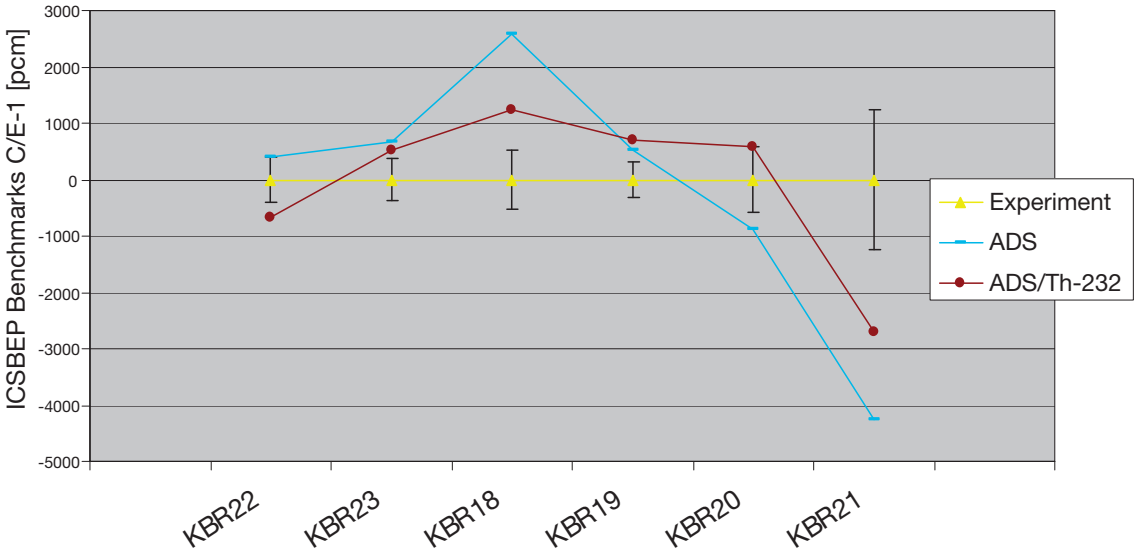

FIG. 6.2. Sensitivity of the KBR benchmarks on ^{232}Th data (ENDF/B-VI.8 versus ENDF/B-VII.β2+).

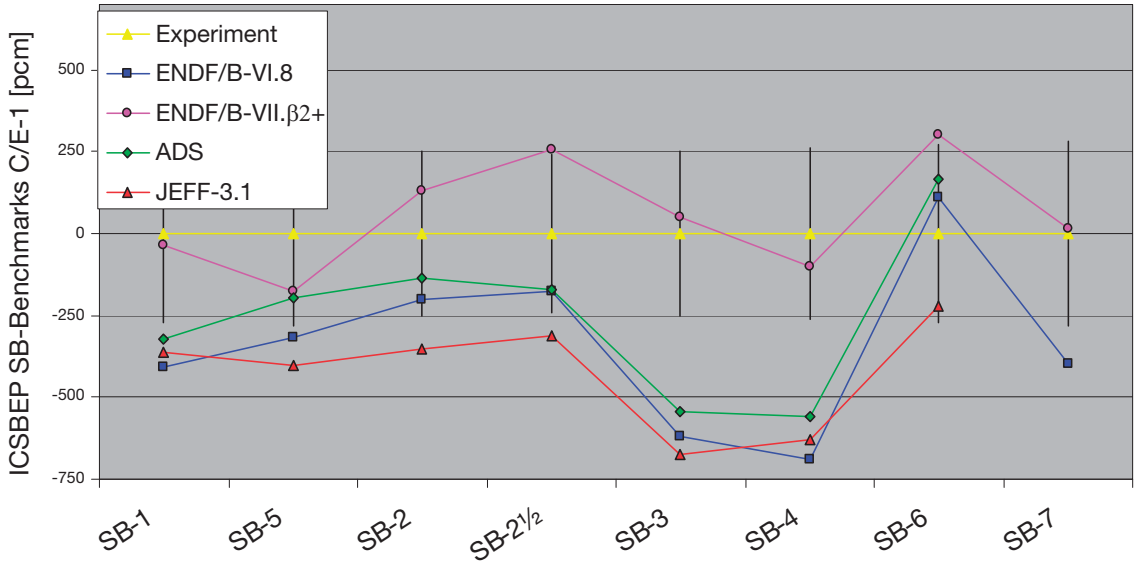

FIG. 6.3. Results of calculations for the SB-n series of benchmarks with different libraries.

6.2.2. SB-n benchmarks

The SB-n series of benchmarks are thermal lattices with a thorium blanket and either a ^{235}U (SB-1 or SB-5) or ^{233}U (other SB lattices) fissile component in the zirconium matrix fuel. As seen from Fig. 6.3, the use of JEFF-3.1 data does not improve the agreement between measurements and calculations compared with the ENDF/B-VI results. However, results with the new ENDF/B-VII.β2+ data lie within the 1σ uncertainty interval, except for lattice SB-6, which is the only outlier (although well within the 2σ uncertainty band).

Sensitivity to the nuclear data of individual nuclides is quite revealing. Starting arbitrarily with the base calculation that uses the ADS library (where ^{232}Th data were taken from ENDF/B-VI.6), data for ^{232}Th, ^{233}U, ^{234}U and zirconium were replaced with data from ENDF/B-VII.β2. Figure 6.4 shows the strong sensitivity of the SB-3 and SB-4 lattices to the ^{232}Th data. Clearly, the new IAEA evaluation for ^{232}Th reduces greatly the scattering in the results. While the introduction of ^{233}U data from ENDF/B-VII.β2 introduces a distinctly positive bias in the lattices that contain ^{233}U, the impact of ^{234}U is virtually negligible. Data for zirconium as the matrix material in the fuel also

produce a positive bias, which together with the ^{233}U data causes an over-prediction of reactivity. The reduction of the average number of neutrons per fission in the ^{233}U data of ENDF/B-VII.β2+ (to be in agreement with the new evaluation of the neutron cross-section standards [6.3]) removes the bias completely, as is evident in Fig. 6.3.

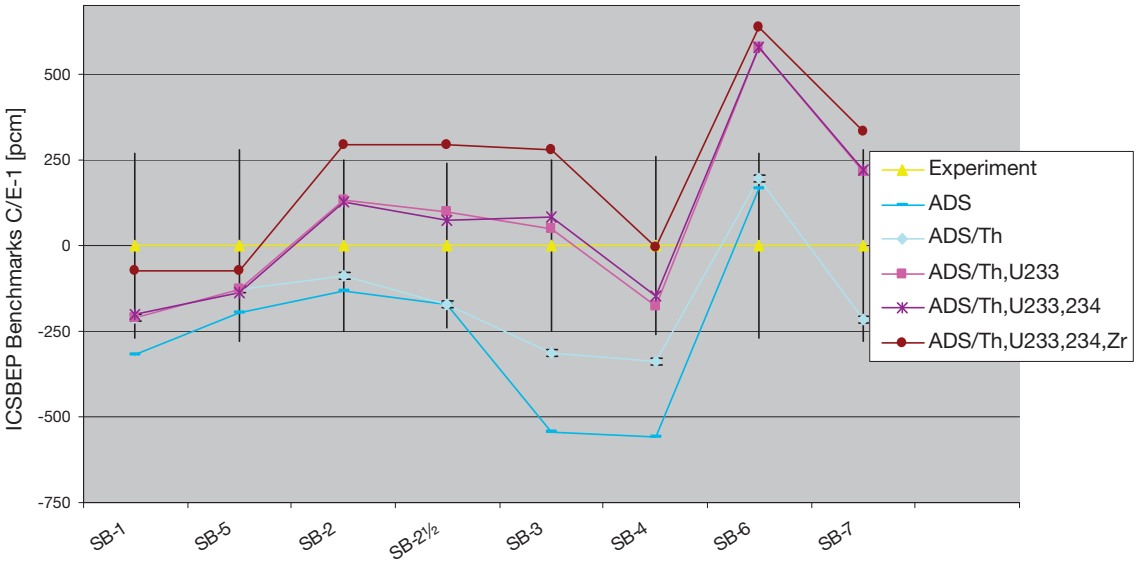

FIG. 6.4. Sensitivity of the SB-n benchmarks on the nuclear data adopted.

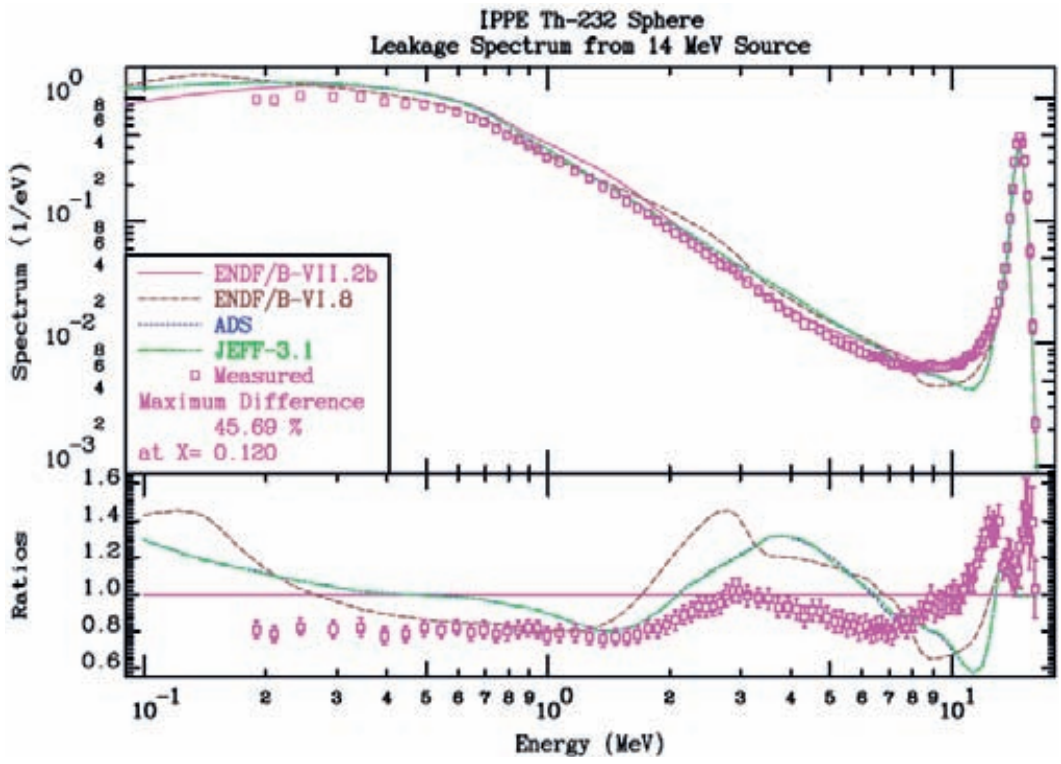

FIG. 6.5. The leakage spectrum from the IPPE (Institute of Physics and Power Engineering (Obninsk)) thorium sphere with a 14 MeV D–T source.

6.2.3. The Thor benchmark

The Thor benchmark is a thorium-reflected plutonium sphere. Interpretation of the results depends strongly on the nuclear data for plutonium. The predicted reactivity is 224 pcm above the benchmark value, but this should be considered with reference to the results for bare plutonium sphere benchmarks, which is outside the scope of the present work.

6.2.4. The IPPE sphere leakage current benchmark

Results based on the SINBAD model and ENDF/B-VII.β2+ data agree with the leakage current measurement to within 20%. The main difference involves the low energy tail of the spectrum, where the (n, 3n) reaction dominates — a reduction of the (n, 3n) cross-section near the threshold would improve the results. This benchmark is strongly influenced by a processing error that occurred when generating the ACE file for ^{232}Th with the older versions of NJOY (Fig. 6.5).

Apart from the discrepancy between measurement and calculation due to the cross-sections, the benchmark model does not include the collimator explicitly, and only represents an approximation to the real configuration. An important recommendation of the benchmark is to model the source spectrum without the sphere in place to simulate the resolution broadening response function. Unfortunately, the available information concerning the benchmark is insufficient to improve the modelling process.

REFERENCES TO SECTION 6

[6.1] NUCLEAR SCIENCE COMMITTEE OF THE OECD NUCLEAR ENERGY AGENCY, International Handbook of Evaluated Criticality Safety Benchmark Experiments, Rep. NEA/NSC/DOC(95)03, OECD Nuclear Energy Agency, Paris (2006).

[6.2] OECD NUCLEAR ENERGY AGENCY, SINBAD Fusion, Neutronics Benchmark Experiments, Rep. NEA-1553, OECD Nuclear Energy Agency, Paris (1990).

[6.3] INTERNATIONAL ATOMIC ENERGY AGENCY, International Evaluation of Neutron Cross-Section Standards, IAEA, Vienna (2007).

7. DECAY AND FISSION PRODUCT YIELD DATA

7.1. EXISTING EXPERIMENTAL AND EVALUATED DATA

The sources of fission product yield data of relevance to the U–Th cycle are listed in Table 7.1. The data in parentheses are new evaluations delivered to the project, based mainly on calculations from the systematics.

The ^{232}Pa half-life [7.5] and fission cross-sections [7.6] are listed in Table 7.2, and are compared with the equivalent data for other nuclides of the Th–U fuel cycle. Although the half-life of ^{232}Pa is rather short, the fission cross-section is very large, especially at the thermal energy point. Therefore, the fission yield data were also evaluated for ^{232}Pa.

Available fission product yield data were compared and the best set recommended. When nuclides possessed no known fission yield data, these yields were generated from the systematics.

TABLE 7.1. DATA FROM EXISTING EVALUATED FISSION YIELD DATA LIBRARIES FOR FISSILE NUCLIDES WITHIN THE Th–U CYCLE

Nuclide	CENDL/FY [7.1]	ENDF/B-VII/FPY [7.2]	JENDL-3.3/FPY [7.3]	JEFF-3.1/FPY [7.4]
Th-232	F	F, H	F, H	F, H
Pa-231	(T[a], F[b], H[c])	F	—	—
(Pa-232)	(T, F, H)	—	—	—
Pa-233	(F, H)	—	—	—
U-232	(T, F, H)	T	—	—
U-233	T	T, F, H	T, F, H	T, F, H
U-234	—	F, H	—	F
U-236	—	F, H	F	F
U-235	T, F, H	T, F, H	T, F, H	T, F, H

[a] T: thermal energy.
[b] F: fission spectrum.
[c] H: approximately 14 MeV neutron energy.

TABLE 7.2. FISSION CROSS-SECTION AND HALF-LIFE OF MINOR ACTINIDES CONCERNING THE Th–U CYCLE

Nuclide	$T_{1/2}$	Thermal	10 keV	1 MeV	5 MeV
Pa-231	3.276×10^4 a	0.0189	0.0003	0.810	0.870
Pa-232	1.31 d	692.490	2.369	1.140	0.938
Pa-233	26.975 d	—	—	0.314	0.417
U-232	68.9 d	73.965	1.530	2.000	2.000
U-234	2.455×10^5 a	0.292	0.0105	1.082	1.343
U-236	2.342×10^7 a	0.0608	0.00562	0.366	0.857

7.2. FISSION YIELD DATA FOR ^{232}Th, ^{233}U AND ^{235}U

Table 7.1 shows that fission yield data are available for ^{232}Th, ^{233}U and ^{235}U in all four major application libraries CENDL/FY, ENDF/B-VII/FPY, JENDL-3.3/FPY and JEFF-3.1/FPY, and at all necessary energy points, except CENDL/FY, which only specifies the yields for ^{232}Th in the fast energy range and ^{233}U at thermal energies. Data were compared from the four libraries [7.7, 7.8]. As a result of this comparison, the JEFF-3.1 data for these nuclides were recommended for adoption.

The ENDF material identifiers (MAT numbers) for some nuclides do not follow the ENDF-6 format recommendation, and therefore they were changed as necessary. Another issue of importance is the definition of a 'stable' nuclide for the purpose of defining cumulative yields (such a definition is not given in the rules for the ENDF-6 format). The JEFF-3.1 evaluation adopts a pragmatic approach by which product nuclides with half-lives greater than 1000 years are not included in the cumulative yields (Table 7.3). Such an assumption is reasonable for applications involving nuclear waste, but most other libraries included all daughter products for which half-lives are defined. This difference in definition had to be taken into account when comparing data.

7.3. FISSION YIELD DATA FOR ^{234}U AND ^{236}U

As can be seen from Table 7.1, the fission yield data for ^{234}U and ^{236}U are only present in the ENDF/B-VII and JEFF-3.1 libraries, while the JENDL-3.3 library contains data for ^{236}U at only one energy point. There is also only a single energy point for both nuclides in JEFF-3.1, but the data are flagged as being energy independent, and are therefore also deemed to be applicable at higher energies. The data were also calculated by the systematics for comparison [7.9].

The reduced χ^2_{ij} for each evaluated library and product nuclide was calculated in order to define the consistency of the evaluated data with respect to equivalent experimental values:

$$\chi^2_{ji} = \frac{1}{N}\sum_{k=1}^{N}\frac{(Y\mathrm{eval}_{ik} - Y\mathrm{exp}_{ik})^2}{\Delta Y\mathrm{exp}^2_{ik}}$$

where the index i represents the product nuclide, the index k represents the experimental data points, N is the total number of experimental data points, and Yeval and Yexp are the evaluated and experimental yields, respectively. The average, $\bar{\chi}^2_j$, for each library j is given by the following equation:

$$\bar{\chi}^2_j = \frac{1}{M}\sum_{i=1}^{M}\chi^2_{ji}$$

where M is the number of product nuclides with experimental data.

TABLE 7.3. PRODUCT NUCLIDES AFFECTED BY THE JEFF-3.1 DEFINITION OF 'STABLE' NUCLIDES

Mass A	79	87	93	99	107*	113
Charge Z	35	38	41	44	47*	49
Mass A	115	126	126	129	135	
Charge Z	50	51	52	54	56	

* Data are not given in JEFF-3.1.

According to the above criteria, the fission yield data from the ENDF/B-VII evaluation agree well with the experimental data. A significant increase in the average $\overline{\chi}_j^2$ for the JEFF-3.1 library arises because the measured yields exhibit a rather strong energy dependence. The yields calculated from the systematics are reasonable, except at the peaks and in the valley region of the distribution. Thus, the data from the ENDF/B-VII library are recommended for the neutron induced fission product yields of ^{234}U and ^{236}U.

7.4. FISSION YIELD DATA FOR ^{231,232,233}Pa AND ^{232}U

There are no fission yield data for ^{231,232,233}Pa and ^{232}U in the available evaluated data libraries, except for ^{232}U at thermal energy. These data had to be calculated from the systematics [7.5]: the mass distribution (chain yield) was calculated by means of the multi-Gaussian model, while the charge distribution (independent yield) was calculated on the basis of the Z_p model. The parameters in the models were determined from suitable fittings of the relevant experimental data. The calculated independent and cumulative yields were assembled in ENDF-6 format by means of the CONVFMTFY code [7.10].

7.5. ASSEMBLY OF A FISSION YIELD DATA FILE

A fission product yield file for nuclides of the U–Th fuel cycle was assembled, following a comparison of the existing data in the JEFF-3.1, ENDF/B-VII, JENDL-3.3 and CENDL/FY libraries with measured values. Yield data for ^{233,235}U and ^{232}Th were taken from the JEFF-3.1 library, data for ^{234,236}U were taken from the ENDF/B-VII library, and yield data for ^{231,232,233}Pa and ^{232}U were calculated from the systematics, since no data for these nuclides were available in any of the fission yield libraries.

Users should be aware that a stable nuclide is not defined in the ENDF-6 format for cumulative yields. The evaluator of the JEFF-3.1 library considered nuclides with a half-life greater than 1000 years as ‘stable’, and therefore excluded specific contributors to the daughter product in the cumulative yields. This convention is applicable to ^{233,235}U and ^{232}Th as taken from JEFF-3.1, but not to the other nuclides. While this difference may represent an inconsistency in the cumulative yields, the anomaly was tolerated for the sake of traceability of the data to the original source.

The data calculated with the systematics need to be improved further, to ensure that their values at the peaks and valleys and variation with incident neutron energy fit the experimental data better. The variation of the systematics with fissile nuclide charge number Z and mass number A, as well as the variation with energy, need to be studied further to achieve such objectives. However, this type of work was beyond the scope of the CRP.

7.6. DECAY DATA FILE

The decay data from the available evaluated nuclear data libraries were reviewed. No separate evaluation was performed. The JEFF-3.1 library [7.4], being the most recent comprehensive library at the time, was adopted for the decay data as needed.

REFERENCES TO SECTION 7

[7.1] ZHIGANG, Ge, et al., “The updated version of the Chinese Evaluated Nuclear Data Library (CENDL-3.1) and China nuclear data evaluation activities”, Nuclear Data for Science and Technology (Proc. Int. Conf. Nice, 2007), (BERSILLON, O., GUNSING, F., BAUGE, E., JACQMIN, R., LERAY, S., Eds), EDP Sciences, Les Ulis (2008) 753–757, http://dx.doi.org/10.1051/ndata:07570

[7.2] CHADWICK, M.B., et al., ENDF/B-VII.0: Next Generation Evaluated Nuclear Data Library for Nuclear Science and Technology, Nucl. Data Sheets **107** (2006) 2931–3060.

[7.3] SHIBATA, K., et al., Japanese Evaluated Nuclear Data Library Version 3, Revision-3: JENDL-3.3, J. Nucl. Sci. Technol. **39** (2002) 1125–1136.

[7.4] KONING, A., et al. (Eds), The JEFF-3.1 Nuclear Data Library, JEFF Rep. 21, NEA No. 6190, OECD Nuclear Energy Agency, Paris (2006).
[7.5] TULI, J.K., Nuclear Wallet Cards, National Nuclear Data Center, Brookhaven Natl Lab., Upton, NY (2005).
[7.6] LIU, Tingjin, et al., China Nuclear Data Center, Beijing, personal communication, 2004.
[7.7] LIU, Tingjin, LIU, Ping, "Intercomparison and recommendation of the current evaluated fission yield libraries", paper presented at 2nd Research Coordination Mtg on Evaluated Nuclear Data for Th–U Fuel Cycle, INDC(NDS)-0468, IAEA, Vienna, 2004.
[7.8] LIU, Tingjin, SUN, Zhengjun, LIU, Ping, "Inter-comparison of ENDF/B-7 and JEFF-3.1 fission yield data", paper presented at 3rd Research Coordination Mtg on Evaluated Nuclear Data for Th–U Fuel Cycle, INDC(NDS)-0494, IAEA, Vienna, 2006.
[7.9] WAHL, A.C., Contribution to Compilation and Evaluation of Fission Yields Nuclear Data, Rep. LA-13928, Los Alamos Natl Lab., NM (2002).
[7.10] SUN, Zhengjun, China Nuclear Data Center, Beijing, personal communication, 2006.

8. SUMMARY

The results of this project on nuclear data for the Th–U fuel cycle are as follows:

(a) A detailed evaluation of the resonance parameters and their covariances for ^{232}Th in the RRR and the URR was performed, taking into consideration the new experimental data from the IRMM laboratory at Geel and the n_TOF project at CERN.
(b) The resonance parameters from Mughabghab were adopted for ^{231}Pa; the resonance parameters for ^{233}Pa were provided by Mourogovskij and Bakhanovich. The resonance parameters were converted into the RM formalism, and their covariances were generated by the retroactive method.
(c) A reaction model of the fission of light actinides which takes into account transmission through a triple humped fission barrier with absorption has been developed. This formalism enables complex structure in the light actinide fission cross-section to be interpreted over a wide energy range, and provides the means of undertaking neutron data evaluations for ^{232}Th and ^{231,233}Pa.
(d) Significant improvements were made in the fission model parameters for light actinides; the triple humped fission barrier model with absorption was incorporated into the EMPIRE-II code. This allowed consistent evaluation of cross-sections and double differential data for ^{232}Th and ^{231,233}Pa above the resonance range.
(e) The same model parameters were used to generate the covariance matrix priors for ^{232}Th and ^{231,233}Pa nuclei by the Monte Carlo technique.
(f) The covariance matrix prior was fed into the GANDR system, which uses the generalized least squares method to combine theoretical priors with selected experimental data. The resultant covariance matrices for ^{232}Th and ^{231,233}Pa nuclei were converted into ENDF-6 format, including cross-reaction correlations.
(g) The evaluation for ^{232}U was adopted directly from the Minsk file.
(h) The recommended ^{233}U data were taken from the Los Alamos evaluation, for the ENDF/B-VII.0 database, except for the prompt fission spectra taken from the Minsk files because they used improved physics models.
(i) The resonance parameters for ^{234}U from ENDF/B-VI were corrected; the cross-sections above the resonance range were taken from the Minsk files. The two components were merged into a consistent file.
(j) The Los Alamos evaluation prepared for ENDF/B-VII.0 was adopted for ^{236}U.
(k) The decay data and the fission product yield data from the JEFF-3.1 library were recommended for adoption.
(l) An extensive validation programme was performed on the basis of criticality benchmarks from the ICSBEP compilation and a 14 MeV benchmark from the SINBAD compilation. The results of benchmark calculations were used to fine-tune the parameters in the evaluation process within their uncertainty intervals.
(m) The evaluated data files were processed using the NJOY code. Application libraries in ACE format for the MCNP family of codes and in MATXS format for deterministic codes are available from the IAEA web site for all the nuclides considered. The data for ^{232}Th and ^{231,233}Pa are implicitly included in the WIMS-D library based on ENDF/B-VII.0 data; the WIMS-D library is also available from the IAEA web site.

Thus, new evaluations for ^{232}Th and ^{231,233}Pa were prepared and improvements to the evaluations for ^{232,233,234,236}U were made; as far as possible, the data were validated against benchmark experiments. These new and substantially improved IAEA data files are available at: http://www-nds.iaea.org/Th-U/

The ENDF/B-VII.0 library was released after the project terminated. Evaluations resulting from the IAEA project for ^{232}Th and ^{231,233}Pa have been adopted for the final version of the ENDF/B-VII.0 library.

PARTICIPANTS IN AND CONTRIBUTORS TO THE COORDINATED RESEARCH PROJECT

Capote, R.	International Atomic Energy Agency
Chadwick, M.	Los Alamos National Laboratory, United States of America
Ganesan, S.	Bhabha Atomic Research Centre, India
Gunsing, F.	Commissariat à l'énergie atomique, France
Hambsch, F.-J.	Institute for Reference Materials and Measurements, Belgium
Ignatyuk, A.V.	Institute of Physics and Power Engineering, Russian Federation
Iwamoto, O.	Japan Atomic Energy Agency, Japan
Janeva, N.B.	Bulgarian Academy of Sciences, Bulgaria
Kawano, T.	Los Alamos National Laboratory, United States of America
Leal, L.	Oak Ridge National Laboratory, United States of America
Lee, Y. Deok	Korea Atomic Energy Research Institute, Republic of Korea
Leeb, H.	Vienna University of Technology, Austria
Liu, Ping	China Institute of Atomic Energy, China
Liu, Tingjin	China Institute of Atomic Energy, China
Maslov, V.M.	Joint Institute for Power and Nuclear Research, Belarus
Schillebeeckx, P.	Institute for Reference Materials and Measurements, Belgium
Sin, M.	University of Bucharest, Romania
Sirakov, I.	Bulgarian Academy of Sciences, Bulgaria
Trkov, A.	International Atomic Energy Agency

Research Coordination Meetings

Vienna, Austria: 25–29 August 2003, 6–9 December 2004,
29 January – 2 February 2006

IAEA
International Atomic Energy Agency

Where to order IAEA publications

In the following countries IAEA publications may be purchased from the sources listed below, or from major local booksellers. Payment may be made in local currency or with UNESCO coupons.

AUSTRALIA
DA Information Services, 648 Whitehorse Road, MITCHAM 3132
Telephone: +61 3 9210 7777 • Fax: +61 3 9210 7788
Email: service@dadirect.com.au • Web site: http://www.dadirect.com.au

BELGIUM
Jean de Lannoy, avenue du Roi 202, B-1190 Brussels
Telephone: +32 2 538 43 08 • Fax: +32 2 538 08 41
Email: jean.de.lannoy@infoboard.be • Web site: http://www.jean-de-lannoy.be

CANADA
Bernan Associates, 4501 Forbes Blvd, Suite 200, Lanham, MD 20706-4346, USA
Telephone: 1-800-865-3457 • Fax: 1-800-865-3450
Email: customercare@bernan.com • Web site: http://www.bernan.com

Renouf Publishing Company Ltd., 1-5369 Canotek Rd., Ottawa, Ontario, K1J 9J3
Telephone: +613 745 2665 • Fax: +613 745 7660
Email: order.dept@renoufbooks.com • Web site: http://www.renoufbooks.com

CHINA
IAEA Publications in Chinese: China Nuclear Energy Industry Corporation, Translation Section, P.O. Box 2103, Beijing

CZECH REPUBLIC
Suweco CZ, S.R.O., Klecakova 347, 180 21 Praha 9
Telephone: +420 26603 5364 • Fax: +420 28482 1646
Email: nakup@suweco.cz • Web site: http://www.suweco.cz

FINLAND
Akateeminen Kirjakauppa, PO BOX 128 (Keskuskatu 1), FIN-00101 Helsinki
Telephone: +358 9 121 41 • Fax: +358 9 121 4450
Email: akatilaus@akateeminen.com • Web site: http://www.akateeminen.com

FRANCE
Form-Edit, 5, rue Janssen, P.O. Box 25, F-75921 Paris Cedex 19
Telephone: +33 1 42 01 49 49 • Fax: +33 1 42 01 90 90
Email: formedit@formedit.fr • Web site: http://www. formedit.fr

Lavoisier SAS, 145 rue de Provigny, 94236 Cachan Cedex
Telephone: + 33 1 47 40 67 02 • Fax +33 1 47 40 67 02
Email: romuald.verrier@lavoisier.fr • Web site: http://www.lavoisier.fr

GERMANY
UNO-Verlag, Vertriebs- und Verlags GmbH, Am Hofgarten 10, D-53113 Bonn
Telephone: + 49 228 94 90 20 • Fax: +49 228 94 90 20 or +49 228 94 90 222
Email: bestellung@uno-verlag.de • Web site: http://www.uno-verlag.de

HUNGARY
Librotrade Ltd., Book Import, P.O. Box 126, H-1656 Budapest
Telephone: +36 1 257 7777 • Fax: +36 1 257 7472 • Email: books@librotrade.hu

INDIA
Allied Publishers Group, 1st Floor, Dubash House, 15, J. N. Heredia Marg, Ballard Estate, Mumbai 400 001,
Telephone: +91 22 22617926/27 • Fax: +91 22 22617928
Email: alliedpl@vsnl.com • Web site: http://www.alliedpublishers.com

Bookwell, 2/72, Nirankari Colony, Delhi 110009
Telephone: +91 11 23268786, +91 11 23257264 • Fax: +91 11 23281315
Email: bookwell@vsnl.net

ITALY
Libreria Scientifica Dott. Lucio di Biasio “AEIOU”, Via Coronelli 6, I-20146 Milan
Telephone: +39 02 48 95 45 52 or 48 95 45 62 • Fax: +39 02 48 95 45 48
Email: info@libreriaaeiou.eu • Website: www.libreriaaeiou.eu

JAPAN
Maruzen Company, Ltd., 13-6 Nihonbashi, 3 chome, Chuo-ku, Tokyo 103-0027
Telephone: +81 3 3275 8582 • Fax: +81 3 3275 9072
Email: journal@maruzen.co.jp • Web site: http://www.maruzen.co.jp

REPUBLIC OF KOREA
KINS Inc., Information Business Dept. Samho Bldg. 2nd Floor, 275-1 Yang Jae-dong SeoCho-G, Seoul 137-130
Telephone: +02 589 1740 • Fax: +02 589 1746 • Web site: http://www.kins.re.kr

NETHERLANDS
De Lindeboom Internationale Publicaties B.V., M.A. de Ruyterstraat 20A, NL-7482 BZ Haaksbergen
Telephone: +31 (0) 53 5740004 • Fax: +31 (0) 53 5729296
Email: books@delindeboom.com • Web site: http://www.delindeboom.com

Martinus Nijhoff International, Koraalrood 50, P.O. Box 1853, 2700 CZ Zoetermeer
Telephone: +31 793 684 400 • Fax: +31 793 615 698
Email: info@nijhoff.nl • Web site: http://www.nijhoff.nl

Swets and Zeitlinger b.v., P.O. Box 830, 2160 SZ Lisse
Telephone: +31 252 435 111 • Fax: +31 252 415 888
Email: infoho@swets.nl • Web site: http://www.swets.nl

NEW ZEALAND
DA Information Services, 648 Whitehorse Road, MITCHAM 3132, Australia
Telephone: +61 3 9210 7777 • Fax: +61 3 9210 7788
Email: service@dadirect.com.au • Web site: http://www.dadirect.com.au

SLOVENIA
Cankarjeva Zalozba d.d., Kopitarjeva 2, SI-1512 Ljubljana
Telephone: +386 1 432 31 44 • Fax: +386 1 230 14 35
Email: import.books@cankarjeva-z.si • Web site: http://www.cankarjeva-z.si/uvoz

SPAIN
Díaz de Santos, S.A., c/ Juan Bravo, 3A, E-28006 Madrid
Telephone: +34 91 781 94 80 • Fax: +34 91 575 55 63
Email: compras@diazdesantos.es, carmela@diazdesantos.es, barcelona@diazdesantos.es, julio@diazdesantos.es
Web site: http://www.diazdesantos.es

UNITED KINGDOM
The Stationery Office Ltd, International Sales Agency, PO Box 29, Norwich, NR3 1 GN
Telephone (orders): +44 870 600 5552 • (enquiries): +44 207 873 8372 • Fax: +44 207 873 8203
Email (orders): book.orders@tso.co.uk • (enquiries): book.enquiries@tso.co.uk • Web site: http://www.tso.co.uk

On-line orders
DELTA Int. Book Wholesalers Ltd., 39 Alexandra Road, Addlestone, Surrey, KT15 2PQ
Email: info@profbooks.com • Web site: http://www.profbooks.com

Books on the Environment
Earthprint Ltd., P.O. Box 119, Stevenage SG1 4TP
Telephone: +44 1438748111 • Fax: +44 1438748844
Email: orders@earthprint.com • Web site: http://www.earthprint.com

UNITED NATIONS
Dept. I004, Room DC2-0853, First Avenue at 46th Street, New York, N.Y. 10017, USA
(UN) Telephone: +800 253-9646 or +212 963-8302 • Fax: +212 963-3489
Email: publications@un.org • Web site: http://www.un.org

UNITED STATES OF AMERICA
Bernan Associates, 4501 Forbes Blvd., Suite 200, Lanham, MD 20706-4346
Telephone: 1-800-865-3457 • Fax: 1-800-865-3450
Email: customercare@bernan.com · Web site: http://www.bernan.com

Renouf Publishing Company Ltd., 812 Proctor Ave., Ogdensburg, NY, 13669
Telephone: +888 551 7470 (toll-free) • Fax: +888 568 8546 (toll-free)
Email: order.dept@renoufbooks.com • Web site: http://www.renoufbooks.com

Orders and requests for information may also be addressed directly to:

Marketing and Sales Unit, International Atomic Energy Agency
Vienna International Centre, PO Box 100, 1400 Vienna, Austria
Telephone: +43 1 2600 22529 (or 22530) • Fax: +43 1 2600 29302
Email: sales.publications@iaea.org • Web site: http://www.iaea.org/books

10-03141

FISSION PRODUCT YIELD DATA FOR THE TRANSMUTATION OF MINOR ACTINIDE NUCLEAR WASTE

STI/PUB/1286 (341 pp.; 2008)
ISBN 92–0–115306–6 Price: €65.00

UPDATE OF X RAY AND GAMMA RAY DECAY DATA STANDARDS FOR DETECTOR CALIBRATION AND OTHER APPLICATIONS (VOLUMES 1 AND 2)

STI/PUB/1287 (210 pp.; 2007)
ISBN 92–0–113606–4 Price: €65.00

INTERNATIONAL EVALUATION OF NEUTRON CROSS-SECTION STANDARDS

STI/PUB/1291 (227 pp.; 2007)
ISBN 92–0–100807–4 Price: €52.00

DATABASE OF PROMPT GAMMA RAYS FROM SLOW NEUTRON CAPTURE FOR ELEMENTAL ANALYSIS

STI/PUB/1263 (251 pp.; 2007)
ISBN 92–0–101306–X Price: €28.00

Considerable improvements have been made to the evaluated nuclear data files for ^{232}Th, ^{231}Pa and ^{233}Pa, and these new data have been adopted, along with additional developments to existing evaluations for ^{232}U, ^{233}U, ^{234}U and ^{236}U for Th–U fuel cycle calculations. These evaluated data files are available on the IAEA web site in ENDF-6 format, as well as the equivalent processed libraries in ACE format for the MNCP family of Monte Carlo codes and in MATXS format for deterministic codes. The resulting evaluations for ^{232}Th and for ^{231}Pa and ^{233}Pa have been adopted in the final version of the US ENDF/B-VII-0 nuclear applications library. This report represents the definitive documentation of this work by members of an IAEA coordinated research project.

INTERNATIONAL ATOMIC ENERGY AGENCY
VIENNA
ISBN 978–92–0–101010–0